WATCHING NEURONS GROW: GUIDANCE RECEPTORS, SIGNAL TRANSDUCTION MACHINERY AND CYTOSKELETAL REGULATORS AFFECT GROWTH CONE MORPHOLOGY AND DYNAMICS IN *C. ELEGANS*

BY

Submitted to the graduate degree program in Molecular Biosciences and the Graduate Faculty of the University of Kansas in partial fulfillment of the requirements for the degree of Doctor of Philosophy

Committee members

Chairperson – Erik Lundquist

_____

Brian Ackley

_____

Yoshiaki Azuma

_____

Paulyn Cartwright

_____

Robert Cohen

_____

Lisa Timmons

_____

Date defended: March 30, 2011

The Dissertation Committee for Adam David Norris certifies that this is the approved version of the following dissertation:

WATCHING NEURONS GROW: GUIDANCE RECEPTORS, SIGNAL TRANSDUCTION MACHINERY AND CYTOSKELETAL REGULATORS AFFECT GROWTH CONE MORPHOLOGY AND DYNAMICS IN *C. ELEGANS*

Chairperson – Erik Lundquist

_____

Date approved: March 30, 2011

Acknowledgements

Boy, this was a lot of fun! Graduate school has been the greatest decision of my short professional life. Thank you to everyone who has made this experience amazing. First and foremost, thanks to the big cheese, Dr. Erik Lundquist, who taught me to work like a scientist, to think like a scientist, to ask questions like a scientist, and to write like a scientist. I owe whatever success and talent I may have in science to his mentorship. So thanks Erik!

Also, thanks to every single person in the Lundquist Lab who has made it the coolest lab at KU. Thanks to Eric Struckhoff, without whom the laboratory would cease to revolve around the sun, and without whom the daily grind would be much more boring and predictable. Thanks to the grad students: Jamie the First, Rafa, Lakshmi and Jamie the Second. You all have been a pleasure to work with, and I honestly have no idea what you will do without me- probably enjoy excess leftover donuts?

Special thanks to the super-cool undergrads who have worked under me: Michelle Winston, the sweetest little thing you ever did see; Samir Hamdeh, who worked hard, accomplished a lot, and managed to make us all laugh; and Zach 'Attach' Roberts, who has done a phenomenal job so far, and is a pretty swell guy. Now Zach, please turn to section 4.6 of this dissertation (Future Directions), and *get cracking!*

A special special thanks to Rafael Demarco, who not only has been the greatest colleague and fellow grad student that one could ask for, but also the greatest friend, roommate, chef, confidante, and lab-mate that one could ask for. In fact, greater than one could ever ask for.

As a graduate student at KU I found an admiration for the process of science, I found an interest in developmental biology, I found a fantastic lab in which to work, I found a deep respect for my fellow scientists, and I found- coming as a complete surprise to myself- the love of my life. Megan, thank you for crossing my path. You have been a blessing to me.

Finally, thank you to my family, who has loved and supported me whole-heartedly since t=0. And to the Author and Perfecter.

Watching neurons grow: guidance receptors, signal transduction machinery and cytoskeletal regulators affect growth cone morphology and dynamics in *C. elegans*

Adam Norris

Mentor: Erik Lundquist

Table of Contents

Chapter I

Introduction

The human nervous system is an incredibly complex network consisting of a myriad of axon tracts, pathways and connections. Proper structure and organization of the nervous system is vital, and many human diseases have been shown to result from improper wiring of the human nervous system, including L1 syndrome, Duane syndrome and corpus callosum agenesis (Engle 2010).

Proper functioning of the nervous system depends on the development of proper neuronal connections, which in turn depends on the proper pathfinding of neurites from their neuronal cells of origin to their eventual synaptic targets. It is the growth cone, which resides at the distal tip of the developing axon, which is able to sense, integrate and respond to guidance information and lead the axon to its destination (Mortimer et al. 2008; Tessier-Lavigne and Goodman 1996). The task of the growth cone is immense, guiding the axon through a complex extracellular milieu, oftentimes over long distances, to reach its target.

The growth cone displays dynamic filopdial and lammellipodial protrusions, which are involved in axon outgrowth and guidance. The lamellipodium is an actin-based, sheet-like structure at the leading edge of the growth cone consisting of a meshwork of actin filaments, which provide the forward motive force of the developing neurite (Gallo and Letourneau 2004). Filopodia, which emanate from the growth cone lamellipodium, consist of bundled filamentous actin (f-actin). Filopodia are thought to be involved in the sensation of directional cues and subsequent changes in directional locomotion (Davenport et al. 1993).

Much work has been done to identify proteins required for axon guidance by studying the developed nervous system *in vivo* of whole organisms (Hedgecock et al. 1987), and by studying developing growth cones *in vitro* (Ming et al. 1997). There has been relatively little work bridging that gap by studying developing growth cones *in vivo* in live organisms. The work here attempts to do that by utilizing the free-living nematode *Caenorhabditis elegans*. For the studies presented here, *C. elegans* as a model system provides three major benefits: ease of genetic manipulation, allowing for the efficient introduction of transgenes as well as a wide variety of existing mutants with which to work; invariant cell lineage and wiring of a relatively simple nervous system, allowing for fully replicable experiments to be performed on the developing nervous system from various animals and with various genetic backgrounds; and a transparent cuticle, facilitating the study of developing neurons in live, intact organisms.

The major class of neurons we chose to focus on were the 13 VDs (Ventral D-type), which along with the 6 DDs (Dorsal D-type) make up 19 of the 26 major GABAergic neurons in *C. elegans*. The VD/DD neurons function to coordinate the characteristic sinusoidal body movement of *C. elegans* by coordinately relaxing the dorsal muscles during ventral muscle contraction, and vice versa. Both VD and DD neurons reside in the ventral nerve cord, and their axons first migrate anteriorly before turning 90 degrees and traveling commissurally until reaching the dorsal nerve cord, at which point they spread both anteriorly and posteriorly and establish their synaptic partners. While the DD

axons develop in embryogenesis, the VD axons develop during larval stages from late L1 to early L2, and are easily observable using a trasngene of *unc*-25 driving GFP to illuminate the D-type neurons (VDs and DDs) (Knobel et al. 1999). The development occurs in a wave, with the most anterior neuron (VD1) sending out growth cones at about 16 hours post-hatching, and the most posterior (VD13) growth cone having completed its commissural trajectory by 19 hours post-hatching. The commissural migration takes about 1 hour to complete in wild-type worms (Knobel et al. 1999). Thus the VD neurons were good candidates to study *in vivo* growth cone development, having a stereotyped and well-described developmental pattern, and being born post-embryonically and in a position easily discernable by fluorescent microscopy.

We also studied the HSNs (Hermaphrodite Specific Neuron) as another class of neurons whose axons migrate ventrally, in contrast to the VDs whose axons migrate dorsally. The HSNs are seretonergic neurons innervating the vulval muscles and facilitating proper egg-laying (Desai et al. 1988). The two bilaterally symmetrical HSN cell bodies are located laterally near the middle of the worm, above to the vulva. Within an hour post-hatching the HSNs begin to send out short protrusions, which continue throughout larval development until about 18 hours post-hatching, by which point the protrusions have consolidated into a robust growth cone. The HSNs continue to send out dynamic protrusions through the L4 stage, by which point the mature axon has finally formed (Adler et al. 2006).

There are a number of well-described genes that cause defects in axon pathfinding and nervous system development (Letourneau 1996; Lundquist 2006; Shakir et al. 2006). We wanted to use the system just described to determine the nature of those axon pathfinding errors and what the activity of the corresponding genes might be at the level of the developing growth cone. We divided known axon-pathfinding genes into three broad categories, and this dissertation will roughly address each of the three categories in three different chapters. First, there are the guidance cues and the receptors that sense those cues, such as UNC-6/Netrin and its receptors UNC-40/DCC and UNC-5 (Chapter III). Next there is the signal transduction machinery that interprets and transduces those cues, such as the Rac GTPases and their GEF (Guanine Nucleotide Exchange Factor) UNC-73/Trio (Chapter IV). Finally, there are the proteins that act directly on the growth cone cytoskeleton, such as the Arp2/3 complex and UNC-34/Enabled (Chapter II and revisited in Chapter IV).

We show here that along with their role in axon pathfinding, each of the genes presented here affects the morphology, dynamics and/or polarity of the developing growth cone. In Chapter II we show that the Arp2/3 complex is indeed involved in axon pathfinding, and that it stimulates filopodia and lamellipodia formation. We similarly show that UNC-115/abLIM is involved in both filopodia and lamellipodia formation. Finally, we show that UNC-34/Enabled is involved in filopodia formation *in vivo*. In Chapter III we show that UNC-6/Netrin and its receptors UNC-40/DCC and UNC-5 are involved in both orienting the polarity of protrusion and in modulating the extent of protrusion in the developing growth

cone. We show a link between repulsive signaling through UNC-5 and inhibition of protrusion, as well as a link between attractive signaling through UNC-40/DCC and stimulation of protrusion. In Chapter IV we show that UNC-73 and the Rac GTPases are required for preventing ectopic axon branching as well as excessive filopodia protrusion. We show that they are likely acting downstream of an UNC-6-repulsed UNC-5/UNC-40 signaling complex, and that they may be upstream of the cytoskeletal regulators UNC-33/CRMP and UNC-44/Ankyrin, which likewise are required for preventing axon branching and excessive filopodia protrusion. Finally, we propose a causal link between the excess filopodia protrusion and the ectopic axon branching phenotypes observed. These studies begin to bridge the gap in understanding between the development of the growth cone *in vivo* and the endpoint axon pathfinding phenotype.

Chapter II

The Arp2/3 complex, UNC-115/abLIM, and UNC-34/Enabled regulate axon guidance and growth cone filopodia formation in *C. elegans*

2.1 Abstract

While many molecules involved in axon guidance have been identified, the cellular and molecular mechanisms by which these molecules regulate growth cone morphology during axon outgrowth remain to be elucidated. The actin cytoskeleton of the growth cone underlies the formation of lamellipodia and filopodia that control growth cone outgrowth and guidance. The role of the Arp2/3 complex in growth cone filopodia formation has been controversial, and other mechanisms of growth cone filopodia formation remain to be described. Here we show that mutations in genes encoding the Arp2/3 complex (*arx* genes) caused defects in axon guidance. Analysis of developing growth cones *in vivo* showed that *arx* mutants displayed defects in filopodia and reduced growth cone size. Time-lapse analysis of growth cones in living animals indicated that *arx* mutants affected the rate of growth cone filopodia formation but not filopodia stability or length. Two other actin modulatory proteins, UNC-115/abLIM and UNC-34/Enabled, that had been shown previously to affect axon guidance had overlapping roles with Arp2/3 in axon guidance and also affected the rate of filopodia initiation but not stability or length. Our results indicate that the Arp2/3 complex is required cell-autonomously for axon guidance and growth cone filopodia initiation. Furthermore, they show that two other actin-binding proteins, UNC-115/abLIM and UNC-34/Enabled, also control growth cone filopodia formation, possibly in parallel to Arp2/3. These studies indicate that, *in vivo*, multiple actin modulatory pathways including the Arp2/3 complex contribute to growth cone filopodia formation during growth cone outgrowth.

2.2 Introduction

The growth cone of a developing axon senses and responds to extracellular cues resulting in the migration of the growth cone and thus axon to its correct target region in the nervous system (Mortimer et al. 2008; Tessier-Lavigne and Goodman 1996). Growth cones display dynamic, actin-based lamellipodial protrusions ringed by filopodia, which together guide the growth cone to its target (Gallo and Letourneau 2004; Pak et al. 2008; Zhou and Cohan 2004). The Arp2/3 complex is a seven-member protein complex that nucleates actin filaments from the sides of pre-existing actin filaments. In cultured cells, the Arp2/3 complex is necessary to form the network of branched actin filaments underlying lamellipodia (Beltzner and Pollard 2007; Borisy and Svitkina 2000; Svitkina and Borisy 1999).

The Arp2/3 complex has been implicated in axon pathfinding *in vivo*. In Drosophila, the Arp2/3 complex and its regulators WAVE/Scar and Kette are required for proper axon pathfinding (Zallen et al. 2002), and in *C. elegans*, the Arp2/3 regulators WAVE-1/WAVE, WASP-1/WASP, GEX-2/Sra-1, and GEX-3/Kette are required for proper axon guidance (Shakir et al. 2008). However, in these studies, the effects of Arp2/3 on growth cone outgrowth were not described. The role of the Arp2/3 complex in growth cone morphology has been controversial. In two studies using cultured hippocampal neurons, inhibition of Arp2/3 activity resulted in increased axon length with little or no effect on growth cone filopodia or morphology (Pinyol et al. 2007; Strasser et al. 2004). Another recent study using cultured hippocampal neurons and neuroblastoma cells

showed that Arp2/3 knock-down resulted in defective actin organization and defective lamellipodia and filopodia formation in the growth cone (Korobova and Svitkina 2008). Studies reported here show that Arp2/3 is indeed required for growth cone morphology and filopodia formation *in vivo*, and and that Arp2/3 is required specifically for the rate of filopodia initiation but not filopodial stability or length. Thus, our studies demonstrate that Arp2/3 is required for growth cone filopodia formation and extend these findings *in vivo*, explaining the axon pathfinding defects observed in Arp2/3 mutants. Furthermore, UNC-115/abLIM has been implicated in axon pathfinding in *C. elegans* (Lundquist et al. 1998; Shakir et al. 2006; Struckhoff and Lundquist 2003) and Drosophila (Garcia et al. 2007), but its role in growth cone dynamics and morphology during outgrowth is not understood. Our results here show that UNC-115/abLIM is also involved in the initiation of growth cone filopodia.

Experiments described here in *C. elegans* show that mutations in genes encoding subunits of the Arp2/3 complex (*arx* genes) cause defects in axon guidance, and that Arp2/3 is required cell-autonomously in neurons for proper axon guidance. Analysis of growth cones during outgrowth *in vivo* revealed that *arx* mutants displayed reduced numbers of growth cone filopodia and also reduced growth cone size. Time-lapse analysis of growth cones in living animals indicated that the Arp2/3 complex controlled the rate of growth cone filopodia initiation but not filopodia stability or length. These results indicate that in *C elegans*, the Arp2/3 complex is a key regulator of growth cone filopodia initiation during outgrowth.

The actin modulatory proteins UNC-34/Enabled and UNC-115/abLIM have been shown previously to affect axon guidance in *C. elegans* (Shakir et al. 2006; Struckhoff and Lundquist 2003; Withee et al. 2004). Enabled is a key regulator of filopodia formation in many systems including neurons and is thought to act by blocking actin-capping activity thus allowing for long filament growth in filopodia (Barzik et al. 2005; Lebrand et al. 2004), although recent studies indicate that Enabled might have anti-capping independent roles (Bear and Gertler 2009) that are involved in filopodia formation (Applewhite et al. 2007).

The actin binding protein UNC-115/abLIM controls axon pathfinding and lamellipodia and filopodia formation in cultured cells and in *C. elegans* neurons (Lundquist et al. 1998; Struckhoff and Lundquist 2003; Yang and Lundquist 2005). We show here that *unc-115* also caused defects in growth cone filopodia initiation and growth cone size, similar to *arx*.

The role of Enabled in growth cone filopodia formation has been described previously, and we found that UNC-34/Enabled affected growth cone filopodia initiation, but did not affect filopodial growth or stability once a filopodium formed. This is in contrast to previous studies that indicated that Enabled also affected filopodial elongation (Lebrand et al. 2004). In sum, our results indicate that three distinct actin modulatory molecules, Arp2/3, UNC-115/abLIM, and UNC-34/Enabled, control filopodia initiation in growth cones *in vivo* that are required for proper axon guidance

2.3 Materials and Methods

Genetic Methods. All experiments were performed at 20°C using standard *C. elegans* techniques (Brenner 1974). The following mutations and transgenic constructs were used: X: *unc-115(mn481* and *ky275), lqIs2[osm-6::gfp), mig-2(mu28)*; I: *arx-7(ok1118), hT2[bli-4(e937) let-?(q782) qIs48] (I;III), lqIs40[gcy-32::gfp];* II: *juIs76[unc-25::gfp]*; III: *arx-4(ok1093), sC1[dpy-1(s2170)]*; IV: *ced-10(n1993), lqIs3[osm-6::gfp], nT1[qIs51] (IV;V); V: arx-2(ok1269), unc-34(e951)*. The chromosomal locations of *lqIs49[gcy-32::gfp]* and *lqIs75[gcy-32::arx-7::mCherry]* were not determined. The *arx-2(+), arx-4(+),* and *arx-7(+)* whole-gene regions were maintained as extrachromosomal arrays. Extrachromosomal arrays were generated by germ line microinjection and integrated into the genome by standard techniques (Mello and Fire 1995).

arx-2, arx-4, and *arx-7* mutations were balanced by the rearrangements *nT1, sC1,* and *hT2*, respectively. *nT1* and *hT2* harbored transgenes that drove *gfp* expression in the pharynx, whereas *sC1* had no *gfp* marker. *arx-2* and *arx-7* homozygotes were identified by lack of pharyngeal GFP, whereas *arx-4* homozygotes were identified by the protruding vulva (Pvl) phenotype in young adults. *arx-4* L1 larvae were not imaged because they could not be unambiguously identified as could *arx-2* and *arx-7*. Double mutants with *ced-10* were confirmed by the gonad misrouting phenotype and by the persistent cell corpse phenotype(Reddien and Horvitz 2000), and doubles with *mig-2* were confirmed by the gonad misrouting phenotype(Zipkin et al. 1997). Double

mutants with *unc-34* and *unc-115* were confirmed by the uncoordinated phenotype of these mutants.

***arx* transgene construction.** The *arx-2, arx-4,* and *arx-7* genes were amplified by polymerase chain reaction (PCR) from wild-type N2 genomic DNA (see Figure 1). The coding regions and splice junctions were sequenced to ensure that no mutations were introduced by PCR. The sequences of all primers and amplified regions used in this work are available upon request.

For cell-specific rescue, the coding regions of *arx-4* and *arx-7* (from the initiator methionine to the stop codon) were amplified from N2 genomic DNA and placed behind the *osm-6* promoter to drive PDE expression, or the *gcy-32* promoter to drive PQR expression. For *arx-7*, the stop codon was not included, and the coding region was fused in frame to the coding region for green fluorescent protein.

Analysis of PDE axon guidance defects. As previously described, PDE axons were visualized with an *osm-6 promoter::gfp* transgene(Struckhoff and Lundquist 2003). *osm-6::gfp*, expressed in all ciliated sensory neurons including PDE, allows unambiguous identification of the PDE axon from other axons(Collet et al. 1998). A PDE axon was considered defective if the axon failed to reach the ventral nerve cord or if it reached the ventral nerve cord at a position greater than a 45^{o} angle from the PDE cell body. Young adult animals were scored, although *arx* mutants were often scored as L3 or L4 larvae. Percentages of defective PDE

axon guidance in each strain was determined, and significance was judged by a two-sided t-test with unequal variance unless otherwise noted.

Imaging and analysis of PQR dendrite development. The PQR dendrite was visualized using *gcy-32::gfp* transgenes(Yu et al. 1997). Larvae were synchronized by washing adults and larvae from a plate with many eggs and allowing the eggs to hatch. Newly-hatched larvae were washed from the plate at 0.5h intervals and allowed to develop for the following times before imaging: 6h, 6.5h, 7h, 7.5h, and 8h. Animals were imaged using a Leica DMR microscope with a Qimaging Retiga EXi camera. Z-stacks of each PQR were captured and were subject to nearest neighbor deconvolution using Openlab software.

Filopodia were defined as growth cone protrusions that were less than 0.5mm in width. The number of filopodial protrusions from the growth cone of PQR neurons at the 7-7.5h timepoint was determined by scrolling through each Z-stack of images. An average number and standard deviation of filopodial protrusions per PQR dendrite was determined, and significance of difference between genotypes was determined by a two-sided T-test with unequal variance unless otherwise noted.

The lamellipodial perimeter of the growth cone was used as an indicator of growth cone size. At the 7-7.5 h timepoint, the distal 3 microns of the tip of the PQR dendritic protrusion was traced (see Figure 6) using ImageJ software, and a value representing the perimeter of this region was derived. An average was derived from multiple tracings, and significance of difference between genotypes

was determined by a two-sided T-test with unequal variance unless otherwise noted.

Time lapse imaging of VD growth cones. VD growth cones were imaged using an *unc-25::gfp* transgene *juIs76* (Jin et al. 1999). Early L2 stage larvae were isolated by washing hatched worms off of a plate and allowing eggs to hatch for one-half hour. Newly-hatched larvae were washed off and allowed to develop at 20°C for 16 hours. Larvae with visible VD growth cones were imaged. Animals were transfered to a 2% agarose pad with a drop of 10mM muscimol (Sigma) in M9 (Weinkove et al. 2008). The drop was allowed to evaporate for 4-5 minutes before a coverslip was placed over the animals. Growth cones that were just emerging from the ventral muscle quadrant were imaged with a Leica DMR microscope with a BD CARV II wide-field light source and qImaging Rolera mGi camera at intervals of 120s. Total duration of time-lapse imaging ranged from 20-60 min.

Dynamic projections emanating from the growth cone, less than 0.5μm in width, were scored as filopodia. Filopodia length was measured using ImageJ software. Growth cone translocation speed was determined by measuring the distance from the distal tip of the lamellipodial portion of the growth cone to a fixed reference point along the axon, often a point at which the axon has crossed a lateral axon tract, which can cause a slight bulge in the axon. Significance of difference was determined by a two-sided t-test with unequal variance.

2.4 Results

Mutations in *arx-2, arx-4,* and *arx-7* cause PDE axon guidance defects. The Arp2/3 complex is composed of seven molecules, Arp2, Arp3, and ArpC1-ArpC5 (Beltzner and Pollard 2007). The *C. elegans* genome contains genes encoding each of these subunits. Deletion mutations in genes encoding three subunits were analyzed; *arx-2 Arp2, arx-4 ArpC2*, and *arx-7 ArpC5* (Figure 1). *arx-2(ok1269)* was a 1330-bp deletion that removed part of exon 4 and all of exons 5 and 6. *arx-4(ok1093)* was a 772-bp deletion that removed the 3' splice site of intron 4 and part of exon 5. *arx-7(ok1118)* was a 1352-bp deletion that removed most of exon 3 of *arx-7* (almost half of the *arx-7* coding region) and extended into the downstream gene *Y54E10BR.1*, removing exon 1 and most of intron 1. While *arx-2(ok1269)* and *arx-4(ok1093)* are predicted to affect only *arx-2* and *arx-4* respectively, *arx-7(ok1118)* might affect both *arx-7* and *Y54E10BR.1*.

From mothers heterozygous for each mutation (wild-type maternal contribution, M+), *arx-2(ok1269M+), arx-4(ok1093M+),* and *arx-7(ok1118M+)* homozygotes grew slowly and arrested as larvae or young adults. Animals that survived to adulthood were sterile and had protruding vulvae (Pvl phenotype). Most *arx-2(ok1269M+)* animals arrested before reaching adulthood in the L3 or L4 larval stage. *arx-7(ok1118)* animals arrested in L4 or early adulthood, and *arx-4(ok1093)* animals survived to adulthood but were sterile and Pvl. RNAi of

arx-2 and *arx-7* caused embryonic lethality due to defects in gastrulation as previously described (Sawa et al. 2003), indicating that *arx-2, arx-7*, and likely *arx-4* have strong maternal contributions that are sufficient for embryonic and larval development. The variation in arrest phenotype of *arx* mutants could be due to differences in maternal contribution and not distinct functions of each *arx* gene.

Axon morphology of the PDE neuron was scored in *arx* homozygous animals. The PDEs are bilateral sensory neurons in the posterior of the animal with single, unbranched axons that extend ventrally to the ventral nerve cord (VNC), where the axons bifurcate and extend anteriorly and posteriorly in the VNC (Figure 2A) (White et al. 1986). In each *arx* homozygous mutant, defects in axon guidance were observed (Figure 2B-D). *arx-2(ok1269M+)* displayed 15% PDE axon guidance defects, *arx-4(ok1093M+)* 34%, and *arx-7(ok1118M+)* 30% (Figure 2E). Defects included failure of the axon to extend straight ventrally with lateral wandering, often never reaching the VNC (Figure 2B). Mutant PDE axons sometimes bifurcated prematurely before reaching the VNC (Figure 2C). Furthermore, some axons appeared to initiate from the sides of the PDE cell body rather than the ventral surface (Figure 2D). This could reflect a defect in polarity of axon initiation or could be a consequence of growth cone misguidance. *arx* mutants did not display a high frequency of ectopic axon formation as do other mutations that also affect PDE axon guidance (e.g. *mig-2, ced-10* and *unc-115*).

To ensure that the phenotype observed in *arx* mutants was due to disruption of the *arx* gene, the entire wild-type genomic region for each locus was amplified by PCR and used in transgenic rescue experiments (see Methods). *arx-4* is the downstream gene in a *C. elegans* operon, and the entire operon region comprised of the genes *K02F3.1*, *K02F3.12*, and *Y6D11A.1* was included in the fragment. The *arx-2(+)* and *arx-4(+)*transgenes rescued the slow growth, sterility and pVul phenotype of *arx-2(ok1269)* and *arx-4(ok1093)*, respectively, and transgenic animals were viable and fertile. Furthermore, PDE axon defects were completely rescued (Figure 2E) (15% to 3% for *arx-2(ok1269M+)* and 34% to 1% for *arx-4(ok1093)*; $p < 0.0001$ for each). The *arx-7(+)* fragment rescued the slow growth and pVul components of the *arx-7(ok1118)* phenotype as well as PDE axon pathfinding defects (30% to 3%; $p < 0.0001$) (Figure 2E). However, *arx-7(ok1118); Ex[arx-7(+)]* animals were still sterile. The *arx-7(ok1118)* deletion also affected the downstream gene *Y54E10BR.1*, which was not included in the rescuing fragment. The sterility of *arx-7(ok118); Ex[arx-7(+)]* transgenic animals might be due to the effects of *ok1118* on *Y54E10BR.1*. These data indicate that the PDE axon guidance defects observed in *arx* mutants are due to mutation of the *arx* genes.

***arx-4* acts cell-autonomously in PDE axon guidance.** To determine if *arx-4* acts in neurons to control axon pathfinding, a transgene was constructed consisting of the *osm-6* promoter upstream of the *arx-4* coding region. The *osm-6* promoter is active exclusively in ciliated sensory neurons including PDE and

has no apparent activity in other tissues (Collet et al. 1998; Struckhoff and Lundquist 2003). *arx-4(ok1093M+)* animals harboring the *Posm-6::arx-4(+)* transgene were slow-growing, Pvl, and sterile, similar to *arx-4(ok1093)* homozygotes alone, confirming that the *Posm-6::arx-4(+)* transgene was not broadly active. However, PDE axon guidance defects were rescued in these animals (34% to 2%; $p < 0.0001$) (Figure 2E), suggesting that expression of *arx-4* in the PDE neurons rescued *arx-4* axon guidance defects. These results suggest that *arx-4* acts cell-autonomously in the PDE neurons in axon guidance.

***arx* mutations enhance mutations in *ced-10/Rac*, *mig-2/RhoG*.** Previous results indicated that the Rac-like molecules CED-10/Rac (Reddien and Horvitz 2000) and MIG-2/RhoG (Zipkin et al. 1997) act redundantly in axon guidance (Lundquist et al. 2001) and that the Arp2/3 activators WVE-1/WAVE and WSP-1/WASP might act in the CED-10/Rac and MIG-2/RhoG pathways, respectively (Shakir et al. 2008). The loss-of-function alleles *ced-10(n1993)* and *mig-2(mu28)* enhanced the PDE axon pathfinding defects of *arx-2(ok1269M+), arx-4(ok1093M+)*, and *arx-7(ok1118M+)* (Figure 2F). For example *ced-10(n1993); arx-4(ok1093M+)* displayed 77% PDE axon guidance defects compared to 34% for *arx-4(ok1093M+)* alone; and *mig-2(mu28); arx-7(ok1118M+)* displayed 68% compared to 30% for *arx-7(ok1118M+)* alone (for all comparisons, $p < 0.0001$). Double mutants did not exhibit ectopic axon formation as observed in *ced-10; mig-2* doubles (Lundquist et al. 2001). That each *arx* mutation was enhanced by both *ced-10(n1993)* and *mig-2(mu28)* suggests that the Arp2/3 complex might

act in both the CED-10 Rac and MIG-2 RhoG pathways in PDE axon guidance. Possibly, both WVE-1/WAVE and WSP-1/WASP pathways converge on regulation of Arp2/3 in axon guidance.

The actin-binding protein UNC-115/abLIM and UNC-34/Enabled have redundant function with Arp2/3 in axon guidance. Previous studies showed that the actin-binding protein UNC-115/abLIM acts downstream of Rac signaling in axon guidance (Struckhoff and Lundquist 2003), raising the possibility that Rac signaling employs multiple actin-modulating pathways in axon guidance (UNC-115/abLIM and Arp2/3). Indeed, *unc-115* mutations enhanced PDE guidance defects of *arx* mutants (Figure 2G). For example, *unc-115(ky275); arx-2(ok1269M+)* displayed 83% PDE axon guidance defects compared to 15% for *arx-2(ok1269M+)* alone (p values for all differences < 0.0001). Double mutants did not display enhanced ectopic axon formation as observed in double mutants of *unc-115* with *ced-10* and *mig-2*. That *unc-115* mutations enhanced PDE axon guidance defects of *arx* mutations indicates that UNC-115/abLIM acts in parallel to Arp2/3 in PDE axon guidance, a result consistent with the idea that Rac GTPases employ both Arp2/3 and UNC-115/abLIM.

Previous studies showed that UNC-115/abLIM and UNC-34/Enabled had redundant roles in PDE axon guidance (Shakir et al. 2006). As predicted by this result, UNC-34/Enabled and Arp2/3 also had parallel function in PDE axon guidance (Figure 2G). Alone, loss-of-function *unc-34(e951)* mutants displayed 8% PDE guidance defects. *unc-34(e951); arx-4(ok1093)* and *unc-34(e951); arx-*

7(ok1118M+) displayed 91% and 97% PDE guidance defects compared to 35% and 35% for the *arx* mutants alone (for each comparison, $p < 0.0001$). Together, these data indicate that Arp2/3, UNC-115/abLIM, and UNC-34/Enabled all act redundantly to control PDE axon guidance.

Ezrin/radixin/moesin (ERM) proteins are regulators of actin organization and interaction with the plasma membrane. The *C. elegans* genome encodes one molecule similar to ezrin, radixin, and moesin called ERM-1. *erm-1(tm677)* is an out-of-frame deletion of the locus (Figure 1) that causes maternal-effect lethality (i.e. homozygotes from a heterozygous mother survive until adulthood). RNAi of *erm-1* results in disrupted morphogenesis of the gut lumen (Gobel et al. 2004; Van Furden et al. 2004). We found that *erm-1(tm677M+)* animals displayed weak but significant defects in PDE axon guidance (9%; Figure 3). Double mutants of *erm-1(tm677M+)* with *unc-115(ky275)* and *unc-34(e951)* displayed PDE axon guidance defects that were not significantly different from the singles alone. These results indicate that ERM-1 has a role in PDE axon guidance but does not act redundantly with UNC-115 and UNC-34. Thus, the synergistic enhancement of *arx* mutants by *unc-34* and *unc-115* is not likely due to general actin cytoskeletal disruption. Rather, these results suggest that the genetic interaction is specific and that Arp2/3, UNC-115, and UNC-34 might act in a common process in axon guidance not affected by ERM-1.

Development of the posterior PQR neurite involves a growth-cone like structure with filopodia. Mutations in *arx* genes caused axon guidance

defects, but the effect of *arx* mutations on the growth cone during neurite extension was unclear. Developing neurites in *arx* mutants were analyzed. Transgenes used to assay PDE axon morphology were not visibly expressed early in PDE development during axon extension, including *osm-6::gfp* (Collet et al. 1998) and *cat-1::gfp* (Duerr et al. 1999). Therefore, the development of a distinct neurite was examined. A *gcy-32::gfp* reporter (Yu et al. 1997) was used to analyze outgrowth of the posterior PQR neurite, which develops into a ciliated sensory dendrite (White et al. 1986).

The PQR neuron, a descendant of the QL neuroblast, is born in the posterior of the L1 larva and migrates to its final position in the tail near the phasmid ganglia (Sulston and Horvitz 1977). At 6.5 hours after hatching, the PQR cell body had reached its final position and differentiation began. At this time, *gcy-32::gfp* expression was evident, revealing a large, wedge-shaped cell body with multiple finger-like filopodial protrusions emanating from around the cell body (Figure 4A). From 6.5 to 7 h, posterior PQR protrusions were oriented to the dorsal-posterior and appeared as thickened, foot-like structures with smaller filopodial extensions (Figure 4B). From 7 to 7.5 h, posterior extensions thinned into neurite-like structures with distal growth cones and multiple filopodial protrusions (Figure 4C). Filopodia also protruded along the lengths of the neurites. Also at this time, the cell bodies of the PQR neurons began to resemble a typical neuronal cell body: they became smaller in size and oval-shaped with fewer filopodial extensions. From 7.5 to 8 h, the neurites were thin and the growth cones at their tips continued to extend (Figure 5D). Filopodial

extensions became mostly restricted to the distal growth cone at this time. By 8.5 h, the neurites had extended completely and the growth cone-like structures were no longer evident. In broad terms, PQR dendritic extension involved initial dorsal-posterior protrusion, consolidation of the protrusion into a neurite with a growth cone, and growth cone extension. This is similar to growth cone advance observed in cultured neurons, which includes a period of growth cone swelling (engorgement) followed by a narrowing and consolidation of the proximal growth cone to form the new axon shaft (Goldberg and Burmeister 1986).

The finger-like extensions on PQR growth cones resembled filopodia. In many systems, including cultured cells and neurons and *C. elegans* neurons (Chang et al. 2006; Drees and Gertler 2008), Enabled activity is required for the formation of filopodia. To confirm that the finger-like protrusions that emanated from the PQR dendrite were filopodia, we determined if they were affected by mutation in *unc-34/Enabled*. Indeed, in *unc-34(e951)* mutants at 7-8 h post-hatching, the average number of finger-like extensions on PQR dendrites (defined as having a thickness of 0.5mm or less) was reduced significantly compared to wild-type (Figure 4I and Figure 6; 4.89 compared to1.48, $p < 0.0001$). That these finger-like protrusions were affected by *unc-34/Enabled* suggests that they are *bona fide* filopodia.

***arx* mutants affect PQR growth cone morphology and filopodia formation.** Posterior PQR neurite extension was assessed in *arx-2(ok1269M+)* and *arx-7(ok1118M+)* living larvae expressing *gcy-32::gfp*. These larvae exhibited a

general growth delay, and timing of PQR dendritic events were slowed by approximately one-half hour. At 7 h, initial wedge-like cell shape with filopodia appeared normal in *arx-2* and *arx-7* mutants (Figure 4E). From 7 to 7.5 hours, *arx-2* and *arx-7* extended dorsal-posterior-foot-like structures. However, these protrusions displayed fewer filopodial extensions than wild-type (Figure 4F). Neurite consolidation appeared normal in *arx-2* and *arx-7*, but from 7.5 to 8.5 hours, the growth cones at the distal tip displayed fewer filopodia (Figure 4G and H). Furthermore, fewer filopodia were evident along the length of the neurites. The posterior protrusions and growth cones of *arx-2* and *arx-7* mutants often appeared thinner and less ramified than in wild-type, possibly indicating a growth cone lamellipodial defect as well (see Figure 5 for additional representative images of wild-type and *arx-7(ok1118M+)* growth cones).

The number of filopodia on the growth cones and neurites of wild-type (7-8 h), *arx-2(ok1269M+)*, and *arx-7(ok1118M+)* (7.5-8.5 h) were counted (see Figure 6A and Methods). Wild-type displayed an average of 4.89 filopodia per neurite whereas *arx-2(ok1269M+)* displayed 2.27 and *arx-7(ok1118M+)* 1.78 ($p < 0.0001$ for each) (Figure 6B).

As mentioned previously, the growth cones of *arx* mutants often appeared less robust and smaller in size than wild-type. To quantify this defect, the perimeters of growth cones (excluding filopodia) from wild type and mutant backgrounds were traced (see Figure 6A and Methods). The growth cone was defined as the widened region at the tip of the neurite, starting at 3mm from the distal growth cone tip. Wild-type growth cones displayed an average perimeter

of 7.96±0.91mm (Figure 6C). *arx-7* displayed a significantly reduced average growth perimeter (6.77±0.51mm; $p < 0.001$).

To determine if these growth cone defects resulted in neurite guidance defects, we scored the final morphology of the PQR dendrites after outgrowth. Initial posterior protrusion, axon consolidation, and outgrowth of the neurite to its normal position in the tail were generally normal in *arx* mutants. However, PQR dendrites did not extend directly to the posterior as in wild-type (Figure 7A). Rather, the dendrites displayed multiple turns, resulting in an undulating dendrite appearance (Figure 7B and C) (45% in *arx-7* compared to 19% in wild-type). These data indicate that *arx-7(ok1118M+)* affects the guidance of the PQR dendrite.

***arx-7* acts cell-autonomously in PQR filopodia regulation.** A transgene consisting of the *gcy-32* promoter driving *arx-7* tagged with coding region for green fluorescent protein was constructed. This transgene was predicted to express full-length ARX-7 with GFP at the C terminus. Animals harboring this transgene showed ARX-7::GFP fluorescence in the URX, AQR, and PQR neurons and nowhere else (data not shown). *arx-7(ok1118M+)* animals harboring this transgene displayed the gross phenotype of *arx-7(ok1118M+)* alone (arrested larvae and sterile, Pvl adults) indicating that *arx-7(+)* activity was not widely provided by the *Pgcy-32::arx-7::gfp* transgene. However, this transgene rescued filopodia formation to wild-type levels in *arx-7(ok1118M+)* PQR neurites (Figure 6B): an average of 5.1 filopodia per neurite compared to

1.78 for *arx-7(ok1118M+)* alone ($p < 0.0001$). *arx-7* rescue was not significantly different than wild-type (5.1 versus 4.89; $p = 0.71$). These data indicate that *arx-7* acts cell-autonomously in the regulation of growth cone filopodia.

unc-115/abLIM* mutation enhanced PQR filopodia defects of *arx-2* and *arx-7. As reported above, *unc-115* mutations enhanced PDE axon guidance defects of *arx-2, arx-4*, and *arx-7*, indicating redundancy of function in PDE axon guidance. The effect of *unc-115* on PQR posterior neurite extension was examined. Alone, *unc-115(ky275)*, a null allele, displayed no defects in PQR posterior neurite filopodia formation (e.g. 4.61 filopodia versus 4.89 for wild-type ($p = 0.51$)) (Figure 6B). However, *unc-115(ky275)* enhanced filopodia defects of *arx-2(ok1269M+)* and *arx-7(ok1118M+)*. *unc-115(ky275); arx-2(ok1269M+)* displayed 1.22 filopodia per neurite compared to 2.27 for *arx-2(ok1269M+)* alone ($p = 0.003$), and *unc-115(ky275); arx-7(ok1118M+)* displayed 1.04 compared to 1.78 for *arx-7(ok1118M+)* alone ($p = 0.007$).

unc-115(ky275) mutants also displayed a reduced growth cone perimeter (Figure 6C) (6.52±0.57mm compared to 7.96±0.91mm for wild-type; $p < 0.001$), indicating that UNC-115 might be involved in growth cone lamellipodium regulation. As opposed to *arx* mutants, *unc-115(ky275)* did not display PQR dendrite guidance defects (the undulating dendrite), and the dendrite reached its normal final position (Figure 7C). Alone, *unc-115(ky275)* had no affect on filopodia, possibly explaining the lack of PQR dendritic guidance defects in this mutant.

unc-115; arx double mutants displayed a defect not seen in *unc-115, arx-2,*or *arx-7* single mutants, a rudimentary or absent posterior PQR neurite (Figure 4J and K): 12/70 PQR neurons from *unc-115(ky275); arx-2(ok1269M+)* and 9/75 *unc-115(ky275); arx-7(ok1118M+)* animals lacked a significant posterior protrusion. Some animals showed a rudimentary posterior protrusion (Figure 4J) whereas other showed no posterior neurite (Figure 4K). These observations suggest that in addition to being required for filopodia formation, the Arp2/3 complex and UNC-115/abLIM might also redundantly control neurite initiation or the ability of a neurite to form and extend.

***unc-34/Enabled* affects filopodia but not growth cone perimeter.** As previously observed in the HSN neuron (Chang et al. 2006), *unc-34(e951)* mutants displayed severely reduced filopodia-like protrusions on the PQR dendritic neurite (Figure 4I and Figure 6; 1.48, $p < 0.0001$). That *unc-34* affected these thin, filopodia-like protrusions supports the notion that they are *bona fide* filopodia, as Enabled molecules have been shown to control filopodia formation in many systems, including *C. elegans* neurons (Chang et al. 2006; Drees and Gertler 2008). *arx-7(ok1118M+); unc-34(e951)* displayed significantly fewer filopodia than each single alone, but an additive effect of the two mutations combined could not be excluded (Figure 6B). Some *arx-7(ok1118M+); unc-34(e951)* double mutants lacked a strong posterior neurite from PQR (2/17), similar to *arx; unc-115* double mutants, suggesting that UNC-34/Enabled and the Arp2/3 complex might control the ability of a neurite to form or to extend. *unc-34*

mutants did not display a reduction in PQR growth cone perimeter (7.78±0.9mm compared to 7.96±0.91mm for wild-type; p = 0.387) (Figure 6C).

These data indicate that Arp2/3 and UNC-115 affect both growth cone filopodia and growth cone perimeter, which might reflect lamellipodial protrusion. In contrast, *unc-34* affected only growth cone filopodia but not growth cone perimeter. Thus, growth cone perimeter and number of filopodia are at least partially-independent processes. For example, *unc-115* alone affected growth cone perimeter but not filopodia, and *unc-34* affected filopodia but not growth cone size. These results indicate that the filopodial defects seen in *arx* mutants might be a specific defect in filopodia and are unliekly to simply be a secondary effect of reduced lamellipodial protrusion.

ARX-7, UNC-115/abLIM, and UNC-34 affect filopodia initiation but not duration or length. The effects of Arp2/3, UNC-115, and UNC-34 on PQR growth cone filopodia formation could be due to decreased filopodial stability or half-life, or could be due to a decrease in the rate of filopodial initiation. We imaged growth cones from wild-type and mutants over time to assess the dynamic effects of these mutations of filopodia formation. The commissural growth cones of the VD motor axons have been used in previous time-lapse studies (Knobel et al. 1999; Weinkove et al. 2008). The VD axons begin extension during the L1/L2 larval molt and continue to extend early in the second larval stage. As the VD commissural growth cones emerge dorsally after transversing the ventral muscle quadrant, they display a spread appearance with

multiple dynamic filopodial extensions (Knobel et al. 1999). Until the growth cones reach the dorsal muscle quadrant, they generally retain a spread morphology with multiple filopodial extensions ((Knobel et al. 1999) and our observations).

To understand the roles of Arp2/3 and UNC-115 in filopodia formation, we imaged VD growth cones as they migrated between the ventral and dorsal muscle quadrants. In wild-type, the VD growth cones displayed dynamic extension and retraction of lamellipodia-like and filopodia-like projections (Figure 8A). In *arx-7, unc-115* and *unc-34* mutants, VD growth cone dynamics appeared generally reduced, and the growth cones displayed a less ramified appearance (Figure 8B-D). Notably, fewer filopodia were observed on the growth cones of mutants, consistent with results in PQR.

Reduced steady-state filopodia number could be due to a defect in filopodia initiation or filopodia stability or duration. We tracked the emergence and dynamics of multiple individual filopodial from multiple growth cones over time (Figure 9A). This analysis revealed that that in wild-type, filopodia had an initiation rate of 0.26 filopodia/minute (approximately one new filopodium initiated every four minutes) (Figure 9B). Filopodia initiation rate was significantly reduced in *arx-7, unc-115,* and *unc-34* mutants (Figure 9B): *arx-7*: 0.16/minute, *unc-115*: 0.17/minute, and *unc-34*: 0.07/minute. Filopodia did occasionally form in these mutants, and we measured their duration time and maximal length. We found no significant difference between wild-type or any of these mutants in filopodial duration (4-5.5 minutes) (Figure 9C) or maximal filopodial length (0.8-1

mm) (Figure 9D). These data indicate that *arx-7*, *unc-115*, and *unc-34* primarily affected the rate of filopodia initiation but did not affect the duration or maximal length of filopodia once they had formed. However, we cannot rule out the possibility that some filopodia initiate but abort before they are detectable in our assay.

We also determined the average translocation rates of wild-type and mutant growth cones (see Methods and Table 1). Wild-type had a translocation rate of 7.38mm/h. This rate is consistent with what has been observed previously for VD growth cones in mounted and anaesthetized larvae (4-8.7 mm/h) (Knobel et al. 1999). *arx-7* and *unc-34* had significantly reduced growth cone translocation rate. *arx-7* had a translocation rate of 4.08mm/h and *unc-34* had 3.84mm/h (Table 1). *unc-115* did not have a significantly reduced translocation rate (7.02mm/h). Variability in translocation rate in each genotype including wild-type was very high, making it difficult to assign a direct effect on growth cone morphology to translocation rate. For example, *unc-115* affected filopodia to the same extent as *arx-7* but did not affect translocation rate. It is possible, however, that these mutants have distinct effects on growth cones aside from filopodia that were not assayed in these studies.

unc-115 and *unc-34* have been shown previously to have VD/DD axon guidance defects (Lundquist et al. 1998; Shakir et al. 2006; Withee et al. 2004). *arx-7* mutants also displayed VD/DD pathfinding defects (compare Figures 10A and B). In *arx-7*, VD and DD axons wandered laterally and crossed other commissural axons in 77% (n=40) of animals (Figure 10C). All *arx-7* VD/DD

axons reached the dorsal nerve cord. Such crossings were occasionally observed in wild-type (38%, n=100), but occured at a significantly higher rate in *arx-7* ($p < 0.0001$). While the penetrance of axon guidance defects of *arx-7, unc-115*, and *unc-34* were similar (Figure 10C), the misguided axons in *arx-7* always reached the dorsal cord, whereas misguided *unc-115* and *unc-34* axons wandered laterally, terminated prematurely, and sometimes failed to reach the dorsal nerve cord (Lundquist et al. 1998; Shakir et al. 2006). The filopodia defects of *arx-7* were as severe as those of *unc-34* and *unc-115*, suggesting that *unc-115* and *unc-34* might have other, non-filopodial roles in axon guidance not shared by *arx-7*.

2.5 Discussion

The Arp2/3 complex controls growth cone size and filopodia formation *in vivo*. The results presented here show that the Arp2/3 complex is required for the initiation of growth cone filopodia of *C. elegans* neurons *in vivo*. The role of Arp2/3 in growth cone morphology has been controversial, based on studies in cultured neurons. Some studies concluded that Arp2/3 was not involved in growth cone filopodia formation (Pinyol et al. 2007; Strasser et al. 2004), while another demonstrated a role for Arp2/3 in growth cone filopodia formation (Korobova and Svitkina 2008). Our results presented here clearly demonstrate that Arp2/3 is required for growth cone filopodia formation *n vivo*. The previous study that found no role of Arp2/3 in cultured hippocampal growth cone filopodia formation used expression of a dominant negative WAVE construct to inhibit Arp2/3 (Strasser et al. 2004), whereas the study that found an effect of Arp2/3 in hippocampal growth cones used siRNA knockdown of the p34-Arc subunit of the Arp2/3 complex (Korobova and Svitkina 2008). Possibly, the dominant-negative WAVE construct did not inhibit Arp2/3 as well as siRNA. In any case, our studies of *C. elegans* growth cones *in vivo* demonstrate that Arp2/3 is a key regulator of growth cone filopodia formation.

A previous study using cultured hippocampal neurons (Korobova and Svitkina 2008) showed that Arp2/3 was present in the growth cone at branch points of actin filaments as observed in other cell types, and filaments with Arp2/3 at their base contributed to filopodial bundles, suggesting that Arp2/3 provides a source of actin filaments for filopodial formation (Korobova and

Svitkina 2008). The nature of the growth cone cytoskeletal defects in *arx* mutant growth cones is difficult to discern, as the growth cones are very small compared to those of cultured hippocampal neurons (< 5mm in diameter compared to ~20mm for cultured hippocampal neurons). However, it is possible that there is reduced nucleation of lamellipodial actin filaments in *arx-7* mutant growth cones resulting in less availability of lamellipodial actin filaments to contribute to filopodial bundles. This idea is consistent with the time-lapse analysis of growth cone filopodia, which showed that *arx* mutants had reduced filopodial initiation rates compared to wild-type (Figure 9). *arx-7* mutant PQR growth cones also displayed a reduction in the size of the growth cone (Figures 4, 5, and 6), consistent with a role of Arp2/3 in the nucleation of growth cone lamellipodial actin filaments. Interestingly, once filopodia formed in *arx*-7 mutants, they had characteristics similar to wild-type, including time of persistence/stability and maximal length. Thus, the Arp2/3 complex might primarily affect the initiation of filopodia and have little role in filopodial stability of extension once a filopodium has initiated. However, we cannot rule out the possibility that filopodia initiate and collapse before they are visible as filopodia in our imaging assays.

The Arp2/3 complex is required for axon guidance. As a growth cone navigates its environment, filopodia are thought to act as sensors of extracellular cues and have a role in guiding the growth cone (Davenport et al. 1993; Dent et al. 2003). Consistent with this idea, we found that *arx* mutants have defects in the guidance of the PDE and VD/DD axons and of the PQR dendrite. Reduction

of filopodia on *arx* mutant growth cones might lead to growth cone guidance defects. However, *arx* axon guidance defects were incompletely penetrant (e.g. 15-34% for the PDEs). This could be due to the action of the remaining few filopodia on *arx* mtant growth cones or could be due to lamellipodial guidance. Indeed, *unc-34/Enabled* mutants lack most or all growth cone filopodia but have relatively weak effects on axon guidance (Chang et al. 2006; Shakir et al. 2006; Withee et al. 2004) (and this work).

Rac GTPases are thought to regulate Arp2/3 activity via the WAVE family of Arp2/3 activators: WAVE is present in a complex with Sra-1 and kette, and Rac-GTP binding to Sra-1 activates WAVE and thus Arp2/3(Eden et al. 2002; Innocenti et al. 2004). Previous studies showed that in *C. elegans* PDE axon guidance, CED-10 Rac acts with WVE-1/WAVE, and that MIG-2/RhoG acts with the WSP-1/WASP molecule, a member of the WASP family of Arp2/3 activators (Shakir et al. 2008). Shown here is that PDE axon guidance defects of *arx* mutations were enhanced by both *ced-10* and *mig-2*, consistent with a role of both CED-10/Rac and MIG-2/RhoG in the Arp2/3 pathway (Figure 11). CED-10/Rac might also control UNC-115/abLIM (Struckhoff and Lundquist 2003), explaining the enhancement of *arx* mutations by *ced-10*.

UNC-115/abLIM controls growth cone size and filopodia formation. As mentioned above, the weak axon guidance defects of *arx* mutants could be explained by the lamellipodial guidance or by the activity of the remaining few filopodia on mutant growth cones, presumably formed by Arp2/3-independent

mechanisms. UNC-115/abLIM has previously been implicated in axon pathfinding, but the role of the molecule in regulation of growth cone dynamics and morphology during outgrowth had not been demonstrated. We found that UNC-115/abLIM also affected the formation of growth cone filopodia. While *unc-115* displayed no significant reduction of filopodia on PQR growth cones, it did enhance filopodia defects of *arx-7.* Furthermore, *unc-115* displayed reduced filopodia initiation rate on VD/DD growth cones. These data indicate that UNC-115/abLIM is also a regulator of filopodia initiation similar to Arp2/3. That *unc-115/abLIM* mutants alone have defects in VD filopodia but not PQR filopodia suggests that different neurons have distinct requirements for UNC-115/abLIM in growth cone filopodia formation. This could be due to different guidance signals detected by these neurons that trigger distinct downstream signal transduction pathways, resulting in different requirements for UNC-115/abLIM.

UNC-115/abLIM binds to actin filaments via the C-terminal villin headpiece domain (VHD), and promotes the formation of lamellipodia and filopodia in *C. elegans* neurons and cultured fibroblasts (Struckhoff and Lundquist 2003; Yang and Lundquist 2005). UNC-115/abLIM might act as a bundling protein in filopodial bundles, or it might produce new actin filaments for use in filopodia, similar to Arp2/3. Indeed, the villin headpiece domain from human villin can nucleate actin polymerization (Friederich et al. 1992), but this activity has not been described for UNC-115/abLIM. Our results here suggest that UNC-115/abLIM might also have a role in lamelliopodia organization similar to Arp2/3, as *unc-115* mutants also displayed reduced PQR growth cone size.

UNC-34/Enabled affects filopodia formation without affecting growth cone morphology. Enabled has been extensively implicated in filopodia formation, including on growth cones, and our results that *unc-34* mutant growth cones had reduced filopodia numbers confirm this role of Enabled. In time-lapse studies, we found that *unc-34* affected the rate of filopodia formation, suggesting that Enabled controls filopodia initiation similar to Arp2/3 and UNC-115/abLIM. This is similar to previous results in cultured neurons in response to netrin (Lebrand et al. 2004). We found that *unc-34* had no effect on filopodia stability or length once a rare filopodium formed, indicating that UNC-34 has no role in filopodia outgrowth or stability. This is in contrast to cultured neurons, where Ena/VASP inhibition also resulted in filopodia extension defects (Lebrand et al. 2004).

In contrast to *arx-7* and *unc-115* mutants, *unc-34* mutant PQR growth cones, while nearly devoid of filopodia, displayed no significant reduction in size. While all three mutations caused reduced filopodia initiation, this difference might hint at distinct mechanisms of action of these molecules. Possibly, Arp2/3 and UNC-115/abLIM primarily affect lamellipodial actin organization such that filaments are less available for filopodia formation in mutants. In contrast, UNC-34/Enabled had a filopodia specific effect, consistent with the role of Ena/VASP molecules as actin anti-capping proteins. It is surprising that *unc-34* had little or no effect on stability or length of the few filopodia that did form in these mutants. Possibly, the anti-capping activity of UNC-34/Enabled is required only during initiation and other proteins can serve its function during elongation. It is also

possible that filopodial initiation requires other actin-interacting properties of Enabled that have been described recently (e.g. filament nucleation or bundling) (Applewhite et al. 2007; Bear and Gertler 2009).

Arp2/3, UNC-115/abLIM, and UNC-34/Enabled act together in axon guidance. Our results indicate that Arp2/3, UNC-115/abLIM, and UNC-34/Enabled are required for growth cone filopodia formation. However, the effects of these mutations on PDE and VD/DD axon guidance and PQR dendritic guidance were incompletely penetrant. Strikingly, double mutants of *arx* with *unc-115* and *unc-34* displayed greatly enhanced PDE axon guidance defects, and previous studies showed that *unc-34* and *unc-115* had overlapping roles in PDE axon guidance. Possibly, perturbing multiple actin modulating molecules had general, nonspecific effects on the cytoskeleton resulting in increased defects. We think this is not the case as these interactions were specific. *erm-1* encodes the sole member of the ezrin/radixin/moesin family of actin-membrane linking proteins, *erm-1* mutation caused weak guidance defects on its own, indicating that ERM- is required for axon guidance. However, *erm-1* did not enhance *unc-115* or *unc-34*, suggesting that the enhancement of *arx, unc-115*, and *unc-34* is specific to these genes and is not the result of general cytoskeletal disruption.

Together, our data indicate that Arp2/3, UNC-115/abLIM, and UNC34/Enabled might act in a common process in axon guidance, namely in the initiation of growth cone filopodia (Figure 11). Indeed, *unc-115* and *unc-34*

enhanced the PQR filopodia defects of *arx-7*, although the enhancement by *unc-34* might simply be an additive effect because *unc-34* mutants alone display severely reduced filopodia numbers. It is also possible that all three molecules affect filopodia formation and have redundant roles in other aspects of growth cone morphology. Indeed, this seems to be the case, as both *unc-115; arx* and *unc-34; arx* doubles displayed severe PQR neurite outgrowth and formation defects. This is surprising for *unc-34/Enabled*, as Ena/VASP molecules were traditionally considered to be anti-capping proteins with specific effects on filopodia. However, recent studies have suggested that Ena/VASP molecules have other effects on actin, including bundling and nucleation (Bear and Gertler 2009), have anti-capping-independent roles in filopodia formation (Applewhite et al. 2007) and control the initiation of neurites in the mammalian central nervous system (Dent et al. 2007; Kwiatkowski et al. 2007). Possibly these other roles of UNC-34/Enabled explain the severe defects in neurite formation in *unc-34; arx* double mutants.

Many molecules have been implicated in axon guidance through genetic, molecular, and biochemical studies. The effects of these molecules on the behavior and dynamics of the growth cone during axon guidance are unclear in many cases. Through a combination of genetic analysis and time-lapse imaging of growth cones during outgrowth, we show that the Arp2/3 complex acts cell autonomously in the initiation of new growth cone filopodia during growth cone outgrowth, possibly explaining the axon guidance defects observed in *arx*

mutants. We show that two other actin modulatory molecules, UNC-115/abLIM and UNC-34/Enabled, also affect growth cone filopodia initiation, which might explain the genetic redundancy of Arp2/3, UNC-115/abLIM, and UNC-34/Enabled in axon guidance. Arp2/3 and UNC-115/abLIM, but not UNC-34/Enabled, also affect the size of the growth cone, possibly reflecting a role in the formation of growth cone lamellipodium. Thus, multiple actin regulatory molecules have shared roles (filopodia initiation) and distinct roles (lamellipodia formation) in the growth cone during axon outgrowth.

Figure 2.1

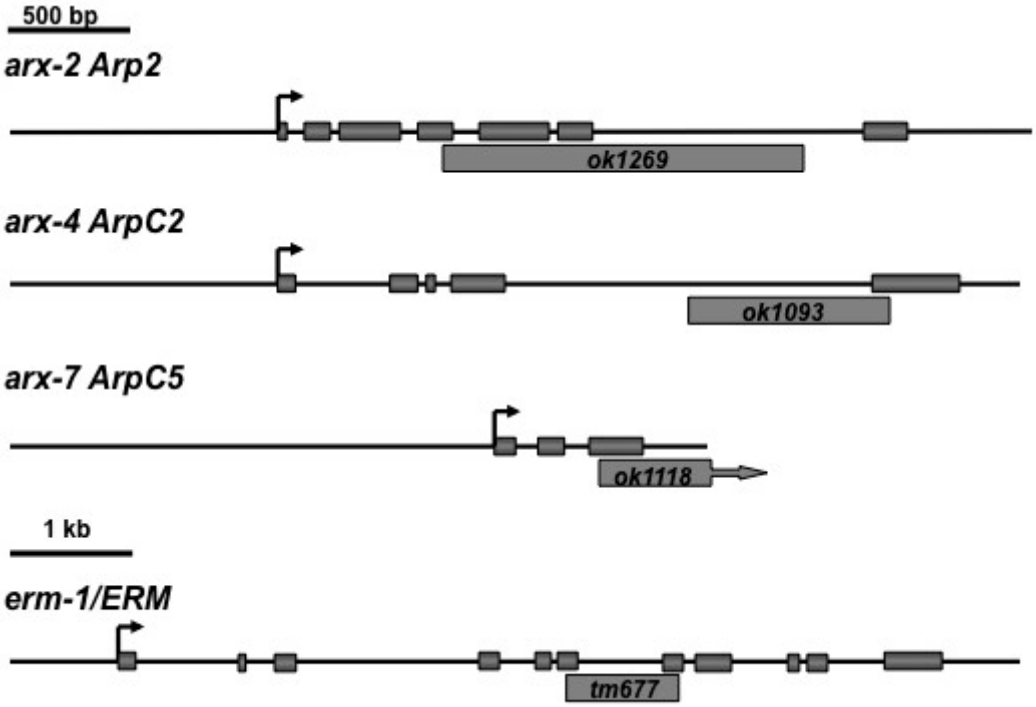
500 bp
arx-2 Arp2
ok1269
arx-4 ArpC2
ok1093
arx-7 ArpC5
ok1118
1 kb
erm-1/ERM
tm677

Figure 2.1. Mutations in *arx-2, arx-4*, *arx-7,* and *erm-1*. The structures of the *arx-2, arx-4, arx-7*, and *erm-1* genes are shown. Filled boxes represent exons; arrows represent translational start sites in putative cDNAs; and 5' is to the left. The extent of deletions in each of the genes is shown below the structure. The *arx-7(ok1118)* deletion extends into the gene to the 3' of *arx-7*.

Figure 2.2

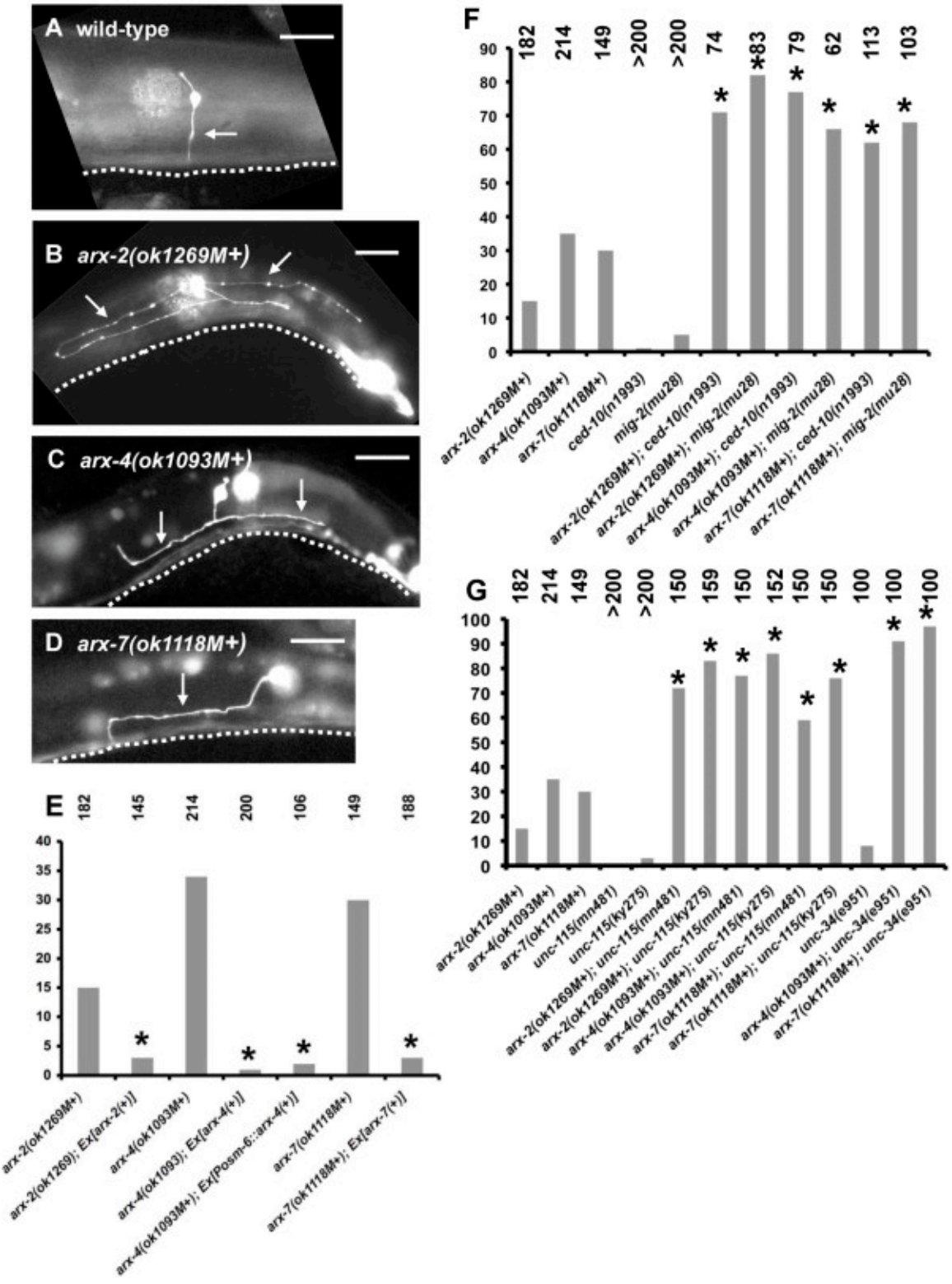
A wild-type
B arx-2(ok1269M+)
C arx-4(ok1093M+)
D arx-7(ok1118M+)
E
182 145 214 200 106 149 188
arx-2(ok1269M+)
arx-2(ok1269); Ex[arx-2(+)]
arx-4(ok1093M+)
arx-4(ok1093); Ex[arx-4(+)]
arx-4(ok1093M+); Ex[Posm-6::arx-4(+)]
arx-7(ok1118M+)
arx-7(ok1118M+); Ex[arx-7(+)]
F
182 214 149 >200 >200 74 *83 * 79 62 113 103
arx-2(ok1269M+)
arx-4(ok1093M+)
arx-7(ok1118M+)
ced-10(n1993)
mig-2(mu28)
arx-2(ok1269M+); ced-10(n1993)
arx-2(ok1269M+); mig-2(mu28)
arx-4(ok1093M+); ced-10(n1993)
arx-4(ok1093M+); mig-2(mu28)
arx-7(ok1118M+); ced-10(n1993)
arx-7(ok1118M+); mig-2(mu28)
G
182 214 149 >200 >200 150 159 150 152 150 150 100 100 *100
arx-2(ok1269M+)
arx-4(ok1093M+)
arx-7(ok1118M+)
unc-115(mn481)
unc-115(ky275)
arx-2(ok1269M+); unc-115(mn481)
arx-2(ok1269M+); unc-115(ky275)
arx-4(ok1093M+); unc-115(mn481)
arx-4(ok1093M+); unc-115(ky275)
arx-7(ok1118M+); unc-115(mn481)
arx-7(ok1118M+); unc-115(ky275)
unc-34(e951)
arx-4(ok1093M+); unc-34(e951)
arx-7(ok1118M+); unc-34(e951)

Figure 2.2. PDE axon pathfinding defects in *arx* mutants. (A-D) Shown are fluorescent micrographs of larval or young adult animals with *osm-6::gfp* expression in the PDE neurons. (A) A wild-type PDE neuron extended a single unbranched axon (arrow) straight ventrally to the ventral nerve cord (VNC), which is out of focus but represented by a dashed line. (B-D) PDE axons were misguided in *arx-2, arx-4*, and *arx-7* mutants. The axons failed to reach the VNC and wandered laterally (B and C) or wandered laterally before extending to the VNC (D). In all micrographs, anterior is to the left and dorsal is up; dashed lines represent the location of the out-of-focus VNC, and scale bars = 10mm. In genotypes, "M+" denotes that the animal had wild-type maternal *arx* contribution. (E-G) Quantitation of PDE axon guidance defects. Genotypes are along the X axis, and proportion of misguided PDE axons is the Y axis. The numbers of PDE axons scored for each genotype is listed above the graph. In (E), *Ex[arx(+)]* indicates that the animals harbored a wild-type *arx(+)* transgene, and *Ex[Posm-6::arx-4]* indicates that the animals harbored a transgene that expressed the *arx-4(+)* gene specifically in the PDEs. The differences between *arx* mutants alone and those harboring transgenes were significant in all cases ($p \leq 0.0001$; indicated by an asterisk).

Figure 2.3

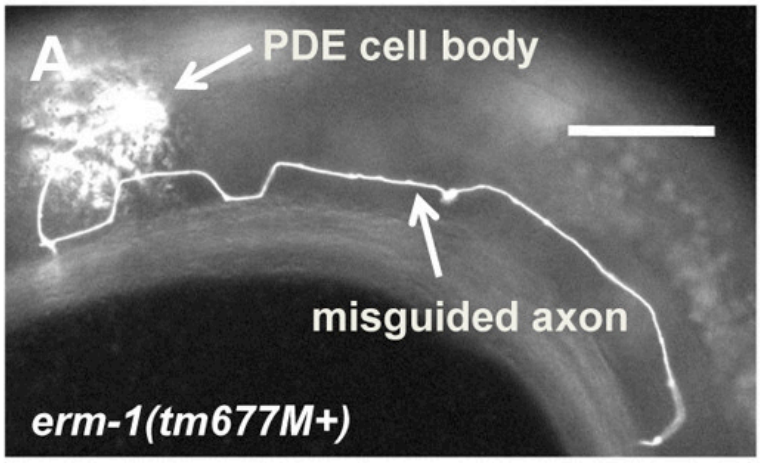
A
PDE cell body
misguided axon
erm-1(tm677M+)

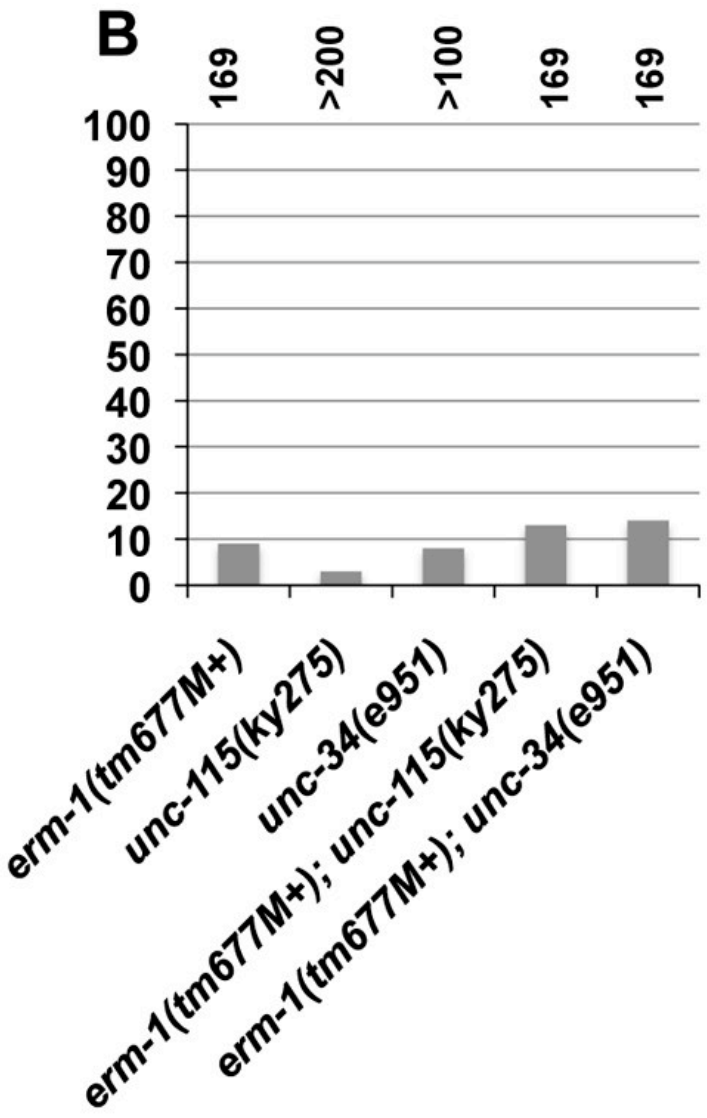
B
169
>200
>100
169
169
100
90
80
70
60
50
40
30
20
10
0
erm-1(tm677M+)
unc-115(ky275)
unc-34(e951)
erm-1(tm677M+); unc-115(ky275)
erm-1(tm677M+); unc-34(e951)

Figure 2.3. PDE axon guidance defects in *erm-1(ok677M+)* and double mutants. (A) A micrograph of a misguided PDE axon in *erm-1(tm677M+)*. The scale bar represents 10mm. (B) Quantitation of PDE axon guidance defects as described in Figure 2.

Figure 2.4

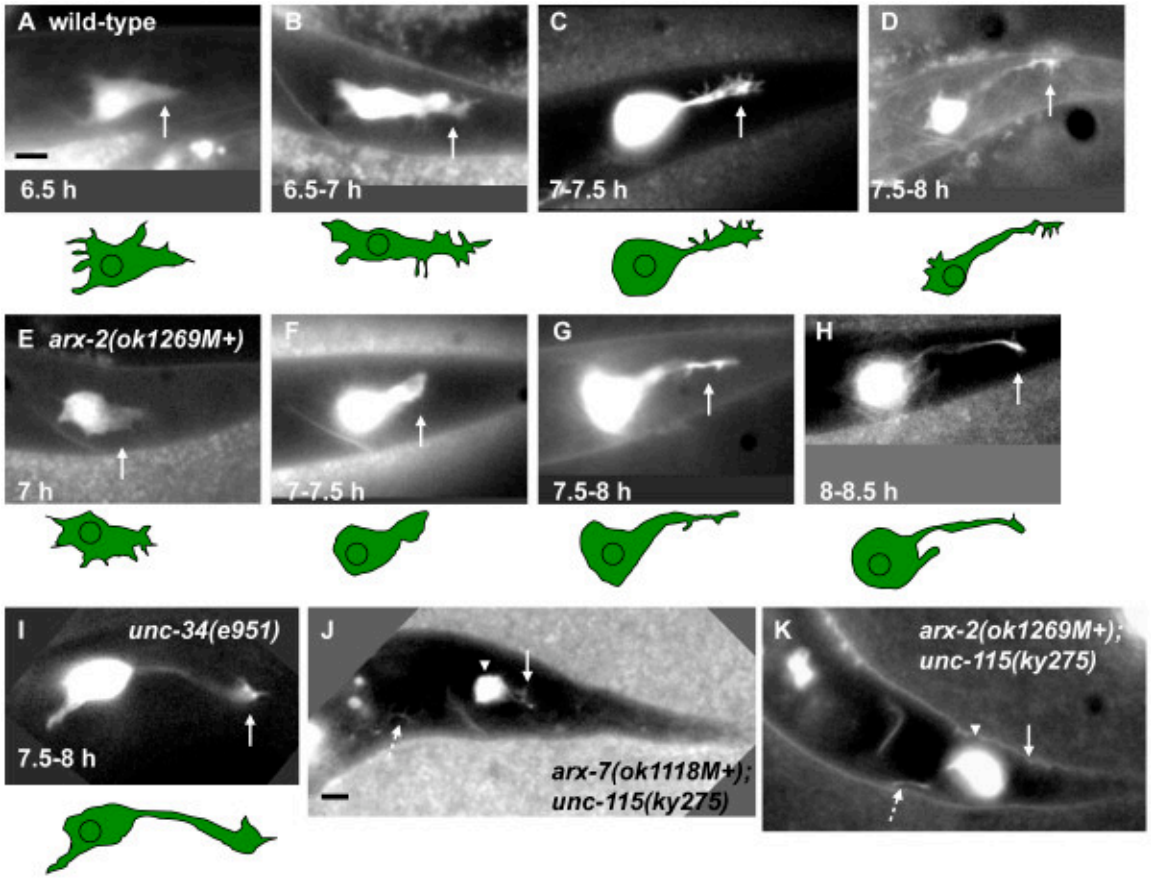
A wild-type
6.5 h
B
6.5-7 h
C
7-7.5 h
D
7.5-8 h
E arx-2(ok1269M+)
7 h
F
7-7.5 h
G
7.5-8 h
H
8-8.5 h
I unc-34(e951)
7.5-8 h
J
arx-7(ok1118M+);
unc-115(ky275)
K
arx-2(ok1269M+);
unc-115(ky275)

Figure 2.4. *arx* mutants display fewer PQR growth cone filopodia. Shown are fluorescent micrographs of living animals with *gcy-32::gfp* expression in the PQR neuron in the tail of the animal posterior to the anus. Below each micrograph is a tracing showing the shape of the PQR neuron. In all micrographs, anterior is to the left and dorsal is up, and the scale bars represent 2mm (A for A-I and J for J-K). (A-D) show a timecourse of wild-type posterior PQR neurite development (arrows). PQR neurons from different animals at particular timepoints are shown. A tracing of the cell and neurite is shown below each micrograph of animals at given timepoints after hatching (see Methods). (E-H) show a PQR posterior neurite development in a representative example of an *arx-2(ok1269M+)* mutant. (I) The PQR posterior neurite from an *unc-34(e951)* mutant. (J-K) show PQR neurons from *unc-115(ky275); arx-2(ok1269M+)* or *unc-115(ky275); arx-7(ok1118M+)* mutants at 9 hours after hatching at a time when wild-type posterior protrusions had fully extended. The PQR in (J) showed a rudimentary posterior protrusion (arrow), and the PQR neuron in (K) showed no obvious posterior protrusion (arrow). The dashed arrows in (J) and (K) point to normal anterior axonal protrusions from these PQR neurons.

Figure 2.5

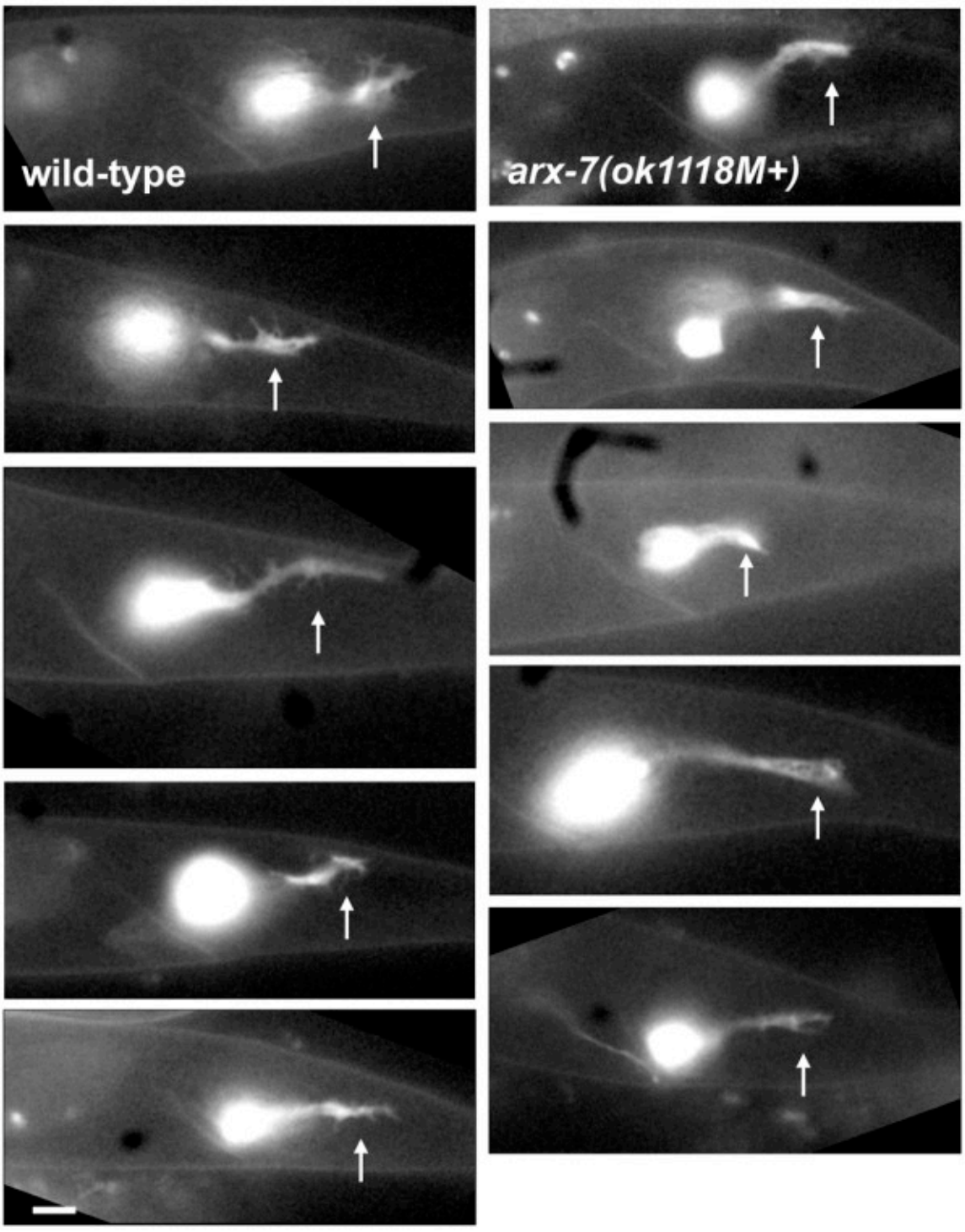

Figure 2.5. *arx-7(ok1118M+)* displayed fewer growth cone filopodia than wild-type. Shown are fluorescent micrographs of posterior PQR neurites in representative samples of wild-type (left column) and *arx-7(ok1118M+)* (right column) at 7-8 hours after hatching. Arrows point to growth cones. For all micrographs, anterior is left, dorsal is up, and the scale bar = 2mm.

Figure 2.6

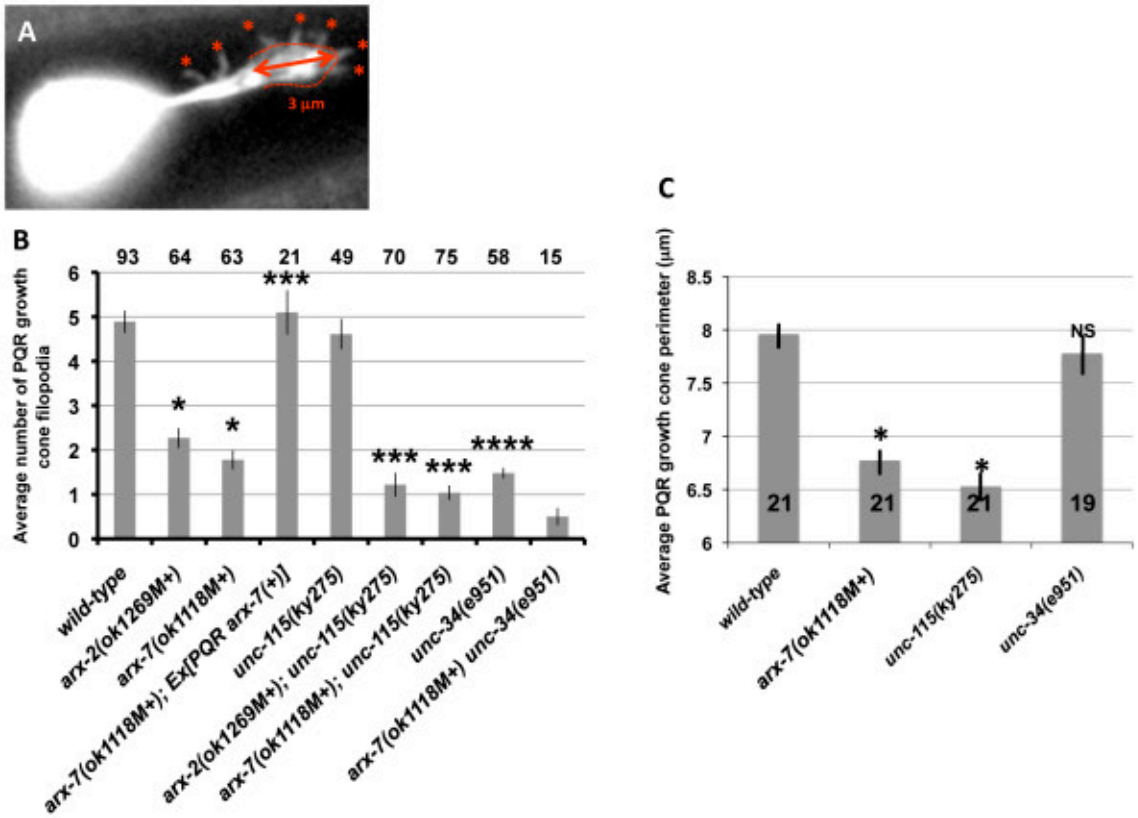
A
3 µm
B
93 64 63 21 49 70 75 58 15
Average number of PQR growth cone filopodia
0 1 2 3 4 5 6
*
*
***
***
***
****
wild-type
arx-2(ok1269M+)
arx-7(ok1118M+)
arx-7(ok1118M+); Ex[PQR arx-7(+)]
unc-115(ky275)
arx-2(ok1269M+); unc-115(ky275)
arx-7(ok1118M+); unc-115(ky275)
unc-34(e951)
arx-7(ok1118M+) unc-34(e951)
C
Average PQR growth cone perimeter (µm)
6 6.5 7 7.5 8 8.5
21
21
21
19
*
*
NS
wild-type
arx-7(ok1118M+)
unc-115(ky275)
unc-34(e951)

Figure 2.6. Quantitation of PQR posterior neurite growth cone filopodia defects. (A) A micrograph demonstrating how filopodia number and growth cone perimeter was quantified. Asterisks mark filopodial protrusions (< 0.5mm in width). The red dashed line is a tracing of the distal 3mm of the growth cone perimeter. (B) The Y axis represents the average number of filopodia present on the PQR posterior neurite growth cone at 7-8 hours after hatching. Error bars represent standard error of the mean. *arx-2(ok1269M+)* and *arx-7(ok1118M+)* displayed significantly fewer filopodia than wild-type ($p < 0.0001$; indicated by a single asterisk). Cell-specific expression of the *arx-7(+)* in PQR via the *Pgcy-32::arx-7(+):: gfp* transgene rescued filopodia defects of *arx-7(ok1118M+)* ($p < 0.0001$; two asterisks). *unc-115(ky275)* was not significantly different from wild-type ($p = 0.51$), but did significantly enhance *arx-2(ok1269M+)* and *arx-7(ok1118M+)* ($p = 0.003$ and 0.007, respectively; three asterisks). *unc-34(e951)* displayed significantly fewer filopodia than wild-type ($p < 0.0001$; four asterisks). (C) Growth cone perimeter (in microns) is the Y axis. Error bars represent standard error of the mean. *arx-7(ok1118M+)* and *unc-115(ky275)* had reduced growth cone perimter compared to wild type (asterisks; $p < 0.001$) whereas *unc-34* did not (NS = not significant).

Figure 2.7

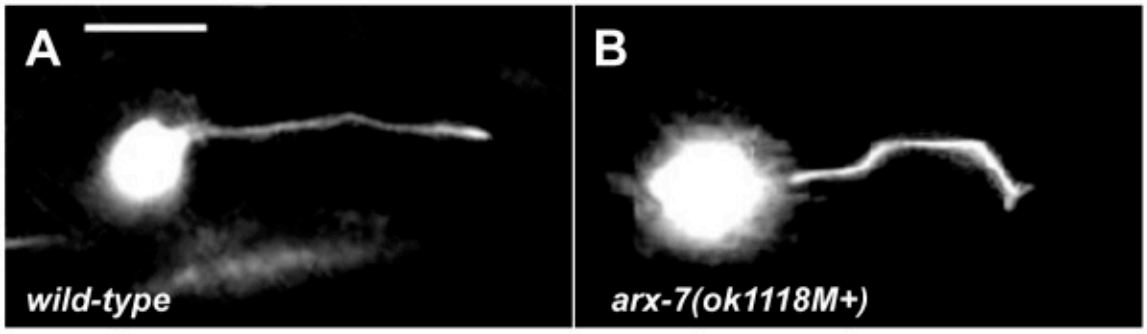

C

Genotype (n > 30)	Percent with misguided dendrite
wild-type	19%
arx-7(ok1118M+)	45%
unc-115(ky275)	41%
unc-34(e951)	67%

Figure 2.7. PQR dendrite guidance defects. (A) and (B) are micrographs of young adult PQR neurons expressing *gcy-32::gfp*. Anterior is to the left, and dorsal is up. In wild-type, the PQR dendrite extends directly to the posterior. In *arx-7(ok118M+)*, the PQR dendrite extends posteriorly but has multiple turns. The scale bar in (A) represents 5mm. (C) Quantitation of PQR dendritic guidance defects.

Figure 2.8

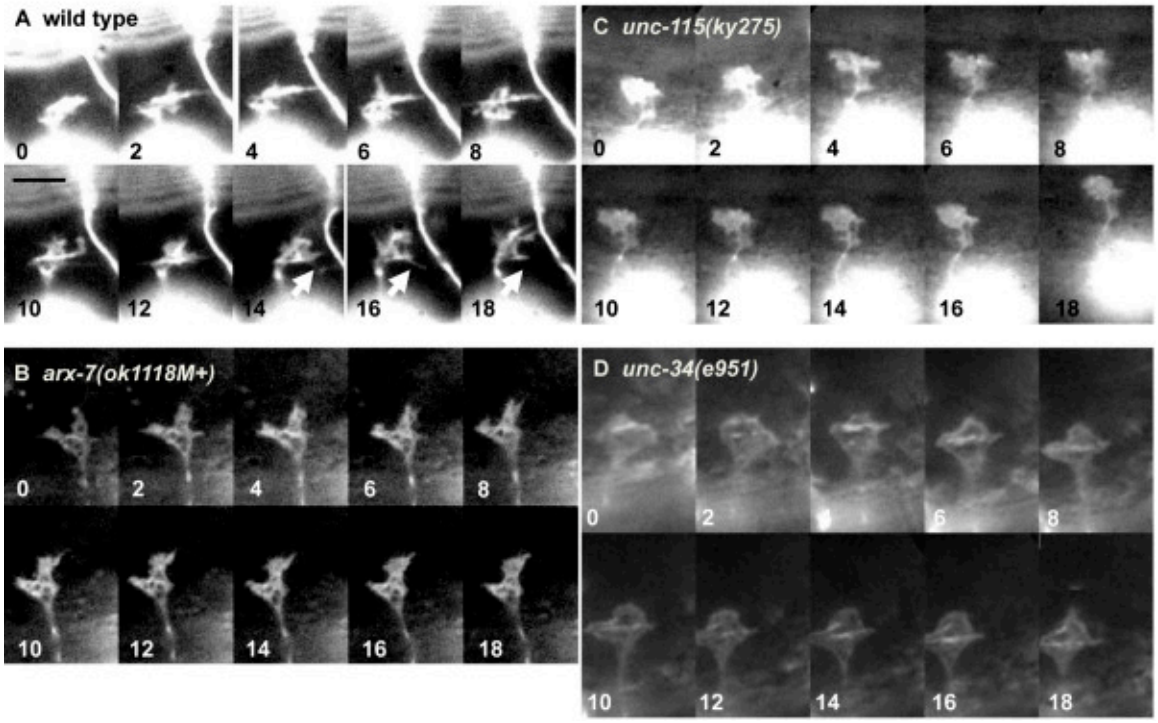
A wild type
0
2
4
6
8
10
12
14
16
18
C unc-115(ky275)
0
2
4
6
8
10
12
14
16
18
B arx-7(ok1118M+)
0
2
4
6
8
10
12
14
16
18
D unc-34(e951)
0
2
6
8
10
12
14
16
18

Figure 2.8. Time lapse images of VD growth cone outgrowth. Series of time-lapse images of VD growth cones in early L2 larvae, as they migrate between muscle quadrants. The time in minutes after initiation of the experiment are shown in the lower left corner of each image. The scale bar represents 5mm. (A) A wild-type VD growth cone displays multiple protrusions. The arrow points to the initiation (at 14 minutes) and retraction (at 18minutes) of a growth cone filopodium. (B) An *arx-7(ok1118M+)* growth cone displayed fewer filopodial protrusions and generally less dynamics than wild type. (C) An *unc-115(ky275)* growth cone displayed few filopodia and generally reduced dynamics. (D) An *unc-34(e951)* growth cone as it spread along a nerve tract as described in (Knobel et al. 1999). The growth cone displayed few filopodial protrusions.

Figure 2.9

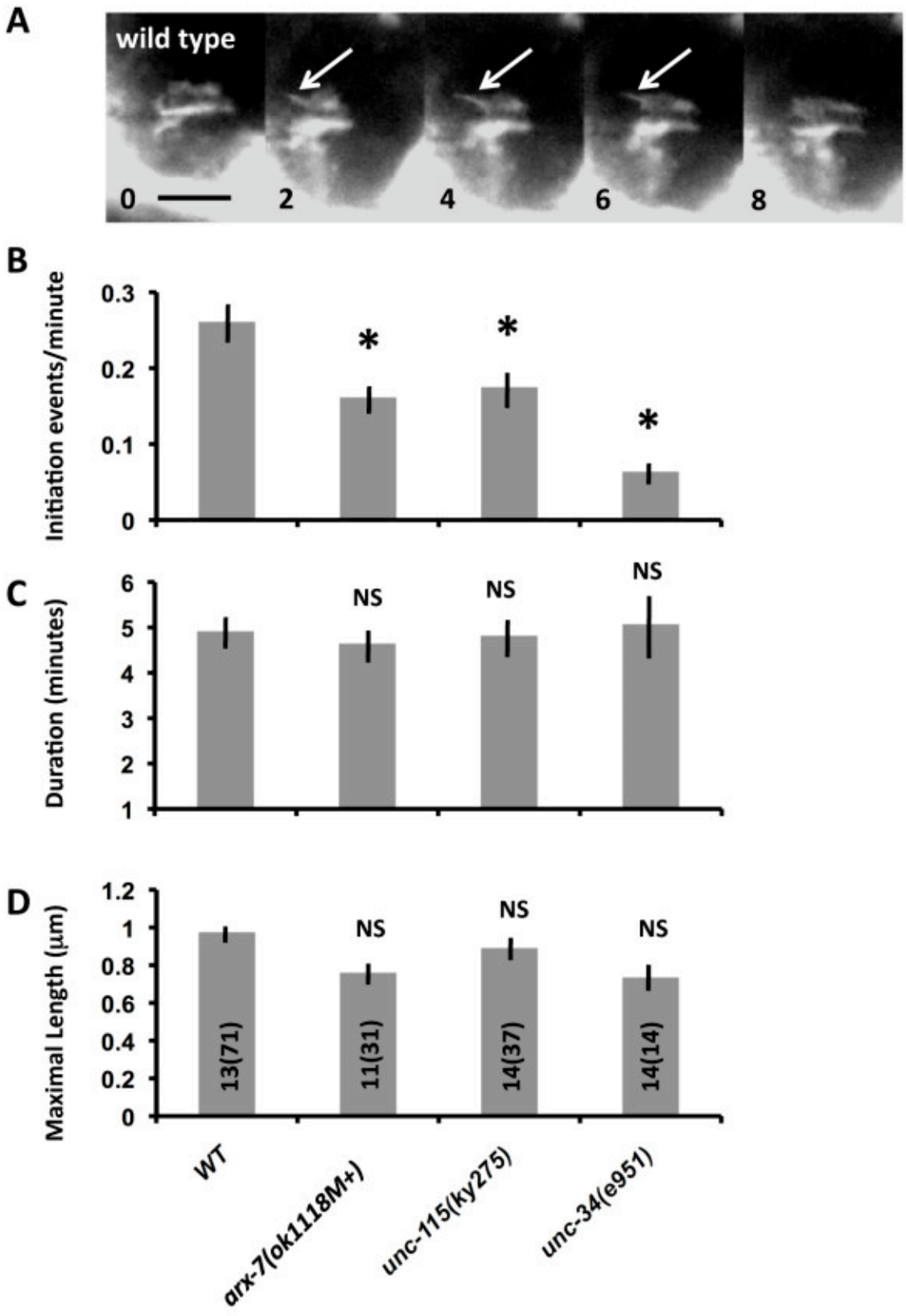
A
wild type
0
2
4
6
8
B
Initiation events/minute
0.3
0.2
0.1
0
*
*
*
C
Duration (minutes)
6
5
4
3
2
1
NS
NS
NS
D
Maximal Length (μm)
1.2
1
0.8
0.6
0.4
0.2
0
NS
NS
NS
13(71)
11(31)
14(37)
14(14)
WT
arx-7(ok1118M+)
unc-115(ky275)
unc-34(e951)

Figure 2.9. Quantitation of VD/DD growth cone dynamics. (A) A time lapse series of a wild-type VD growth cone showing the emergence and retraction of an individual filopodium (arrows). The scale bar represents 5mm, and the time after the start of the time lapse experiment is indicated in the lower left of each panel. B-D) Quantitation of filopodia initiation rate, stability, and maximal length. Error bars represent standard error of the mean. Asterisks indicate significant differences between wild type and the mutant ($p < 0.0006$). NS = not significantly different. The number of growth cones analyzed and the total number of filopodia (in parentheses) is indicated in the bars in (D). (B) Initiation rates of filopodia (average initiation events per minute); (C) average filopodial duration (in minutes); and (D) average filopodial maximal length.

Figure 2.10

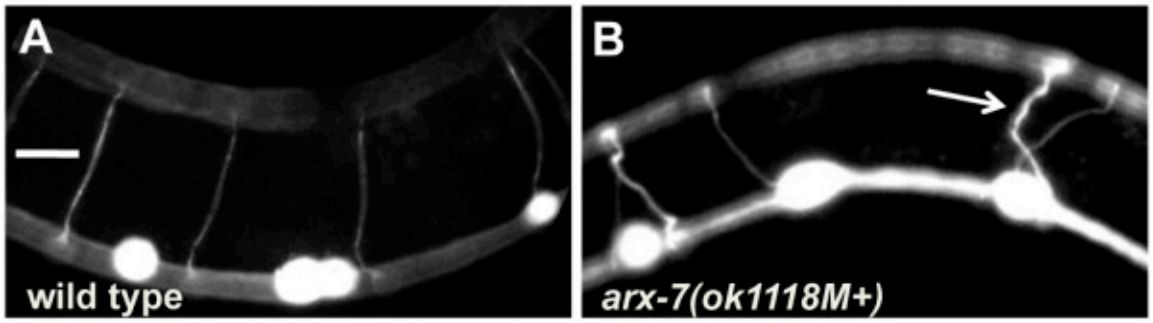

C

Genotype (n)	Percent of animals with misguided VD/DD axons
wild-type (>100)	38%
arx-7(ok1118M+) (40)	77%
unc-115(ky275) (>100)	80%
unc-34(e951) (>100)	100%

Figure 2.10. VD/DD axon guidance defects. (A) and (B) are micrographs of young adult animals with *unc-25::gfp* expression in the VD/DD motor axons. In wild type, the commissural axons generally extend directly from ventral to dorsal. In *arx-7(ok1118M+)*, axons often wandered laterally and crossed other commissures before reaching the dorsal cord (arrow). (C) Percentage of animals with misguided VD/DD commissural axons.

Figure 2.11

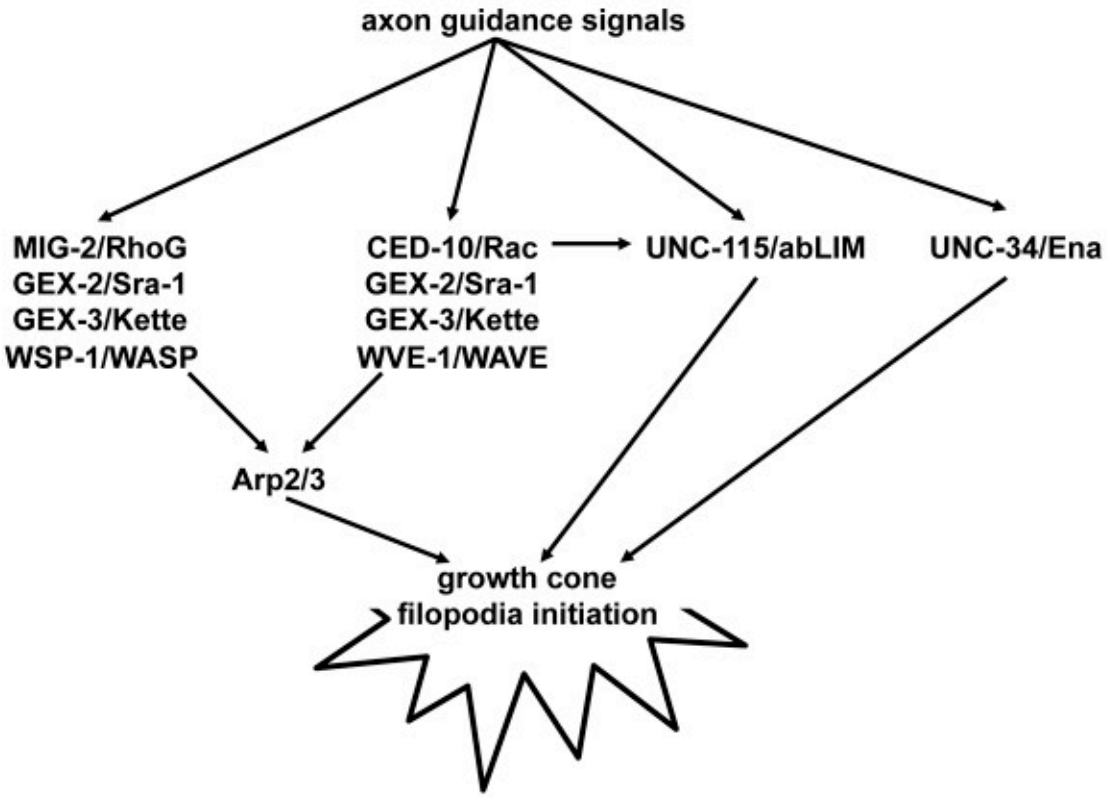
axon guidance signals
MIG-2/RhoG
GEX-2/Sra-1
GEX-3/Kette
WSP-1/WASP
CED-10/Rac
GEX-2/Sra-1
GEX-3/Kette
WVE-1/WAVE
UNC-115/abLIM
UNC-34/Ena
Arp2/3
growth cone
filopodia initiation

Figure 2.11. A model of Arp2/3, UNC-115/abLIM, and UNC-34 in growth cone filopodia formation. Arp2/3 might act downstream of both CED-10/Rac and MIG-2/RhoG and in parallel to UNC-115/abLIM and UNC-34/Enabled. CED-10/Rac might also regulate UNC-115/abLIM.

Chapter III

UNC-6/Netrin and its receptors UNC-40/DCC and UNC-5 modulate extent and polarity of growth cone protrusion

4.1 Abstract

A great deal is known about the roles of UNC-6/Netrin and its receptors UNC-40/DCC and UNC-5 in axon pathfinding, but little is known about how they directly affect the growth cone *in vivo* in developing organisms. The lamellipodia and filopodia of the growth cone are actin-based structures that sense the extracellular environment and power the forward motion of the growth cone. We show here that in UNC-6-repelled VD growth cones and in UNC-6-attracted HSN growth cones, mutations in *unc-6*, *unc-40* and *unc-5* affected lamellipodia and filopodia, both in the extent of lamellipodial and filopodial protrusion and in the polarity of protrusion. *unc-6* mutants exhibited a loss of polarity in both VD and HSN filopodia protrusions and decreased the extent of protrusion in the HSNs. u*nc-40* mutants exhibited a loss of polarity and decreased the extent of protrusion in the HSNs, while activated *unc-40* caused decreased extent of protrusion in the VDs and increased extent of protrusion in the HSNs. Finally, *unc-5* mutants exhibited a loss of polarity and increased extent of protrusion in the VDs. The loss of polarity extended to the actin cytoskeleton, as filamentous actin, normally polarized to the leading edge of the growth cone, lost its polarity in *unc-5* and *unc-6* mutants in VD growth cones. The findings presented here suggest that UNC-6-mediated repulsion through UNC-5 corresponds to a decreased extent of growth cone protrusion, while UNC-6-mediated attraction through UNC-40 corresponds to an increase in growth cone protrusion. These studies show that UNC-6/Netrin and its receptors UNC-40/DCC and UNC-5 are

required *in vivo* to correctly orient and modulate the extent of protrusions in the developing growth cone.

4.2 Introduction

Developing axons are tipped with growth cones, dynamic actin-based structures that sense and respond to extracellular cues, driving the forward motion of the axon (Mortimer et al. 2008; Tessier-Lavigne and Goodman 1996). Growth cones consist of lammelipodial protrusions of a branched actin meshwork and filopodial protrusions of bundled actin filaments, which are both involved in the proper growth of an axon to its target destination (Gallo and Letourneau 2004; Pak et al. 2008; Zhou and Cohan 2004).

The laminin-like UNC-6/Netrin guidance cue and its receptors UNC-40/DCC (Deleted in Colorectal Carcinoma) and UNC-5 have been strongly implicated in axon pathfinding in mouse, *Drosophila, C. elegans* and other organisms (Chan et al. 1996; Hong et al. 1999; Leonardo 1997; Montell 1999; Pan et al. ; Shekarabi and Kennedy 2002). In *C. elegans*, UNC-6 is secreted by neurons in the ventral nerve cord and is necessary for guidance of circumferential neurons (Ishii et al. 1992). The receptor UNC-40 is expressed in growth cones and mediates an attractive response to UNC-6, driving the ventral guidance of circumferential axons, while the receptor UNC-5 is expressed in dorsally-guided growth cones and mediates a repulsive response to UNC-6, driving the dorsal guidance of circumferential axons (Hedgecock et al. 1990; Hong et al. 1999).

UNC-40/DCC and UNC-5 both respond to UNC-6/Netrin by the formation of receptor dimers. In neurons expressing only UNC-40/DCC, UNC-6/Netrin binding causes the formation of an UNC-40/DCC homodimer, leading to an

attractive response by the growth cone. In neurons expressing both UNC-5 and UNC-40/DCC, UNC-6/Netrin binding leads primarily to the formation of UNC-5 homodimers or UNC-5-UNC-40/DCC heterodimers, both of which mediate a repulsive response (Hong et al. 1999; MacNeil et al. 2009).

While the role of UNC-6/Netrin and its receptors have been studied extensively in axon pathfinding endpoint analyses and in *in vitro* growth cone experiments, little is known about how they affect the growth cone *in vivo* during the developmental process. Previous studies have shown that UNC-6/Netrin can affect the polarity of growth cone protrusions in *C. elegans* (Adler et al. 2006), and the morphology of the growth cone in neurons *in vitro (Shekarabi and Kennedy 2002; Shekarabi et al. 2005).* This led us to the hypothesis that UNC-6/Netrin and its receptors may play an important role in modulating the extent and polarity of protrusion in *C. elegans* growth cones, and that this may affect the final axon pathfinding outcomes.

We endeavored to understand how UNC-6/Netrin and its receptors UNC-40/DCC and UNC-5 affect axon pathfinding, growth cone morphology and dynamics in circumferential neurons in *C. elegans*, using methods we have previously developed which allow *in vivo* analysis of *C. elegans* growth cones. We show here that UNC-6/Netrin and its receptors UNC-40/DCC and UNC-5 are involved in polarity of growth cone protrusiveness and in modulating the extent of protrusion.

4.3 Materials and Methods

Genetic methods

Experiments performed at 20°C using standard *C. elegans* techniques. These mutations and transgenics were used: X: *unc-6*(*ev400* and *e78*), *lqIs170* [*rgef-1::vab-10ABD::gfp*]; I: *unc-40*(*n324* and *e1430*), *unc-73*(*rh40*); II: *juIs76* [*unc-25::gfp*] ; IV: *kyIs179* [*unc-86::gfp*], *unc-5*(*e53* and *e152*). Chromosomal locations for the following transgenes were not determined: *lqIs128* [*unc-25::myr::unc-40*], *lqIs129* [*unc-25::myr::unc-40*], *lqIs164* [*myo-3::cfp*], *lqIs182* [*unc-86::myr::gfp*], and *lhIs6* [*unc-25::mCherry*]. Extrachromosomal arrays were attained by injection into the germline, and then integrated into the genome via standard techniques (Mello and Fire 1995). Double mutants with *unc-6*, *unc-5* and *unc-40* were confirmed by the uncoordinated movement phenotype, axon pathfinding phenotype, and PCR genotyping.

Imaging of axon guidance defects

VD neurons were visualized with an *unc-25::gfp* (Jin et al. 1999) or *unc-25::mCherry* transgene (gift of Brian Ackley), which is expressed in all GABAergic neurons, including the 16 VDs. VD axons were considered defective if the axon failed to reach the dorsal nerve cord or if it branched or turned at an angle greater than 45° before reaching the dorsal nerve cord. To determine severity of defects, a *myo-3::cfp* transgene was introduced to mark the ventral and dorsal muscle quadrants. Using an *unc-25::mCherry* construct we could then

determine whether an axon's trajectory went awry before or after reaching the dorsal edge of the ventral muscle quadrant.

HSNs were visualized with an *unc-86::gfp* transgene (Shen and Bargmann 2003), which is expressed in numerous neurons, including the two HSNs. HSN axons were considered defective if the axon failed to reach the ventral nerve cord, or if it branched or turned at an angle greater than 45° before reaching the ventral nerve cord.

Growth cone time-lapse imaging

VD growth cones were imaged as previously described (Norris et al. 2009). Briefly, animals harboring the *juIs76* [*unc-25::gfp*] transgene were selected 16 h post-hatching at 20°C and placed on a 2% agarose pad with a drop of 10mM muscimol (Sigm-Aldrich, St. Louis, MO USA) in M9 (Weinkove et al. 2008), which was allowed to evaporate for 3 to 4 minutes before placing coverslip. Growth cones were imaged with a Qimaging Rolera mGi camera on a Leica DMR microscope with BD CARV II wide-field light source. Images were acquired at intervals of 120 s, with total duration of time lapse ranging from 20 to 60 minutes. HSN growth cone time-lapse imaging was performed identically, except that animals were selected at 19 h post hatching.

Dynamic projections less than 0.5 μm in width emanating from the growth cone were scored as filopodia. Filopodia length and growth cone area were measured using ImageJ software. Polarity of filopodia protrusion was determined in ImageJ by dividing the growth cone into four equally-sized quadrants (dorsal-

anterior, dorsal-posterior, ventral-anterior and ventral-posterior) and determining from which quadrant each filopodium emanated. Significance of difference was determined in all cases by a two-sided *t*-test with unequal variance or a fisher's exact test.

4.4 Results

UNC-5, UNC-6 and UNC-40 control dorsal-ventral axon pathfinding.

The secreted laminin-like molecule UNC-6/Netrin and its receptors UNC-40/DCC and UNC-5 define an evolutionarily-conserved dorsal-ventral axon and cell migration system (Moore et al. 2007). In *C. elegans*, UNC-6 is secreted by ventral cells, creating an asymmetry of UNC-6 from the ventral to dorsal. Circumferential axons respond differentially to UNC-6 (Hedgecock et al. 1990; Ishii et al. 1992). Those that are attracted to UNC-6 grow ventrally toward UNC-6, and those that are repelled from UNC-6 grow dorsally away from UNC-6. The UNC-6/Netrin receptors mediate attraction versus repulsion. UNC-40 is required for both attractive ventral growth and repulsive dorsal growth, and UNC-5 is required specifically for dorsal repulsive growth (Hedgecock et al. 1990). Studies in vertebrate systems indicate that growth cones with active UNC-40/DCC homodimers are attracted to UNC-6, and growth cones with active UNC-40/UNC-5 heterodimers are repelled from UNC-6 (Hong et al. 1999). In *C. elegans*, *unc-6* and *unc-40* mutants display guidance defects in both ventrally-directed and dorsally-directed circumferential axons, and *unc-5* mutants display defective pathfinding in dorsally-directed circumferential axons (Hedgecock et al. 1990). We confirmed and quantified defects in *unc-5, unc-6*, and *unc-40* mutants in the dorsally-directed VD motor neurons that are repelled from UNC-6, and in the ventrally-directed HSN axons that are attracted to UNC-6. Consistent with previous results, *unc-5* and *unc-6* mutants displayed a nearly complete failure of

VD axons to reach the dorsal nerve cord, whereas *unc-40* mutants had a weaker effect on VD axon pathfinding (Figure 1A-D). In contrast, *unc-6* and *unc-40* mutants had strong HSN axon guidance defects whereas *unc-5* mutants did not (Figure 1E-G). Thus, UNC-6 is required for both repulsion (VDs) and attraction (HSNs), UNC-40 is required for attraction and weakly for repulsion, and UNC-5 is required for repulsion. In support of this model, the *unc-6(e78)* allele, which results in a cysteine to tyrosine substitution in domain V-3 that disrupts interaction with UNC-5 but not UNC-40/DCC (Lim and Wadsworth 2002), more strongly affected dorsal repulsive growth than ventral attractive growth as previously reported (Figure 1A and E). These results are consistent with previous findings that UNC-6/Netrin and UNC-40/DCC, but not UNC-5, are required for ventral migration (Hedgecock et al. 1990).

UNC-5 and UNC-6 inhibit growth cone protrusion

While it is established that UNC-6/Netrin signaling affects circumferential axon guidance, the effects of these molecules on the growth cone during outgrowth *in vivo* are less well understood. We started by timelapse imaging of the growth cones of the VD motor neurons that are repelled from UNC-6/Netrin. VD growth cones were imaged in animals at 16 hours post-hatching at a time when the VD growth cones have begun their commissural migrations (see Materials and Methods for imaging methods). We measured growth cone area as well as the dynamic parameters of filopodia initiation rate, filopodia duration, and maximal filopodial length (see Material and Methods for parameter measurement). Wild-

type VD growth cones had an average area of 6.7 μm^2. Wild-type growth cones also displayed multiple dynamic filopodia that formed at an average rate of 0.26 per minute (one initiation event every 3.8 minutes). The average wild-type filopodium had a duration of 4.9 minutes (between the time it was first noticeable to the time it was no longer apparent) and had an average maximal length of 0.96 μm. These parameters are similar to those previously observed for wild-type VD growth cones.

unc-5 caused an increase in growth cone protrusiveness in VD growth cones. Growth cone area was significantly increased (6.8 μm^2 in WT compared to 8.7 μm^2 in *unc-5(e152)* and *unc-5(e53)*; $p < 0.01$) (Figure 2E), as was filopodia duration (4.9 minutes in wild type versus 7.1 and 7.3 minutes in *unc-5(e152)* and *unc-5(e53)*; $p < 0.01$) (Figure 2A). Average maximal filopodial length was also increased significantly. However, filopodial length appeared biphasic in *unc-5* mutants, with many filopodia that were comparable to wild-type length and some that grew very long (greater than two standard deviations from average wild-type length; 12% and 15% in *unc-5(e152)* and *unc-5(e53)*) (Figure 2D; Figure S1). Some of these long filopodia were observed to endure throughout the growth cone imaging period, suggesting that they are very stable growth cone protrusions not observed in wild-type. These data indicate that UNC-5 is normally required to limit the extent of protrusion of growth cones that are repelled from UNC-6. However, *unc-5* mutants did not affect the rate of filopodia formation (Figure 2B) suggesting that UNC-5 might affect filopodial dynamics after a filopodium has been formed.

Surprisingly, the *unc-6(ev400)* null mutation had no significant effect on any of the VD growth cone parameters we measured. However, the *unc-6(e78)* mutation that specifically disrupts the repulsive, UNC-5-dependent role of UNC-6 (Lim and Wadsworth 2002), resembled *unc-5* mutants in all parameters measured (increased growth cone area, increased filopodial duration, and unusually long filopodia with no effect on filopodia initiation rate). Thus, UNC-6 also normally inhibits filopodial dynamics and growth cone area. That these effects are reduced in the *unc-6* null suggests that they are due to a non-UNC-5 mediated role of UNC-6, possibly interaction with UNC-40. Indeed, as we show below, loss of UNC-40 suppressed the increased filopodial dynamics in *unc-5* mutants and in *unc-6(e78)*, indicating that UNC-40 is required for increased filopodial dynamics in these mutants.

Constitutively-active MYR::UNC-40 inhibits VD growth cone protrusion.

Two putative null mutations in *unc-40*, *e1430* and *n324*, had very little effect on VD growth cone dynamics and morphology, with the only significant effect being a reduction in maximal filopodial length compared to wild-type (Figure 2C). This is surprising given that UNC-40 is thought to cooperate with UNC-5 in repulsive axon guidance. To probe the role of UNC-40 in VD growth cone dynamics in more detail, we constructed a constitutively-active version of UNC-40, based upon Gitai et al., 2003, by adding an N-terminal myristoylation signal to the cytoplasmic domain of UNC-40. MYR::UNC-40 lacks the transmembrane domain and the extracellular domains, which function to inhibit

dimerization in the absence of UNC-6/Netrin, and is targeted to membranes by the myristoylation sequence. MYR::UNC-40 is thought to dimerize and be constitutively active even in the absence of UNC-6/Netrin. *myr::unc-40* was then expressed in the VD neurons using the *unc-25* promoter. In a wild-type background, MYR::UNC-40 caused a marked decrease in VD growth cone protrusiveness. MYR::UNC-40 growth cones exhibited a decrease in growth cone area and filopodial formation rate (Fig. 2). When filopodia did form, they had reduced maximal length (0.96 μm in WT compared to 0.76 μm in *lqIs128*; $p < 0.01$) and reduced duration (4.9 minutes in WT compared to 3.9 minutes in *lqIs128*; $p < 0.01$). MYR::UNC-40 growth cones appeared very small (6.8 μm^2 in WT compared to 4.6 μm^2 in *lqIs128*; $p < 0.01$) with few filopodial protrusions, and exhibited a "treadmilling" behavior in which there was some movement around the edges of the growth cone but very little growth cone advance (Figure S2). Thus, constitutively-active MYR::UNC-40 inhibited growth cone protrusion suggesting that UNC-40 normally has a role in inhibition of protrusion. In contrast to loss of function of *unc-5* and *unc-6(e78)*, *myr::unc-40* also affected filopodia initiation rate (0.26 per minute in WT compared to 0.16 per minute in *lqIs128*; $p < 0.01$) (Figure 2B). Thus UNC-40 might also be involved in inhibition of filopodial initiation. Alternatively, filopodia might form at a normal rate in *myr::unc-40* but are inhibited before they are visible in our imaging conditions, which might not be able to distinguish short or transient filopodia. Consistent with these defects in growth cone morphology, *myr::unc-40* caused defects in VD

and DD dorsal axon pathfinding as determined by end point analysis (55% defective axons in *lqIs128*) (Figure 1A).

Constitutively-active MYR::UNC-40 requires UNC-5 to inhibit VD protrusion

We next tested if the MYR::UNC-40-mediated reduction in growth cone protrusion was dependent on the presence of other Netrin signaling components. We found that the MYR::UNC-40 phenotype was not dependent on UNC-6, as *unc-6(ev400); myr::unc-40* double mutant VD growth cones resembled *myr::unc-40* alone (Figure 3). This result is consistent with the idea that MYR::UNC-40 is an UNC-6-independent constitutively-active molecule. MYR::UNC-40 was also not dependent on endogenous UNC-40 (Figure 3). However, MYR::UNC-40 inhibition of protrusion was dependent upon function UNC-5 (Fig. 3, Fig. S3). Growth cone area (4.6 μm^2 in *lqIs128* compared to 7.2 μm^2 in *unc-5(e53); lqIs128*; $p < 0.01$) and filopodia initiation rate (0.16 per minute in *lqIs128* compared to 0.21 per minute in *unc-5(e53); lqIs128*; $p < 0.01$), maximal length (0.76 µm in *lqIs128* compared to 1.1 µm in *unc-5(e53); lqIs128*; $p < 0.01$), and duration (3.9 minutes in *lqIs128* compared to 7.4 minutes in *unc-5(e53); lqIs128*; $p < 0.01$) were restored in *unc-5(e53); myr::unc-40* mutants to levels comparable to or greater than that of wild-type and in fact resembled the excessive protrusion seen in *unc-5* mutants alone.

These results suggest that MYR::UNC-40 acts in a complex with UNC-5 to inhibit growth cone protrusion, consistent with previous results suggesting that an UNC-40/UNC-5 heterodimer mediates growth away from UNC-6/Netrin. These

results also suggest that formation of a putative MYR::UNC-40/UNC-5 heterodimer is independent of UNC-6/Netrin as would be expected of a ligand-independent constitutively-active molecule.

VD growth cone over-protrusive phenotypes of *unc-5* and *unc-6(e78)* are suppressed by *unc-40* mutation

unc-5 null and *unc-6(e78)* mutants but not *unc-6(ev400)* null mutants displayed increased growth cone protrusion, suggesting a role of UNC-6 in stimulating VD growth cone protrusion in the absence of UNC-5. We speculated that this might involve UNC-40. We constructed *unc-5; unc-40* double mutants and found that they did not exhibit the over-protrusive phenotypes seen in the *unc-5* single mutants: growth cone size (8.7 μm^2 in *unc-5(e53)* compared to 6.5 μm^2 in *unc-40(n324); unc-5(e53)*; $p < 0.01$), filopodia length (1.1 µm in *unc-5(e53)* compared to 0.92 µm in *unc-40(n324); unc-5(e53)*; $p < 0.01$) and duration (7.3 minutes in *unc-5(e53)* compared to 5.0 minutes in *unc-40(n324); unc-5(e53)*; $p < 0.01$) were all returned to near-wild-type levels in the double mutants using two distinct null alleles of *unc-40* (Fig. 4). Likewise, *unc-40(n324)* was required for the over-protrusive growth cones of *unc-6(e78)* mutants, as *unc-6(e78); unc-40(n324)* double mutants had near-wild-type levels of protrusion (for example, 8.5 μm^2 growth cone size in *unc-6(e78)* compared to 6.6 μm^2 in *unc-40(n324); unc-5(e53)*; $p < 0.01$) (Figure 4). These results suggest that UNC-40 and UNC-6 might have roles in stimulating VD growth cone protrusion in addition to roles in inhibition of protrusion along with UNC-5, as demonstrated by the MYR::UNC-40

results above. This also might explain why *unc-6* null mutants and *unc-40* mutants display less severe growth cone protrusion defects than *unc-5* mutants (i.e. UNC-6 and UNC-40 are required both to stimulate and to inhibit protrusion, and when they are gone an equilibrium between the two is maintained).

Axon pathfinding defects of *unc-5* mutants are reduced by *unc-40* mutation

Previous studies indicated that UNC-5 homodimers mediate repulsion while close to the UNC-6/Netrin source, whereas UNC-5/UNC-40 heterodimers mediate repulsion at locations more distant from the UNC-6/Netrin source (MacNeil et al. 2009). We labeled the ventral and dorsal muscle quadrants with CFP and the VD axons with mCherry, allowing us to quantify the number of axon trajectories that go awry before passing the ventral muscle quadrant, close to the normal source of UNC-6/Netrin (Fig. 5) (Ishii et al. 1992). Indeed, most VD axon pathfinding defects in *unc-40* mutants occurred after the axon passed the ventral muscle quadrant (90% in *unc-40(e1430)*, whereas *unc-5(e53)* null and *unc-6(e78)* defects occurred in or before the ventral muscle quadrant, with some axons apparently not emerging from the ventral nerve cord. *unc-5(e53)* and *unc-6(e78)* null also had more severe defects than the *unc-6(ev400)* null (67% in *unc-5(e53)* and 63% in *unc-6(e78)*, compared to 33% in *unc-6(ev400)*). *unc-40(n324); unc-5(e53)* double mutants were less severe than *unc-5(e53)* alone, and had guidance defects of comparable severity to *unc-6(ev400)* alone (67% for *unc-5(e53)* alone compared to 41% for *unc-40(n324); unc-5(e53)* and 33% for *unc-6(ev400)*; $p < 0.01$). These data indicate that in *unc-5* mutant VD growth

cones, UNC-40/DCC may be mediating an attractive response to UNC-6/Netrin, causing these axons to become attracted to rather than repelled from UNC-6/Netrin and thus misguided sooner than in the complete absence of UNC-6/Netrin.

Netrin signaling component mutants modulate extent of protrusion of HSN growth cones

Axons that contain UNC-40 but not UNC-5 are normally attracted to UNC-6/Netrin and thus navigate ventrally (MacNeil et al. 2009). To study the roles of UNC-6 and UNC-40 in growth cones that are attratced to UNC-6/Netrin, we turned to the HSN neurons. The bilateral HSN cell bodies reside laterally just behind the hermaphrodite vulva in the midsection of the animal. The HSN axons extend ventrally to the ventral nerve cord and then anteriorly to innervate the vulva. As previously reported, the axons of the HSN neurons require UNC-6 and UNC-40 for their ventral-ward migration (Figure 1E-G) (Adler et al. 2006). In *unc-6* and *unc-40* mutants, the HSN axons often extend laterally instead of ventrally. The HSN displays a prominent growth cone at 18-19 h post-hatching in the late L1 stage. At this time, the growth cone resembles a thickened protrusion from the ventral region of the cell body with multiple filopodial protrusions, as previously reported (Adler et al. 2006). Over the next 12 hours into the mid L4 larval stage, the HSN growth cone remains dynamic and migrates ventrally to the ventral nerve cord. We analyzed HSN growth cones in time lapse at 19 hours

post-hatching. At this time the wild-type HSN growth cone is on average 11.2 μm^2 in size, with filopodia that form at an average rate of one every 4.4 minutes and endure for 5.2 minutes, with a maximal filopodial length of 0.9 μm (Fig. 6, Fig. S4). The HSN growth cone is larger, but all dynamic filopodial characteristics are similar to those of the VD growth cones.

unc-40 and *unc-6* null mutant HSN growth cones exhibited a decrease in protrusiveness, with a decrease in growth cone size (11.2 μm^2 in WT compared to 8.2 μm^2 in *unc-6(ev400)* and *unc-40(n324)*; $p < 0.01$), filopodia length (0.9 μm in WT compared to 0.73 and 0.78 μm in *unc-6(ev400)* and *unc-40(n324)*; $p < 0.01$), and duration (5.2 minutes in WT compared to 3.2 and 3.6 minutes in *unc-6(ev400)* and *unc-40(n324)*; $p < 0.01$). *unc-6* mutants but not *unc-40* mutants exhibited a decrease in filopodia formation rate as well (0.23 per minute in WT compared to 0.14 per minute in *unc-40(n324)*; $p < 0.01$). These results indicate that UNC-6/Netrin and UNC-40/DCC are required for robust HSN growth cone protrusion.

We drove the expression of MYR::UNC-40 in the HSNs using the *unc-86* promoter. In contrast to VDs, MYR::UNC-40 caused an increase in protrusiveness in the HSNs, with an increase in growth cone size (11.2 μm^2 in WT compared to 15.1 μm^2 in *myr::unc-40*; $p < 0.01$), filopodia duration (5.2 minutes in WT compared to 7.8 minutes in *myr::unc-40*; $p < 0.01$) and length (0.9 μm in WT compared to 1.3 μm in *myr::unc-40*; $p < 0.01$) (Fig. 6). This is the opposite effect seen with MYR::UNC-40 in the VDs, and suggests that in axons

that do not express UNC-5, the MYR::UNC-40 molecules form an attractive complex that stimulates growth cone protrusion.

Considered with the results in the VD growth cones, these data suggest that UNC-6/Netrin and it receptors UNC-40/DCC and UNC-5 control the extent of growth cone protrusion, including growth cone size and the maximal length and duration of growth cone filopodia. However, in the VD growth cones, *unc-6* and *unc-40* mutants have only weak effects on growth cone protrusiveness but very strong VD axon guidance defects, indicating that regulation of growth cone protrusion is not the only role of these molecules in growth cones.

UNC-5, UNC-6, and UNC-40 affect polarity of growth cone filopodia protrusion

Wild type VD and HSN growth cones display highly polarized filopodial protrusion: in VD growth cones, most filopodia protrude dorsally away from UNC-6; and in HSN growth cones, most filopodia protrude ventrally toward UNC-6. We next determined if orientation of filopodial protrusion was altered in *unc-5, unc-6* and *unc-40* mutants. To quantify polarity of filopodial protrusion, we divided the growth cones into four quadrants along the A-P and D-V axes, based upon the orientation of the animal, regardless of the direction that the growth cone is navigating (some growth in mutants were misguided and were migrating laterally or even ventrally). In wild type VD neurons growing along naked epidermis, the majority of filopodia (70%) extended from the dorsal half of the growth cone, toward their target in the DNC. *unc-5* and *unc-6* null mutations

abolished this polarity such that filopodia protruded nearly equally in the dorsal and ventral directions (54% and 45% of filopodia directed ventrally in *unc-5(e53)* and *unc-6(ev400)* mutants) (Figure 7). Anterior-posterior filopodial protrusion was not significantly different in wild-type growth cones or in *unc-5* and *unc-6* mutants (Figure 6G). *unc-40* null mutations had no significant effect on dorsal ventral polarity of VD growth cone filopodial protrusion, nor did MYR::UNC-40.

In wild-type HSN growth cones, the majority of filopodia extended from the ventral half of the growth cone, toward their target in the VNC. Loss of UNC-5 did not affect this polarity, which is consistent with the observation that UNC-5 is not expressed in the HSN. However, loss of UNC-40/DCC or UNC-6/Netrin abolished the polarity of filopodia extension (Fig. 7E-H), and the growth cone often extended laterally instead of ventrally (Figure G). These results are consistent with previous results showing that UNC-6 localizes UNC-40 to the ventral surface of the HSN, and in an *unc-6* mutant, UNC-40 localizes uniformly around the cell body and protrusions extend from around the cell body (Xu et al. 2009). These results indicate that UNC-5, UNC-6, and UNC-40 control the polarity of filopodial protrusion from growth cones that are repelled (VDs) or attracted (HSNs) to UNC-6/Netrin.

UNC-5 and UNC-6 control polarity of growth cone filamentous actin

Growth cone protrusion, including the lamellipodial growth cone body and filopodial extensions, involves dynamic regulation of the actin cytoskeleton (Quinn and Wadsworth 2008). In the VDs and the PQR dendrite growth cones,

the actin regulators Arp2/3, UNC-115/abLIM, and UNC-34/Enabled are required for robust filopodial extensions (Norris et al. 2009). We assayed filamentous actin (F-actin) in the VD growth cones, using a construct in which the F-actin binding domain (Kim et al.) of the spectraplakin VAB-10 is fused to GFP that has been used to monitor F-actin in other cells in living *C. elegans*. In wild-type VD growth cones, this VAB-10ABD::GFP construct localized preferentially to the dorsal leading edge of the lamellipodia (Fig. 8A-C). In *unc-6* and *unc-5* null mutants, VAB-10ABD::GFP no longer showed a preferential dorsal leading edge (Fig. 8D-F). Rather, VAB-10ABD::GFP distribution was randomized across the growth cone and sometimes showed a ventral bias. No obvious differences in overall levels of f-actin were detected, but slight changes would not be distinguished using this assay. *unc-40* null mutations had no effect on VAB-10ABD::GFP distribution. These results suggest UNC-5 and UNC-6 control the distribution of f-actin in the VD growth cone away from the UNC-6/Netrin source and toward the protrusive dorsal edge of the growth cones.

4.5 Discussion

UNC-6/Netrin and its receptors modulate extent of growth cone protrusion

Migrating growth cones navigate to their destinations employing a balance of cytoskeletal-based protrusion toward attractive cues and inhibition of protrusion toward repulsive cues. Thus it is necessary to correctly interpret the extracellular signal and transmit the information into the appropriate cytoskeletal response (Gallo and Letourneau 2004; Pak et al. 2008).

We show that in UNC-6-repulsed VD neurons, which express both UNC-40/DCC and UNC-5, loss of *unc-5* causes an increase in protrusive activity. We show that this is likely due to an increase in protrusion-stimulating binding of UNC-6/Netrin to UNC-40/DCC homodimers in the absence of the protrusion-limiting UNC-5.

In the HSNs we also show that loss of UNC-6/Netrin or UNC-40/DCC causes a reduction in the extent of growth cone protrusion, likely due to a loss of attractive signaling.

Relationship between growth cone attraction and protrusion

Our findings suggest that there is a link between an attractive cue and stimulation of protrusion, and between a repulsive cue and inhibition of protrusion in the growth cone. When the repulsive receptor UNC-5 is removed in VDs, the result is an overly-protrusive phenotype. When the attractive UNC-40/DCC

receptor, or its ligand UNC-6/Netrin, are removed in HSNs, the result is reduced protrusiveness.

Similarly, when an activated version of the attractive receptor UNC-40/DCC is expressed in HSNs, it causes an increase in protrusiveness. However, when it is expressed in VDs containing UNC-5, it causes excess inhibition of protrusion, likely through the formation of repulsive, protrusion-limiting UNC-5/UNC-40/DCC heterodimers.

These findings suggest a broader theme in which sensation of an attractive cue causes stimulation of protrusion, while a repulsive cue causes inhibition of protrusion. These *in vivo* morphological results are supported by previous *in vitro* studies as well (Shekarabi and Kennedy 2002; Shekarabi et al. 2005).

UNC-6/Netrin and its receptors affect polarity of protrusion

Previous studies have shown that UNC-6/Netrin is involved in establishment of initial protrusion polarity in the growth cone (Adler et al. 2006). We expand upon these findings and show that UNC-6/Netrin, UNC-40/DCC and UNC-5 are all involved in controlling the polarity of protrusion in the growth cone.

We show here that UNC-6/Netrin is required for appropriately polarizing the protrusions of VD and HSN growth cones. In *unc-6* mutants, both VD and HSN growth cones lose filopodia and F-actin polarization. We also show that in VDs UNC-5 is required for appropriate polarization of filopodia and F-actin, and

that in the HSNs UNC-40/DCC is required for appropriate polarization of filopodia.

Activation of UNC-40/DCC causes differential context-dependent effects

We created an activated form of UNC-40/DCC by removing the extracellular domain and adding a myristoylation sequence, thus driving it to membranes, including the cell membrane. Removal of the extracellular domain has been shown to constitutively activate the receptor, as it removes the dimerization-inhibiting extracellular domain, allowing the receptor to constitutively dimerize even in the absence of ligand (Gitai et al. 2003). A similar construct has previously been shown to lead to increased protrusion in adult HSNs (Gitai et al. 2003).

We confirm these results in the HSN growth cones, which express only UNC-40/DCC, but we observe the opposite effect in VDs, which express both UNC-40/DCC and UNC-5 and exhibit a marked decrease in protrusion upon introduction of MYR::UNC-40. We suspect that the differences between the two phenotypes are dependent on the formation of attractive, protrusion-stimulating dimers of UNC-40/DCC and MYR::UNC-40 in the HSNs, while repulsive, protrusion-inhibiting dimers of UNC-5 and MYR::UNC-40 are formed in the VDs. This hypothesis is supported by the fact that the decreased protrusion phenotype seen in MYR::UNC-40 in the VDs is suppressed by *unc-5(e53)*.

Thus we have shown that UNC-6/Netrin, UNC-40/DCC and UNC-5 are not only required for axon pathfinding from an endpoint analysis standpoint, but that

they are also necessary developmentally for orienting and modulating the extent of growth cone protrusions.

Figure 3.1

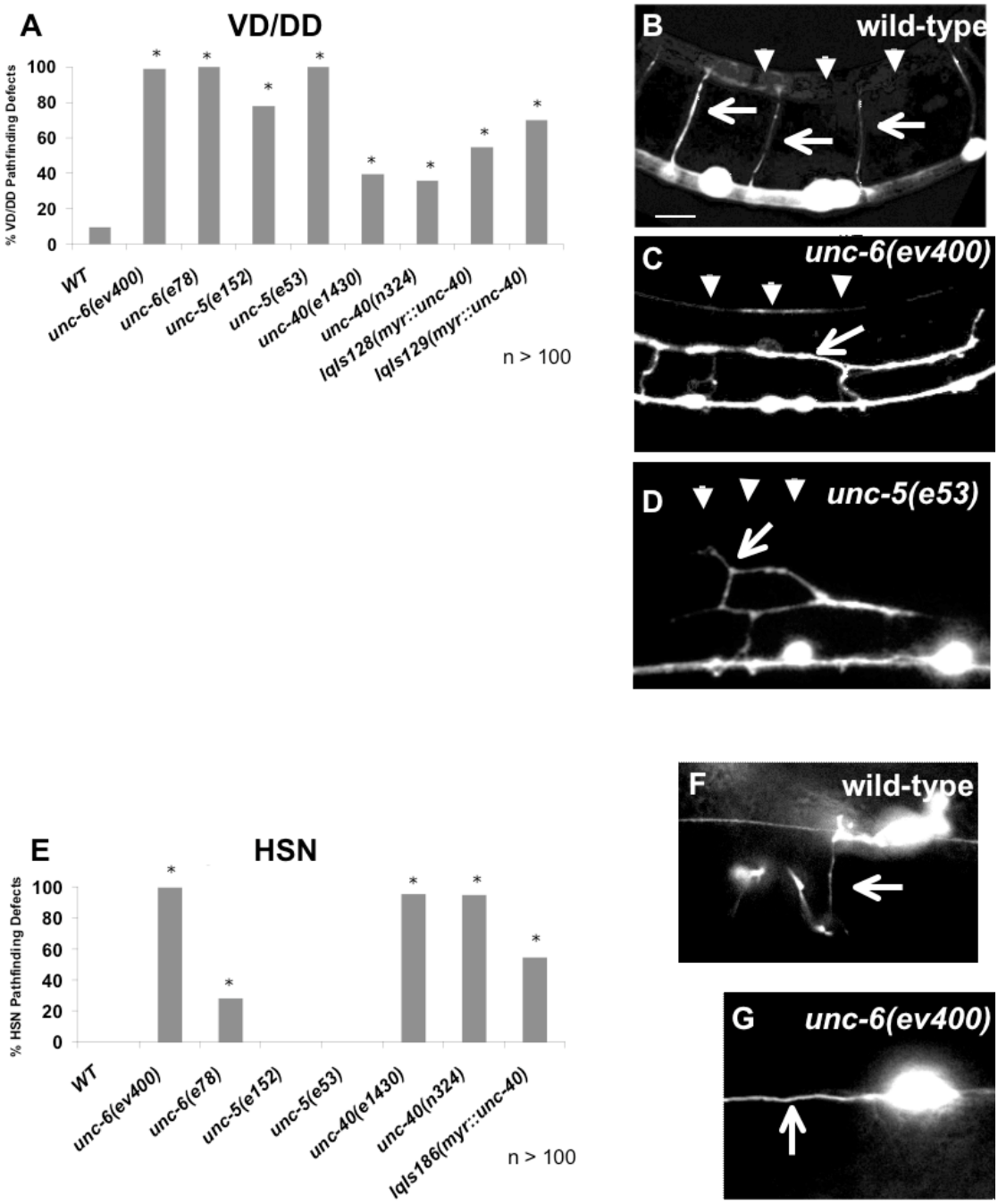
A
VD/DD
% VD/DD Pathfinding Defects
100
80
60
40
20
0
WT
unc-6(ev400)
unc-6(e78)
unc-5(e152)
unc-5(e53)
unc-40(e1430)
unc-40(n324)
lqIs128(myr::unc-40)
lqIs129(myr::unc-40)
n > 100
B
wild-type
C
unc-6(ev400)
D
unc-5(e53)
E
HSN
% HSN Pathfinding Defects
100
80
60
40
20
0
WT
unc-6(ev400)
unc-6(e78)
unc-5(e152)
unc-5(e53)
unc-40(e1430)
unc-40(n324)
lqIs186(myr::unc-40)
n > 100
F
wild-type
G
unc-6(ev400)

Figure 3.1 Netrin signaling mutants cause axon pathfinding defects. (A) Percentage of VD axons with pathfinding defects. (B-D) Fluorescent micrograph L4 VD axons; (B) normal pathfinding in WT axons; (C) misguided and prematurely stopped axons in *unc-6(ev400);* and (D) prematurely stopped and improperly branched axon in *unc-5(e53).* (E) Percentage of HSN axons with pathfinding defects. (F-G) Fluorescent micrographs of WT and *unc-6(ev400)* HSN axons; (F) normal pathfinding in WT; and (G) failure to migrate ventrally in *unc-6(ev400)*. Arrowheads delineate dorsal nerve cord, arrows point to axons. Asterisk denotes significant difference between wild type and the mutant ($p < 0.01$); $n \geq 100$; scale bar represents 5 μm.

Figure 3.2

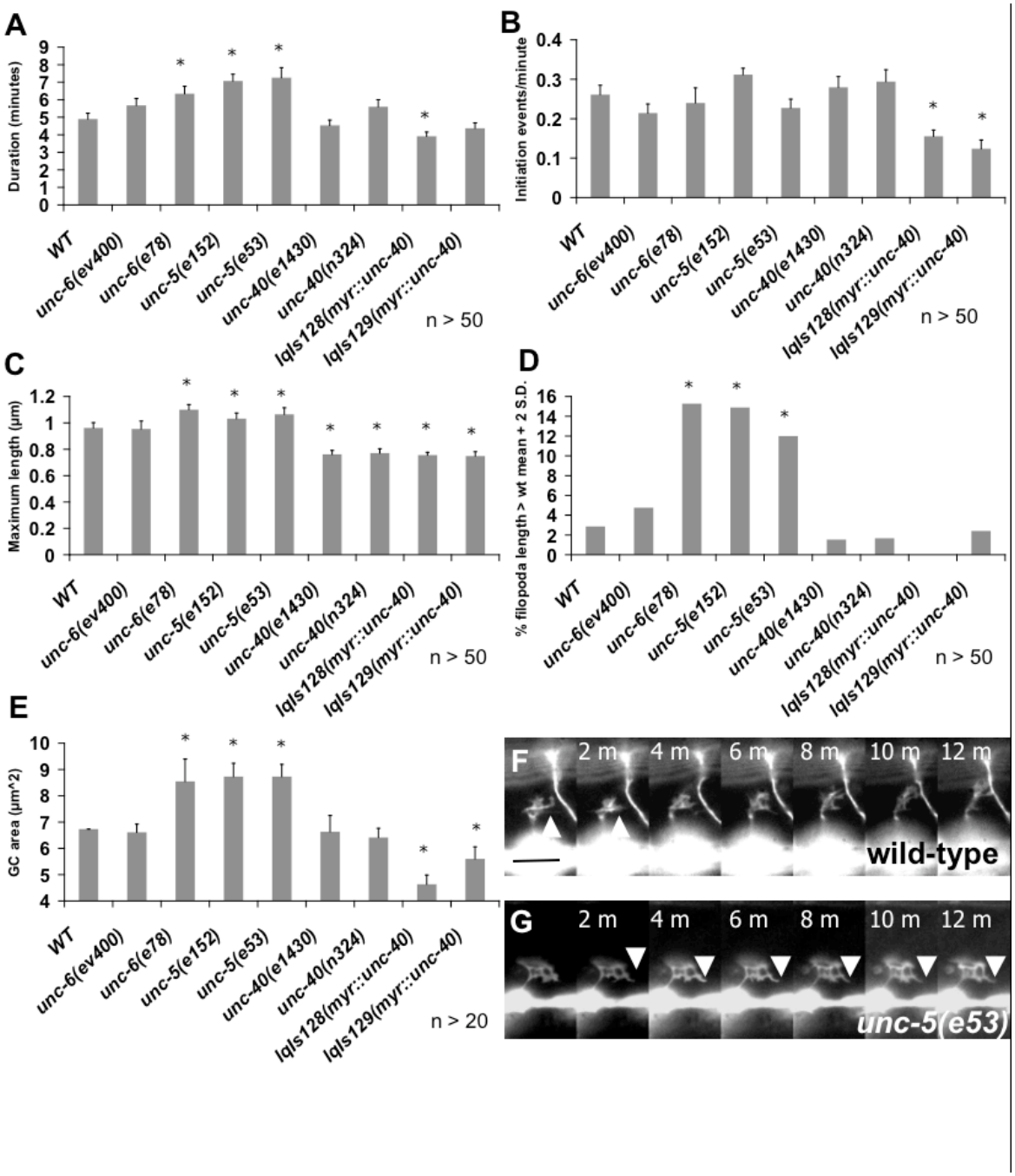
A
Duration (minutes)
B
Initiation events/minute
C
Maximum length (µm)
D
% filopoda length > wt mean + 2 S.D.
E
GC area (µm^2)
WT
unc-6(ev400)
unc-6(e78)
unc-5(e152)
unc-5(e53)
unc-40(e1430)
unc-40(n324)
lqIs128(myr::unc-40)
lqIs129(myr::unc-40)
n > 50
n > 20
F
2 m
4 m
6 m
8 m
10 m
12 m
wild-type
G
unc-5(e53)

Figure 3.2 Netrin signaling mutants cause VD growth cone morphology and dynamic defects. (A-D) Quantification of filopodia dynamics in VD growth cones. (A) Duration of filopodia once formed, in minutes; (B) Filopodia formation rate, in initiation events per minute; (C) Maximum filopodia length, in μm; and (D) Percentage of filopodia greater than the WT average + 2 standard deviations in length. (E) Growth cone area in μm^2. (F-G) Timelapse series of live growth cones, taken at 2 minutes per frame. (F) WT VD growth cone; and (G) *unc-5(e53)* growth cone. Arrows point to representative filopodia. Error bars represent standard error of the mean; asterisk denotes significant difference between wild type and the mutant ($p < 0.01$); $n \geq 50$; scale bar represents 5 μm.

Figure 3.3

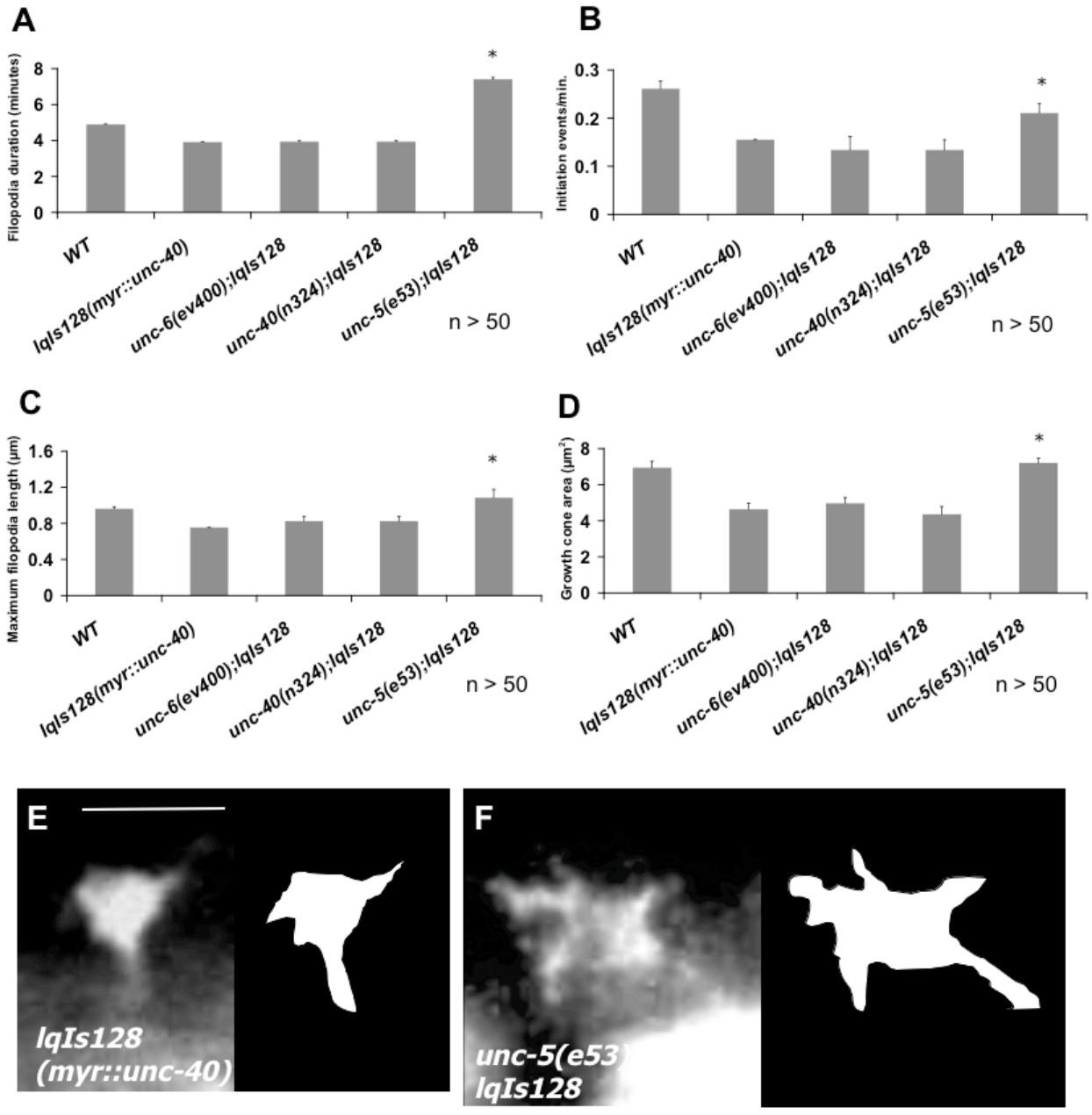
A
Filopodia duration (minutes)
0
2
4
6
8
*
WT
lqIs128(myr::unc-40)
unc-6(ev400);lqIs128
unc-40(n324);lqIs128
unc-5(e53);lqIs128
n > 50
B
Initiation events/min.
0
0.1
0.2
0.3
*
WT
lqIs128(myr::unc-40)
unc-6(ev400);lqIs128
unc-40(n324);lqIs128
unc-5(e53);lqIs128
n > 50
C
Maximum filopodia length (µm)
0
0.4
0.8
1.2
1.6
*
WT
lqIs128(myr::unc-40)
unc-6(ev400);lqIs128
unc-40(n324);lqIs128
unc-5(e53);lqIs128
n > 50
D
Growth cone area (µm²)
0
2
4
6
8
*
WT
lqIs128(myr::unc-40)
unc-6(ev400);lqIs128
unc-40(n324);lqIs128
unc-5(e53);lqIs128
n > 50
E
lqIs128
(myr::unc-40)
F
unc-5(e53)
lqIs128

Figure 3.3 Under-protrusive MYR::UNC-40 VD phenotypes are rescued by loss of UNC-5. (A-C) Quantification of filopodia dynamics in VD growth cones. (A) Duration of filopodia once formed, in minutes; (B) Filopodia formation rate, in initiation events per minute; (C) Maximum filopodia length, in μm. (D) Growth cone area in μm^2 (E-F) Fluorescent micrographs of mutant VD growth cones, showing inhibition of myr::unc-40 phenotype in an *unc-5(e53)* mutant background. Error bars represent standard error of the mean; asterisk denotes significant difference between *lqIs128* and the mutant ($p < 0.01$); $n \geq 50$; scale bar represents 5 μm.

Figure 3.4

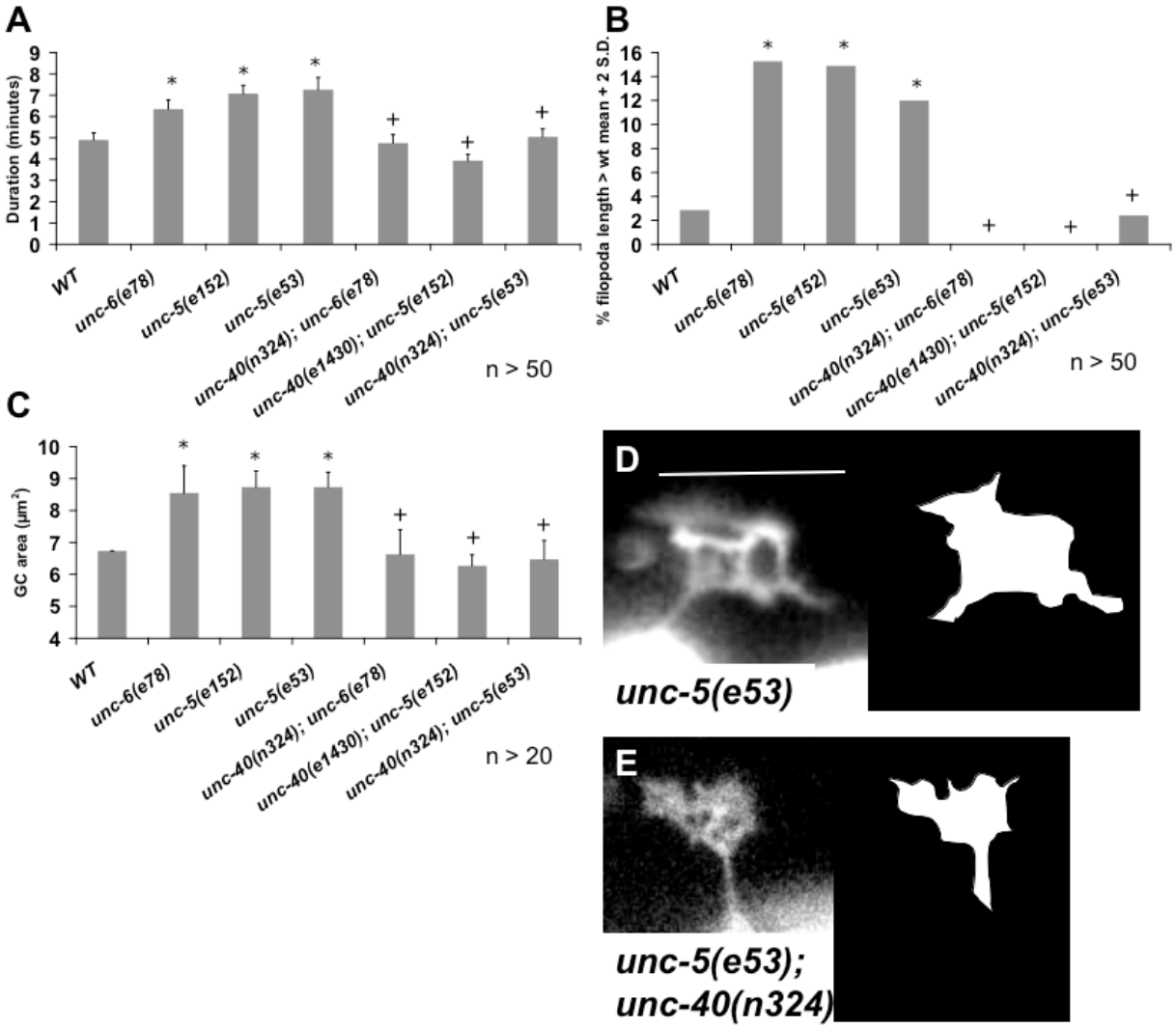
A
Duration (minutes)
WT
unc-6(e78)
unc-5(e152)
unc-5(e53)
unc-40(n324); unc-6(e78)
unc-40(e1430); unc-5(e152)
unc-40(n324); unc-5(e53)
n > 50
B
% filopoda length > wt mean + 2 S.D.
n > 50
C
GC area (μm²)
n > 20
D
unc-5(e53)
E
unc-5(e53);
unc-40(n324)

Figure 3.4 Over-protrusive *unc-5* VD phenotypes are mediated by UNC-40/DCC. Quantification of filopodia dynamics in VD growth cones. (A) Filopodia duration once formed, in minutes; and (B) Percentage of filopodia greater than WT length + 2 standard deviations. (C) Growth cone area, in μm^2. (D-E) Fluorescent micrographs showing reduction of over-protrusive phenotypes between *unc-5(e53)* single mutant and *unc-5(e53); unc-40(n324)* double mutant. Error bars represent standard error of the mean; asterisk denotes significant difference between wild type and the mutant ($P < 0.01$); plus sign denotes significant difference between double mutant and its respective protrusion-stimulating mutant ($p < 0.01$); $n \geq 50$; scale bar represents 5 μm.

Figure 3.5

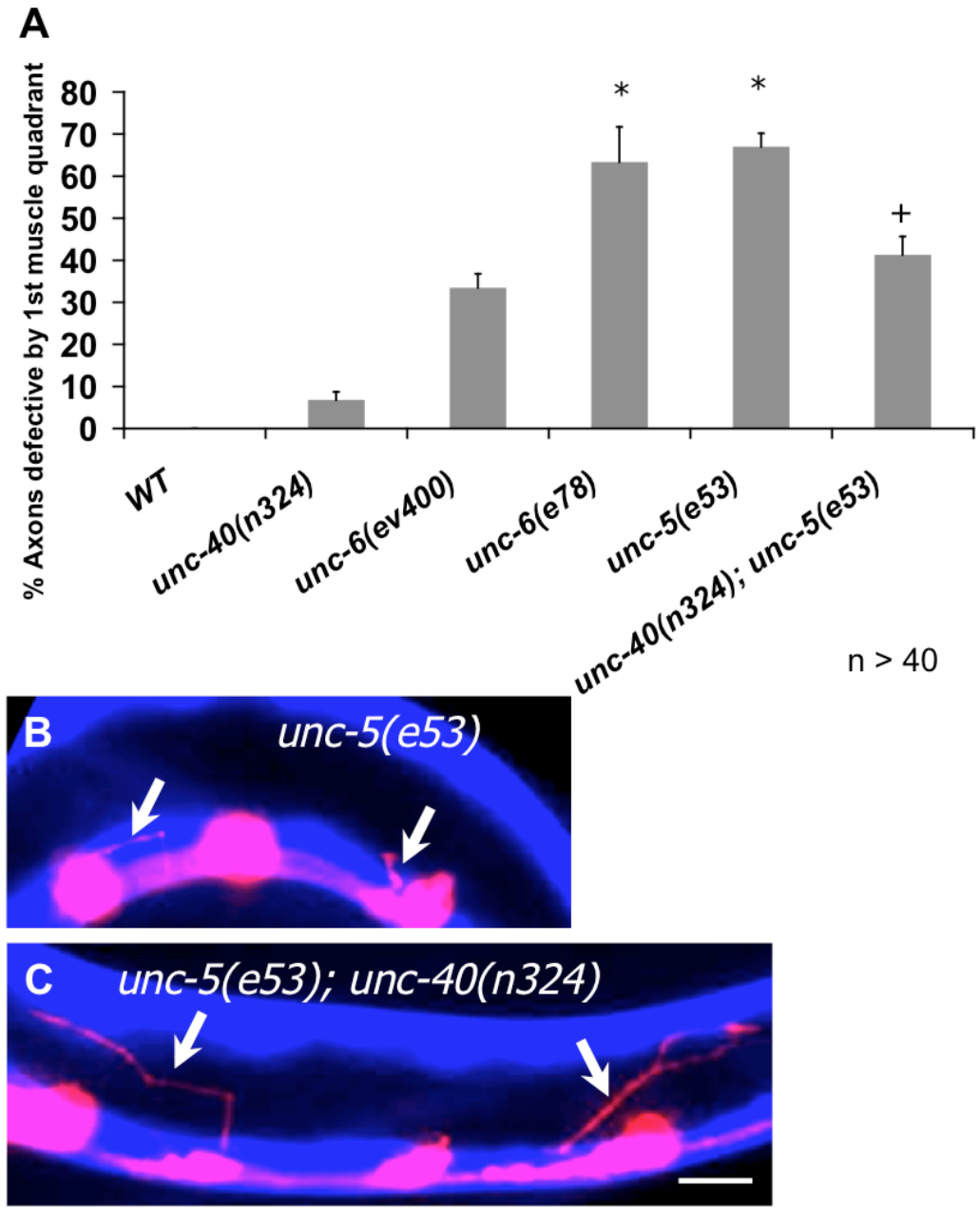
A
% Axons defective by 1st muscle quadrant
80
70
60
50
40
30
20
10
0
*
*
+
WT
unc-40(n324)
unc-6(ev400)
unc-6(e78)
unc-5(e53)
unc-40(n324); unc-5(e53)
n > 40
B
unc-5(e53)
C
unc-5(e53); unc-40(n324)

Figure 3.5 Severity of *unc-5(e53)* axon pathfinding defects is mitigated by loss of *unc-40.* (A) Percentage of VD axons that have pathfinding errors by the time they reach the dorsal edge of the ventral muscle quadrant. (B-C) Representative images showing VD axons in red and muscles in blue, demonstrating more severe axon pathfinding defects in the *unc-5(e53)* single mutant than in *unc-5(e53); unc-40(n324)* double mutant. Error bars represent standard error of the mean; asterisk denotes significant difference between wild type and the mutant ($P < 0.01$); plus sign denotes significant difference between double mutant and its respective protrusion-stimulating mutant ($p < 0.01$); $n \geq 50$; scale bar represents 5 μm.

Figure 3.6

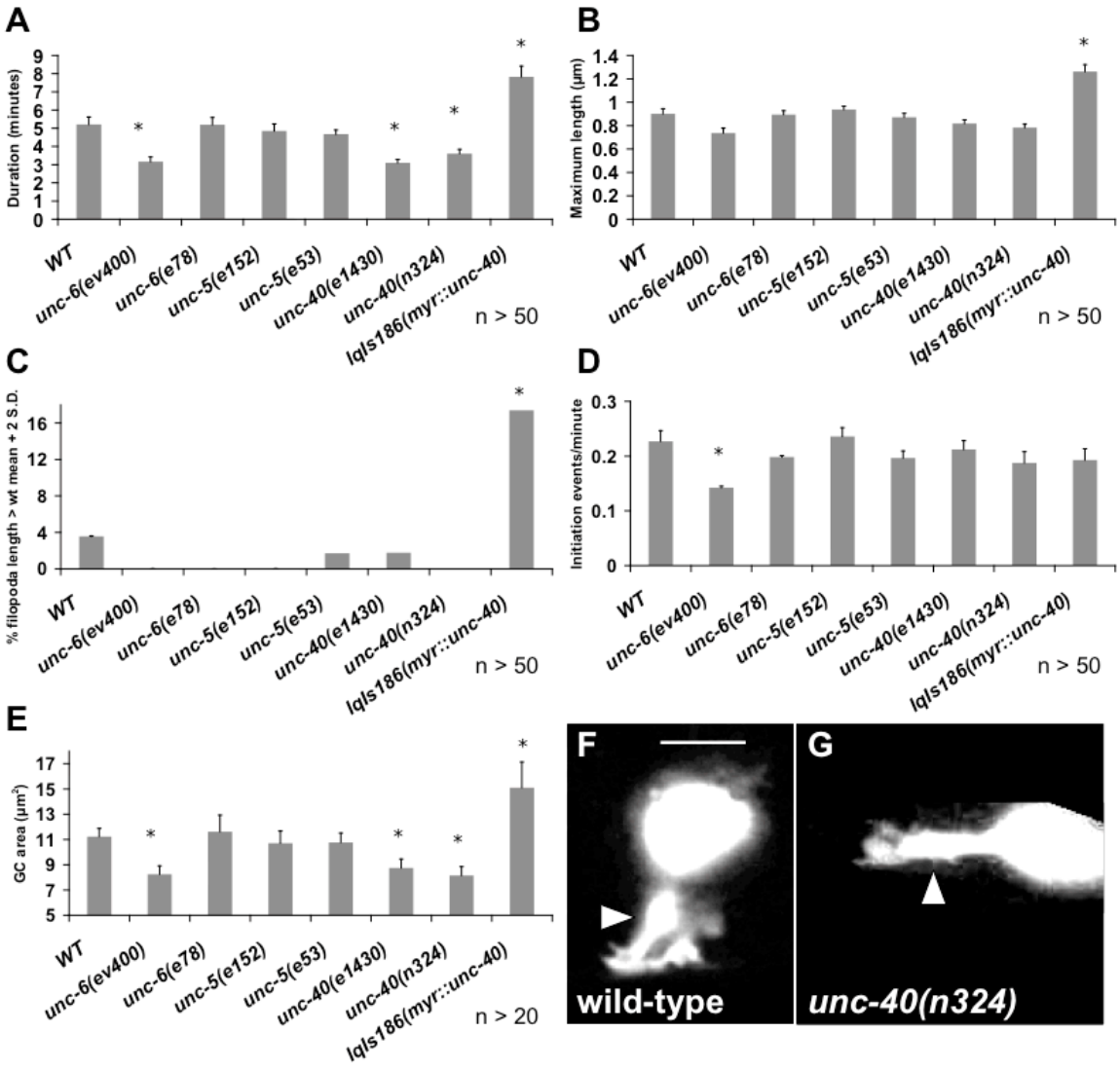
A
Duration (minutes)
B
Maximum length (μm)
C
% filopoda length > wt mean + 2 S.D.
D
Initiation events/minute
E
GC area (μm²)
WT
unc-6(ev400)
unc-6(e78)
unc-5(e152)
unc-5(e53)
unc-40(e1430)
unc-40(n324)
lqIs186(myr::unc-40)
n > 50
n > 20
F
wild-type
G
unc-40(n324)

Figure 3.6 Netrin signaling mutants cause HSN growth cone morphology and dynamic defects. (A-D) Quantification of filopodia dynamics in HSN growth cones. (A) Duration of filopodia once formed, in minutes; (B) Filopodia formation rate, in initiation events per minute; (C) Maximum filopodia length, in μm; and (D) Percentage of filopodia greaterthan the WT average + 2 standard deviations in length. (E) Growth cone area in μm^2. (F) WT HSN growth cone. (G) *unc-40(n324)* HSN growth cone. Error bars represent standard error of the mean; asterisk denotes significant difference between wild type and the mutant ($p < 0.01$); $n \geq 50$; scale bar represents 5 μm.

Figure 3.7

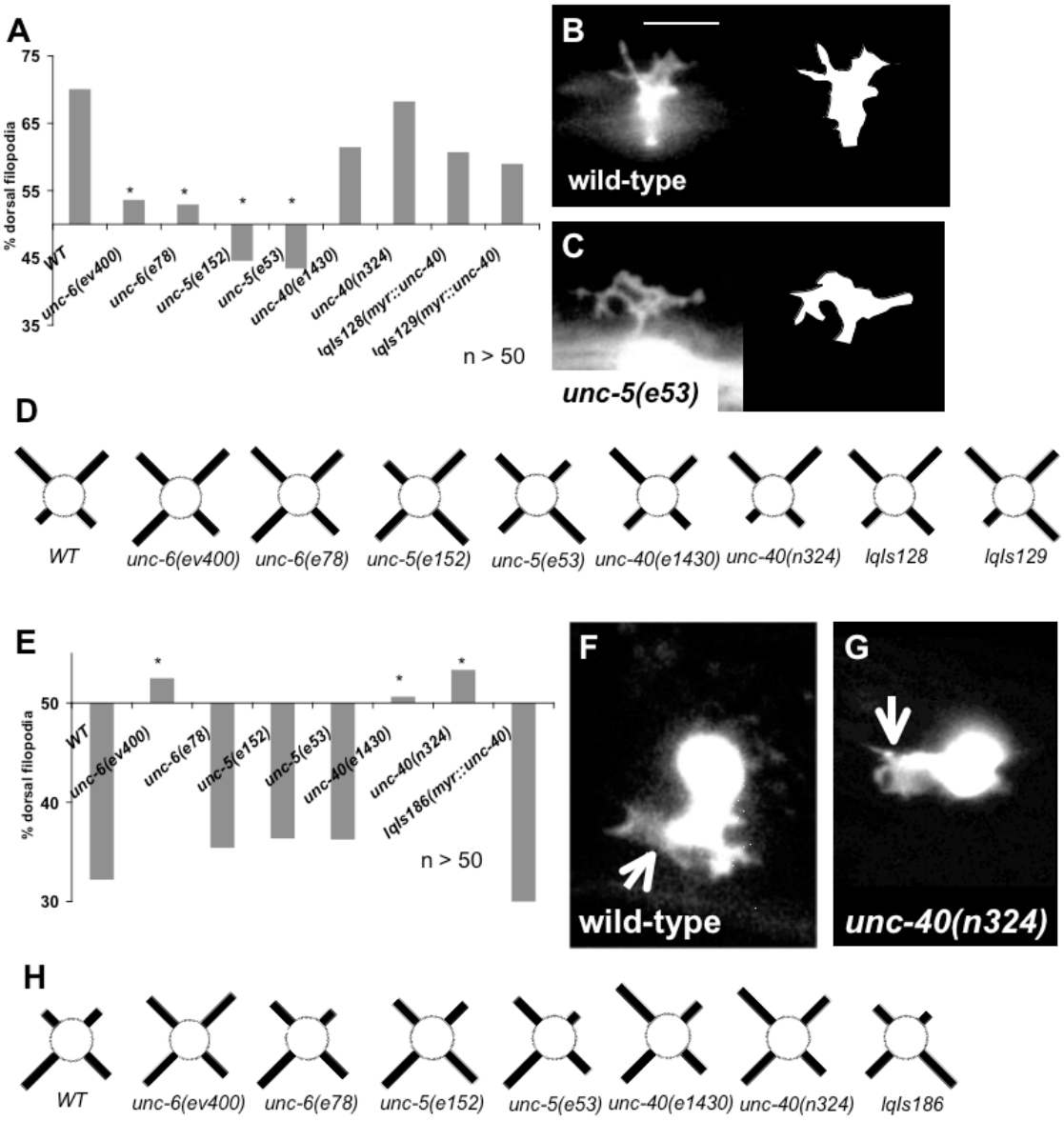
A
% dorsal filopodia
75
65
55
45
35
WT
unc-6(ev400)
unc-6(e78)
unc-5(e152)
unc-5(e53)
unc-40(e1430)
unc-40(n324)
lqIs128(myr::unc-40)
lqIs129(myr::unc-40)
n > 50
B
wild-type
C
unc-5(e53)
D
WT
unc-6(ev400)
unc-6(e78)
unc-5(e152)
unc-5(e53)
unc-40(e1430)
unc-40(n324)
lqIs128
lqIs129
E
% dorsal filopodia
50
40
30
WT
unc-6(ev400)
unc-6(e78)
unc-5(e152)
unc-5(e53)
unc-40(e1430)
unc-40(n324)
lqIs186(myr::unc-40)
n > 50
F
wild-type
G
unc-40(n324)
H
WT
unc-6(ev400)
unc-6(e78)
unc-5(e152)
unc-5(e53)
unc-40(e1430)
unc-40(n324)
lqIs186

Figure 3.7 Netrin signaling mutants cause growth cone polarity defects. (A) Percentage of filopodia protruding dorsally from VD growth cones. (B-C) Representative images of *WT* and *unc-6(ev400)* growth cones, with arrowheads marking filopodia. (D) Percentage of filopodia protruding dorsally from HSN growth cones. (E-F) Representative images of *WT* and *unc-40(n324)* growth cones, with arrowheads marking filopodia. (Leung-Hagesteijn) Graphical representation of percentage of filopodia protruding from each quadrant of the growth cone, dorsal is up and anterior to the left; (G) VD growth cones; and (H) HSN growth cones. Asterisk denotes significant difference between wild type and the mutant ($p < 0.01$); $n \geq 50$; scale bar represents 5 μm.

Figure 3.8

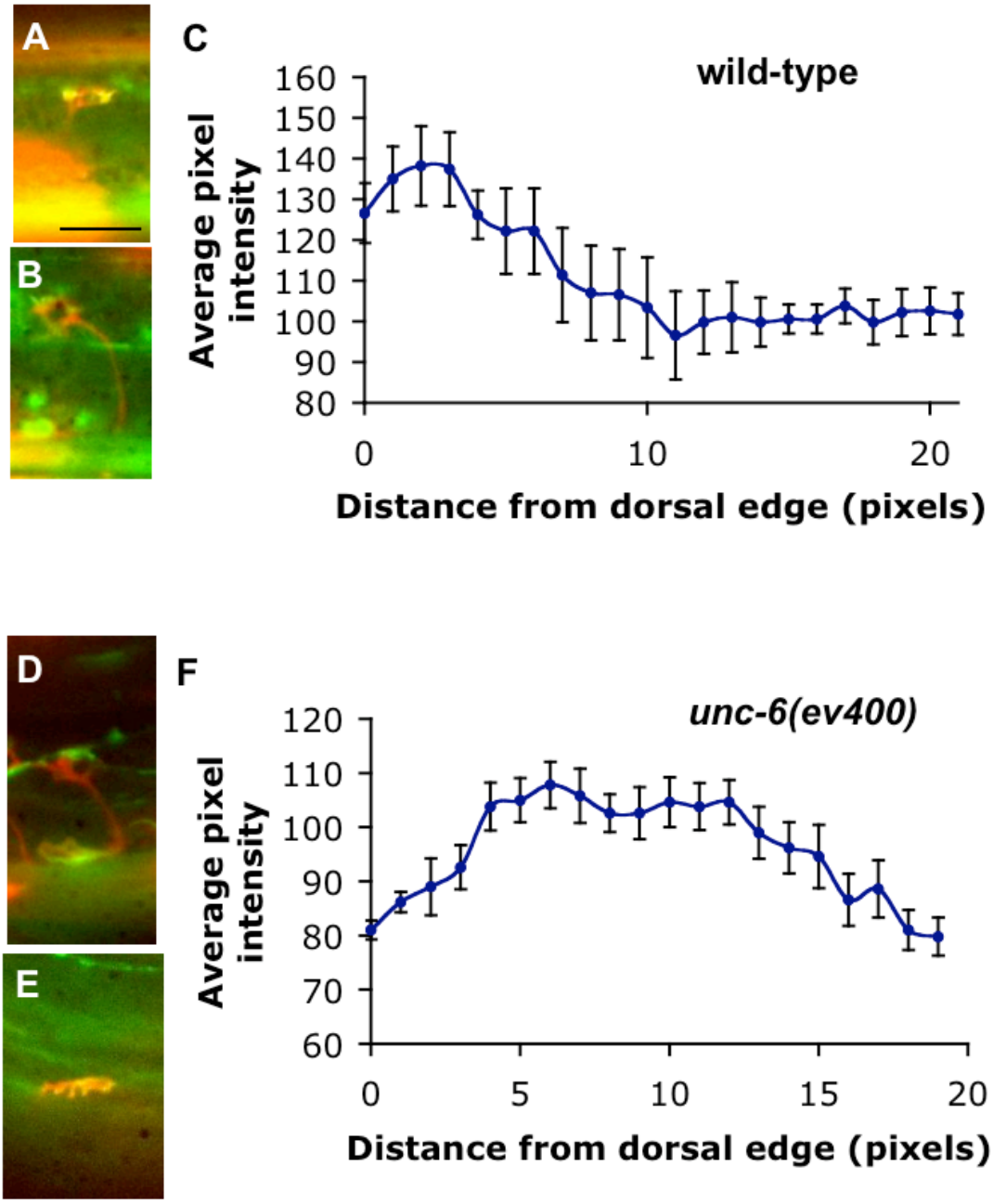
A
B
C
wild-type
Average pixel intensity
160
150
140
130
120
110
100
90
80
0
10
20
Distance from dorsal edge (pixels)
D
E
F
unc-6(ev400)
Average pixel intensity
120
110
100
90
80
70
60
0
5
10
15
20
Distance from dorsal edge (pixels)

Figure 3.8 Netrin signaling mutants cause loss of growth cone F-actin polarity. Representative images of WT growth cones; cytoplasmic mCherry in red, F-actin binding domain fused to GFP in green. (C) Representative line-plot of WT growth cone; X-axis represents distance (in pixels) from the dorsal edge of the growth cone of a line drawn vertically from the dorsal growth cone membrane to the ventral growth cone membrane, Y-axis represents average ABD::GFP pixel intensity (n=5 lines drawn through growth cone). (D-E) Representative images of *unc-6(ev400)* growth cones, as in (Gatlin et al.). (F) Representative line-plot of *unc-6(ev400)* growth cone, as in (C). Scale bar represents 5 μm.

Chapter IV

UNC-73/Trio, the Rac GTPases, UNC-33/CRMP and UNC-44/Ankyrin are required for limiting the extent of filopodia protrusion and ectopic axon branching in *C. elegans*

4.1 Abstract

The growth cone consists of actin-based lamellipodial and filopodial protrusions which provide both propulsive force and the sensation of extracellular guidance cues. While many molecules involved in axon pathfinding have been identified, little is known about their role in the developing growth cone. Here we show that UNC-73/Trio, the Rac GTPases, UNC-33/CRMP and UNC-44/Ankyrin, which are all known axon guidance genes, were required for the inhibition of excessive axon branching and the inhibition of filopodia protrusion in developing growth cones. The *unc-73* mutant phenotype was rescued by an activated *mig-2* construct, indicating that MIG-2 likely acts downstream of UNC-73. The ectopic axon defects seen in each of these mutants appeared to be a direct consequence of the filopodia protrusive defects. The genes studied here may be downstream of a repulsive UNC-40/UNC-5 heterodimer, as they suppressed an ectopically-expressed UNC-5-dependent activated UNC-40 phenotype in the VD growth cones. Thus we have described a developmental role for a series of genes known to be important for proper axon guidance, arriving at a developmental explanation for the defects seen in the endpoint analysis of the nervous system.

4.2 Introduction

The growth cone, located at the distal tip of a developing axon, senses and responds to guidance cues, directing the axon to its target destination (Mortimer et al. 2008; Tessier-Lavigne and Goodman 1996). The growth cone consists of a dynamic lamellipodium, a sheet-like structure consisting of an actin meshwork, and filopodia, spike-like protrusions consisting of bundled actin filaments (Pak et al. 2008; Zhou and Cohan 2004). Filopodia are thought to be involved in the sensation of directional cues and subsequent changes in directional locomotion (Gallo and Letourneau 2004).

The Rac GTPases are involved in axon pathfinding, through modulation or the actin cytoskeleton and stimulation of growth cone lamellipodia (de Curtis 2008; Hall and Lalli 2010). In *C. elegans* the Rac GTPases MIG-2 and CED-10 act redundantly to control axon outgrowth and guidance (Lundquist et al. 2001; Lundquist 2006). The Rho/Rac GEF UNC-73/Trio has been shown to act upstream of the Rac GTPases in *Drosophila* and *C. elegans* to control cytoskeletal rearrangements necessary for proper axon guidance (Bateman et al. 2000; Blangy et al. 2000; Kishore and Sundaram 2002; Lundquist et al. 2001; Steven et al. 1998).

The collapsin response mediator (CRMP) orthologue UNC-33 and the Ankyrin orthologue UNC-44 are both cytoskeletal regulators that are necessary for proper axon guidance, and physically interact with each other in *C. elegans* (Colavita and Culotti 1998; Fukata et al. 2002; Li 1992; A. J. Otsuka, Franco, R.,

Yang, B., Shim, K.-H., Tang, L.Z., Zhang, Y.Y., Boontrakulpoontawee, P., Jeyaprakash, A., Hedgecock, E., and Wheaton, V.I. 1995; Tsuboi et al. 2005; Zallen et al. 1999). Both proteins have been shown to act directly on the cytoskeleton, and thus are good candidates for genes that could be downstream effectors of axon pathfinding signal transduction pathways.

While much is known about the requirements of UNC-33, UNC-44, UNC-73 and the Rac GTPases from endpoint axon-pathfinding analysis, little is known about their effects on the developing growth cone. We thus set out to examine how these genes affect the dynamics and morphology of the developing growth cone, and how these growth cone effects impinge upon axon pathfinding. We show that *unc-73, unc-33, unc-44* and *mig-2; ced-10* mutants have strong increases in filopodia length and longevity, perhaps leading to the excessive ectopic axon branches observed in endpoint analyses. In contrast, constitutively active *mig-2* causes significant reductions in filopodia length and longevity. We also provide evidence that these genes may act in a linear pathway downstream of an UNC-40/UNC-5 Netrin-repulsed signaling complex.

4.3 Materials and Methods

Genetic methods

Experiments performed at 20°C using standard *C. elegans* techniques (Brenner 1974). These mutations and transgenics were used: X: *mig-2(mu28)*; I: *unc-73*(*rh40*); II: *juIs76* [*unc-25::gfp*]; IV: *unc-5*(*e53*), *unc-33(e204), unc-44(e362), ced-10(n1993)*. Chromosomal locations for the following transgenes were not determined: *lqIs128* [*unc-25::myr::unc-40*], and *lqIs182* [*unc-25::mig-2(G16V)*]. Extrachromosomal arrays were attained by injection into the germline, and then integrated into the genome via standard techniques (Mello and Fire 1995). Double mutants were confirmed by uncoordinated movement phenotype, axon pathfinding phenotype, and PCR genotyping. The *mig-2(mu28); ced-10(n1993M+)* strain was balanced with the nT1 balancer.

Imaging of axon guidance defects

VD neurons were visualized with an *unc-25::gfp* transgene (Jin et al. 1999), which is expressed in all GABAergic neurons, including the 16 VDs. VD axons were considered defective if the axon failed to reach the dorsal nerve cord or if it branched or turned at an angle greater than 45° before reaching the dorsal nerve cord.

Growth cone time-lapse imaging

VD growth cones were imaged as previously described (Norris et al. 2009). Briefly, animals harboring the *juIs76* [*unc-25::gfp*] transgene were selected 16 h post-hatching at 20°C and placed on a 2% agarose pad with a drop of 10mM muscimol (Sigm-Aldrich, St. Louis, MO USA) in M9 (Weinkove et al. 2008), which was allowed to evaporate for 3 to 4 minutes before placing coverslip. Growth cones were imaged with a Qimaging Rolera mGi camera on a Leica DMR microscope with BD CARV II wide-field light source. Images were acquired at intervals of 120 s, with total duration of time lapse ranging from 20 to 60 minutes. HSN growth cone time-lapse imaging was performed identically, except that animals were selected at 19 h post hatching.

Dynamic projections less than 0.5 μm in width emanating from the growth cone were scored as filopodia. Filopodia length and growth cone area were measured using ImageJ software. Significance of difference was determined in all cases by a two-sided *t*-test with unequal variance or a fisher's exact test.

4.4 Results

Mutations in *unc-73* and *mig-2; ced-10* cause defects in axon pathfinding.

UNC-73/Trio acts as a GEF for Rac and Rho GTPases and to be required for proper neuronal migration and axon guidance (de Curtis 2008). In *C. elegans* we can distinguish the Rac and Rho GEF activity of UNC-73 by utilizing the *unc-73(rh40)* mutation, which causes a Ser-1216 to Phe substitution, disrupting the Rac-GEF domain of UNC-73 but leaving the Rho-GEF domain intact (Lundquist et al. 2001; Steven et al. 1998) . We scored axon pathfinding defects in the VD/DD neurons in an *unc-73(rh40)* mutant background and found significant axon pathfinding errors, including ectopic axon branching. UNC-73 is a GEF for the Rac GTPases MIG-2 and CED-10 in *C. elegans (Lundquist et al. 2001; Steven et al. 1998).* We also scored axon pathfinding defects in these mutants, and found that in either single mutant there were little to no axon pathfinding defects, but in the *mig-2(mu28); ced-10(n1993M+)* double mutants there was a significant increase in pathfinding defects, including ectopic branches (Figure 1). The pathfinding defects were highly similar to *unc-73(rh40)* mutants (0% ectopic branches in wild-type, compared to 48% and 51% ectopic branches in *unc-73(rh40)* and *mig-2(mu28); ced-10(n1993M+)*; $p < 0.01$) (Figure 1).

Mutations in *unc-73* and *mig-2; ced-10* cause defects in growth cone dynamics.

To further probe the nature of the axon pathfinding errors we observed in *unc-73(rh40)* and *mig-2(mu28); ced-10(n1993M+),* we turned to live growth cone

analysis of the VDs as they developed beginning at 16 hours post-hatching. We found that both *unc-73(rh40)* and *mig-2(mu28); ced-10(n1993M+)* growth cones had significant increases in filopodia protrusiveness, exhibiting longer filopodia (0.96 μm in wild-type compared to 1.44 and 1.30 μm in *unc-73(rh40)* and *mig-2(mu28); ced-10(n1993M+);* $p < 0.01$) and longer duration of the filopodia once formed (4.9 minutes in wild-type compared to 10.5 and 8.0 minutes in *unc-73(rh40)* and *mig-2(mu28); ced-10(n1993M+)*; $p < 0.01$) (Figure 2). Indeed, some filopodia endured throughout the length of the experiment (greater than 20 minutes), and in some cases the growth cone appeared to disintegrate, and the exceptionally long filopodia seemed to consolidate into the appearance of a prematurely terminated axon with ectopic branches, similar to the previously-described ectopic axon branches seen in adults.

Ectopically expressed constitutively-activated *mig-2* causes growth cone defects and rescues the *unc-73* phenotype.

We next asked what effect a gain-of-function mutation in the Rac GTPase MIG-2 would have on the dynamics of the growth cone. The Gly-16 to Val substitution results in a constitutively GTP-bound, active version of MIG-2(Lundquist et al. 2001). We expressed this construct in VD/DD motorneurons and found that growth cone filopodia protrusiveness was inhibited, with a reduction in filopodia duration (4.9 minutes in wild-type compared to 3.6 minutes in *mig-2(G16V)*; $p < 0.01$) and length (0.96 μm in wild-type compared to 0.68 μm in *mig-2(G16V)*; $p < 0.01$) (Figure 3). This phenotype is the opposite of the

phenotype observed in *unc-73* and *mig-2; ced-10* mutants. This prompted us to ask whether or not the active *mig-2(G16V)* could rescue the defects seen in the *unc-73(rh40)* background. Indeed, in *unc-73(rh40); mig-2(G16V)* double mutants we observed a significant reduction in filopodia protrusiveness when compared to the *unc-73(rh40)* single mutant, with a decrease in filopodia duration (10.5 minutes in *unc-73(rh40)* compared to 3.9 minutes in *unc-73(rh40); mig-2(G16V)*; $p < 0.01$) as well as filopodia length (1.44 μm in *unc-73(rh40)* compared to 0.79 μm in *unc-73(rh40); mig-2(G16V)*; $p < 0.01$) (Figure 3). All of these data are consistent with the idea that MIG-2, and perhaps CED-10 as well, work downstream of and are activated by UNC-73.

The cytoskeletal-binding mutants *unc-33* and *unc-44* have similar increases in ectopic axon branches and excessive filopodia protrusion to *unc-73* and *mig-2; ced-10* mutants.

The cytoskeletal regulators UNC-33/CRMP and UNC-44/Ankyrin are involved in tubulin and actin dynamics, and necessary for proper axon outgrowth and guidance (Colavita and Culotti 1998; Fukata et al. 2002; Li 1992; A. J. Otsuka, Franco, R., Yang, B., Shim, K.-H., Tang, L.Z., Zhang, Y.Y., Boontrakulpoontawee, P., Jeyaprakash, A., Hedgecock, E., and Wheaton, V.I. 1995; Tsuboi et al. 2005; Zallen et al. 1999). We observed that both mutants had similar endpoint axon pathfinding defects to those seen in *unc-73* and *mig-2; ced-10* mutants (48% ectopic branches in *unc-73(rh40)* compared to 48% and 56% in *unc-33(e204)* and *unc-44(e362)*) (Figure 1). They also had similar growth

cone filopodia protrusion phenotypes, with increases in filopodia duration (10.5 minutes in *unc-73(rh40)* compared to 9.3 minutes in *unc-33(e204)* and *unc-44(e362);* $p < 0.01$) and length (1.44 µm in *unc-73(rh40)* compared to 1.30 µm in *unc-33(e204)* and *unc-44(e204);* $p < 0.01$) (Figure 4). These findings raised the possibility that *unc-33* and *unc-44* could be functioning in the same pathway as *unc-73*, *ced-10* and *mig-2.* Further evidence for this hypothesis was provided by the fact that both *unc-33* and *unc-73* suppressed an activated UNC-40 and thus may be downstream effectors (see below).

unc-73, unc-33 and _unc-44_ rescue the morphological phenotypes in a constitutively active MYR::UNC-40/UNC-5 repulsive signaling complex in VD growth cones

We had previously constructed a constitutively active form of UNC-40/DCC based on (Gitai et al. 2003), by adding an N-terminal myristoylation signal to the cytoplasmic domain of UNC-40 lacking the transmembrane and extracellular domains, which normally function to inhibit receptor dimerization in the absence of UNC-6/Netrin. Introduction of this construct into VD growth cones caused MYR::UNC-40 to constitutively dimerize with UNC-5 and mediate a repulsive response, which resulted in a morphological phenotype similar to the *mig-2(G16V)* construct described here, and opposite of the *unc-73, mig-2; ced-10*, *unc-33* and *unc-44* mutants (Norris et al. 2009). We thus tested whether the genes described here might be downstream of this active MYR::UNC-40/UNC-5 signaling complex. Indeed, both of the mutants tested suppressed the filopodia

dynamics defects observed in *myr::unc-40*. Filopodia duration (for example, 3.9 minutes in *myr::unc-40* compared to 8.2 minutes in *unc-73(rh40);* $p < 0.01$) and length (for example, 0.76 µm in *myr::unc-*40 compared to 1.52 µm in *unc-73(rh40); myr::unc-40*); $p < 0.01$) (Figure 5) were restored to levels comparable to or greater than wild-type in the double mutants.

These results suggest that *unc-73, unc-33* and *unc-44* are required for the repulsive, anti-protrusive phenotypes observed in a *myr::unc-40* growth cone.

mig-2(G16V) fails to suppress the *unc-5* gain-of-protrusion phenotype in VD growth cones

We had also previously shown that loss of *unc-5* in VD growth cones caused an over-protrusive phenotype that was dependent on UNC-40, probably mediated by an active, attractive, pro-protrusive UNC-40 homodimer (Norris et al. 2009). The observation that UNC-73 was in the same pathway as the anti-protrusive MYR::UNC-40/UNC-5 heterodimer led us to test whether UNC-73, and its effector MIG-2, might also be in the same pathway as the pro-protrusive UNC-40/UNC-40 homodimer. Interestingly, *unc-5(e53); mig-2(G16V)* double mutants failed to rescue any of the morphological defects seen in *unc-5(e53)* mutants alone (for example, filopodia duration of 7.26 minutes in *unc-5(e53)* compared to 7.06 minutes in *unc-5(e53); mig-2(G16V);* $p > 0.05$) (Figure 3).

These findings suggest that UNC-73 and the Rac GTPases are acting downstream of MYR::UNC-40/UNC-5 heterodimers which act to inhibit growth cone protrusion, but not downstream of UNC-40/UNC-40 homodimers which act

to stimulate growth cone protrusion.

4.5 Discussion

UNC-73 signals through MIG-2 to limit axon branching and limit the extent of filopodia protrusion

The results presented here show that UNC-73/Trio and the Rac GTPases are required to limit the extent of filopodia protrusion. Loss of *unc-73* or *mig-2* and *ced-10* led to a significant increase in filopodia length and longevity, while a constitutively active *mig-2* led to a significant decrease in filopodia length and longevity. This activated *mig-2* rescues defects observed in the *unc-73* background, suggesting that *unc-73* may regularly be functioning to activate *mig-2* in VD growth cones. UNC-73/Trio has previously been shown to regulate the Racs in axon pathfinding (Kishore and Sundaram 2002; Lundquist et al. 2001; Steven et al. 1998), and here we show that their role may be in limiting the extent of filopodia protrusion in the growth cone. This is somewhat unexpected given the fact that the Rac GTPases are usually thought to be involved in the stimulation of lamellipodial protrusion (Hall and Nobes 2000; Hall 2005; Hall and Lalli 2010), while our studies here show that the Rac GTPases are involved in the inhibition of filopodia and have no apparent defects on the lammelipodium *in vivo* in *C. elegans* VD growth cones.

UNC-33 and UNC-44 are required to limit the extent of filopodia protrusion

UNC-33/CRMP and UNC-44/Ankyrin are both cytoskeletal-binding proteins (Fukata et al. 2002; A. J. Otsuka et al. 2002). It has previously been

shown that UNC-33/CRMP binds tubulin and is required for proper axonal migration, and that UNC-44/Ankyrin binds actin (via spectrin) and is likewise required for proper axonal migration (Fukata et al. 2002; Hopitzan et al. 2006). It has furthermore been shown that UNC-33 and UNC-44 interact physically, and that their individual mutant phenotypes resemble each other in endpoint axon pathfinding analyses (Li 1992; A. J. Otsuka, Franco, R., Yang, B., Shim, K.-H., Tang, L.Z., Zhang, Y.Y., Boontrakulpoontawee, P., Jeyaprakash, A., Hedgecock, E., and Wheaton, V.I. 1995). We confirmed that *unc-33* and *unc-44* mutants have similar axon pathfinding phenotypes in the VD/DD motorneurons, exhibiting a high degree of ectopic axon branching, at levels similar to *unc-73* or *mig-2; ced-10* mutants. We also showed that they have similar growth cone morphology phenotypes, exhibiting an increase in filopodia length and duration, similar to the *unc-73* and *mig-2; ced-10* phenotypes. We have thus elucidated the roles of two cytoskeletal regulators in growth cone morphology and dynamics.

UNC-73, the Rac GTPases, UNC-33 and UNC-44 may function downstream of an UNC-40/UNC-5 repulsive guidance response

We demonstrate that mutations in either *unc-73, unc-33* or *unc-44* were able to suppress a constitutively active *myr::unc-40* construct expressed in the VDs. We previously demonstrated that this construct acts in an *unc-5*-dependent manner to limit protrusion, probably through the formation of MYR::UNC-40/UNC-5 heterodimers that act as a constitutively repulsive signaling complex in VD growth cones (Norris et al. 2009). Based on the observation that both of the

mutants tested suppressed the under-protrusive phenotypes observed in the *myr::unc-40* background, we hypothesize that *unc-73* and *unc-33* are likely required for an UNC-40/UNC-5 repulsive growth cone response to limit the extent of filopodia protrusion in VD neurons.

On the other hand, loss of *unc-5* in the VDs resulted in an over-protrusive phenotype, including greater filopodia protrusion. We previously showed that this phenotype is likely due to increased UNC-40 homodimerization in the growth cone, leading to over-stimulation of growth cone protrusion (Norris et al. 2009). We showed here that while an ectopically expressed *mig-2(G16V)* construct rescued the over-protrusive phenotypes observed in an *unc-73* loss of function, it failed to rescue the over-protrusive phenotypes observed in an *unc-5* loss of function, suggesting that the Rac GTPases may not be required for an UNC-40/UNC-40 attractive growth cone response. Taken together, these results suggest that *unc-73,* the Rac GTPases and *unc-33* may act downstream of an UNC-40/UNC-5 repulsive signal, but not downstream of an UNC-40/UNC-40 attractive signal.

Relationship between the extent of filopodia protrusion and ectopic axon branching

We have shown here that for each case in which a mutant displayed excessive filopodia length and duration in the growth cone, it also displayed excessive ectopic branches in axons of the developed nervous system. We interpret this to mean that the ectopic axon branches observed in the adults may

be a direct result of the growth cone defects observed in the developing larvae. This idea is strengthened by the observation that at times the developing mutant growth cones with excessively long filopodia appeared to disintegrate and leave stable protrusions, similar in appearance to axon branches, where the dynamic filopodia once were. Thus these studies provide a link between the dynamics of growth cone protrusion and the endpoint analysis of axon pathfinding.

4.6 Future Directions

There remain a number of interesting questions to be asked in this project. One of the most direct questions is whether or not *unc-33* and *unc-44* suppress the *mig-2(G16V)* construct. If they do, it would further support our model of *unc-33* and *unc-44* acting downstream of *unc-73* and the Rac GTPases as effectors of filopodia protrusion inhibition.

Similarly, having already implicated *unc-33* as being downstream of the MYR::UNC-40 inhibition-of-protrusion phenotype, it will be instructive to know whether or not *unc-44* acts similarly.

Furthermore, it would be interesting to know whether or not CED-10 acts similarly to MIG-2 to limit filopodial protrusions, and whether or not it suppresses *unc-73(rh40)*. Unfortunately, the necessary construct has yet to be successfully transformed into worms.

The *unc-73(rh40); mig-2(G16V)* strain has yet to be scored for axon pathfinding and branching phenotypes. If the *mig-2(G16V)* were to rescue the branching phenotype seen in the *unc-73(rh40)* single-mutant, it would support the idea that excessive filopodia protrusion directly leads to ectopic axon branching.

Finally, it would be useful to observe growth cones with excessively long filopodia, rescue the worms onto plates, then re-image the worms in adulthood to see if in fact whether or not the seemingly stable filopodia have consolidated into

mature axons with ectopic branches. This would be a final piece of information needed to confirm the hypothesis that the filopodia dynamic defects observed in these mutants directly leads to the axon pathfinding defects.

Figure 4.1

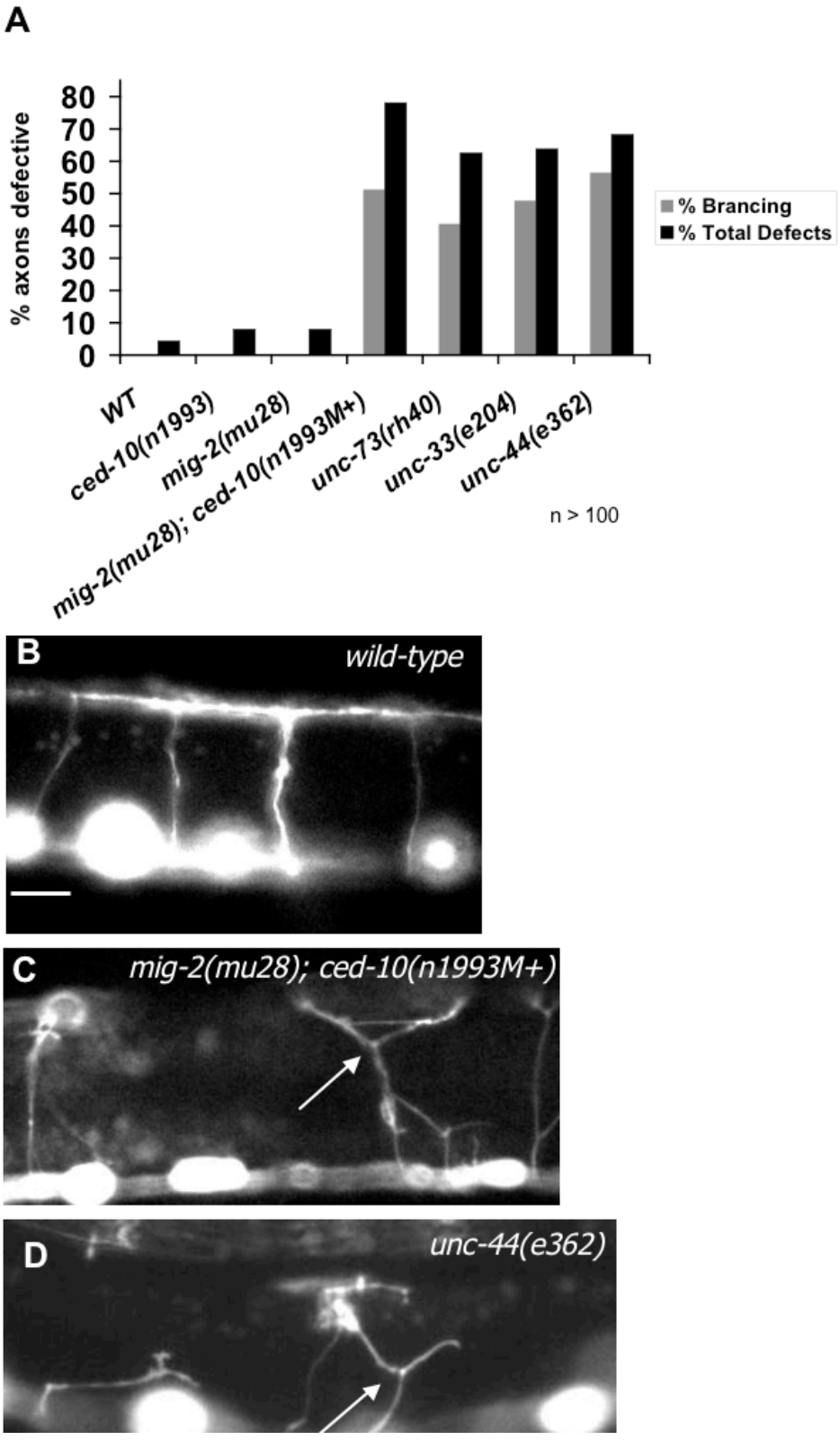
A
% axons defective
80
70
60
50
40
30
20
10
0
% Brancing
% Total Defects
WT
ced-10(n1993)
mig-2(mu28)
mig-2(mu28); ced-10(n1993M+)
unc-73(rh40)
unc-33(e204)
unc-44(e362)
n > 100
B
wild-type
C
mig-2(mu28); ced-10(n1993M+)
D
unc-44(e362)

Figure 4.1 Mutations in Rac GTPases and in the Rac GEF UNC-73/Trio cause defects in VD/DD axon pathfinding (A) Quantification of VD/DD axon pathfinding defects and ectopic axon branches. (B-D) Representative fluorescent micrographs of VD/DD axons demonstrating axon pathfinding and branching errors. (B) Wild-type; (C) *mig-2(mu28); ced-10(n1993M+*; and (D) *unc-44(e362)* VD/DD axons. Arrows point to ectopic axon branches.

Figure 4.2

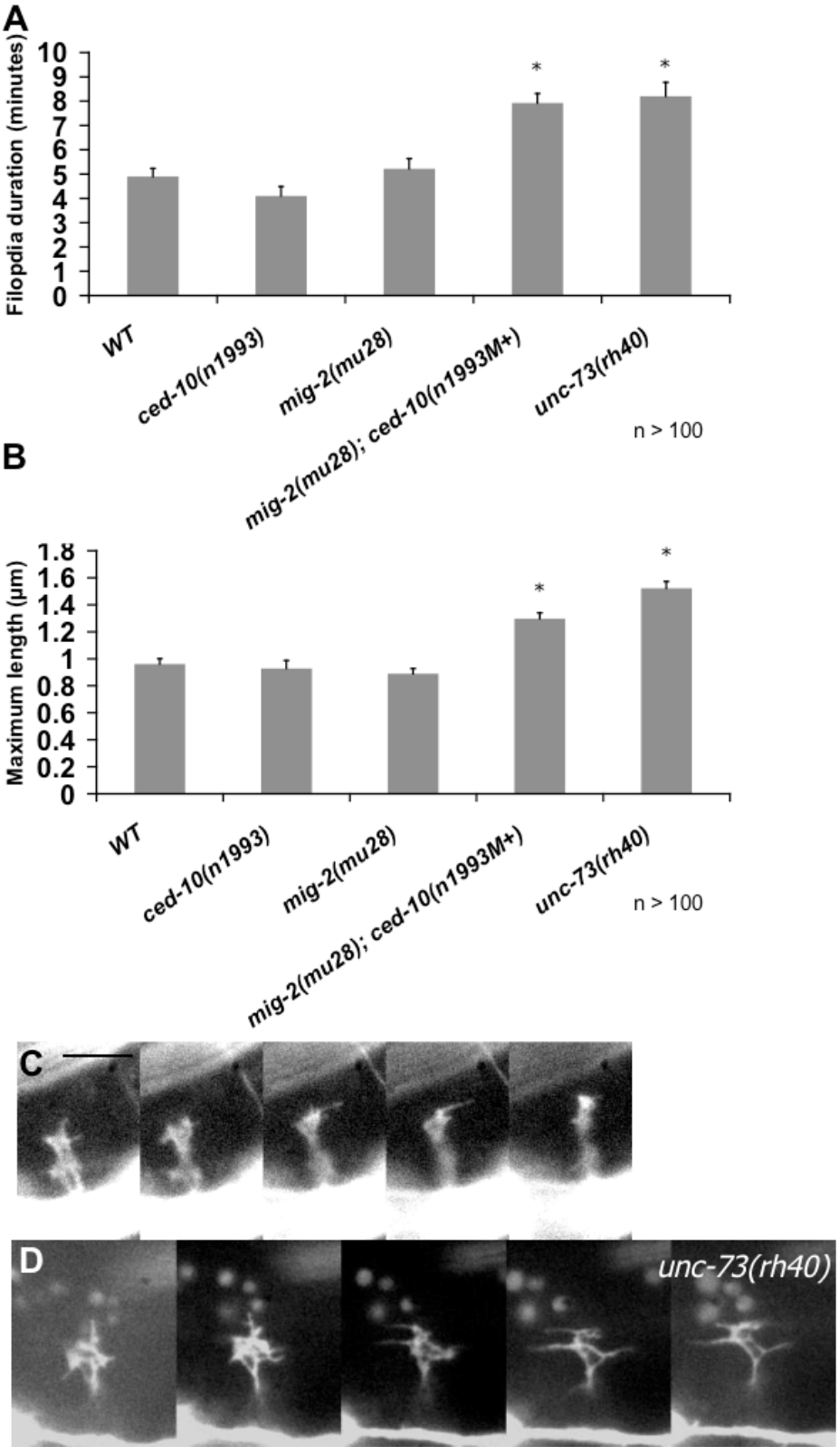
A
Filopdia duration (minutes)
10
9
8
7
6
5
4
3
2
1
0
*
*
WT
ced-10(n1993)
mig-2(mu28)
mig-2(mu28); ced-10(n1993M+)
unc-73(rh40)
n > 100
B
Maximum length (µm)
1.8
1.6
1.4
1.2
1
0.8
0.6
0.4
0.2
0
*
*
WT
ced-10(n1993)
mig-2(mu28)
mig-2(mu28); ced-10(n1993M+)
unc-73(rh40)
n > 100
C
D
unc-73(rh40)

Figure 4.2 Mutations in Rac GTPases and in the Rac GEF UNC-73/Trio cause defects in VD growth cone filopodia dynamics. Quantification of filopodia dynamic defects in VD growth cones. (A) Filopodia duration (in minutes); and (B) Maximum filopodia length (in μm). (C-E) Timelapse series of live growth cones, taken at 2 minutes per frame. (C) Wild-type growth cone; and (D) *unc-73(rh40)* growth cone. Error bars represent standard error of the mean; asterisk denotes significant difference between wild-type and the mutant ($p < 0.01$); $n \geq 100$; scale bar represents 5 μm.

Figure 4.3

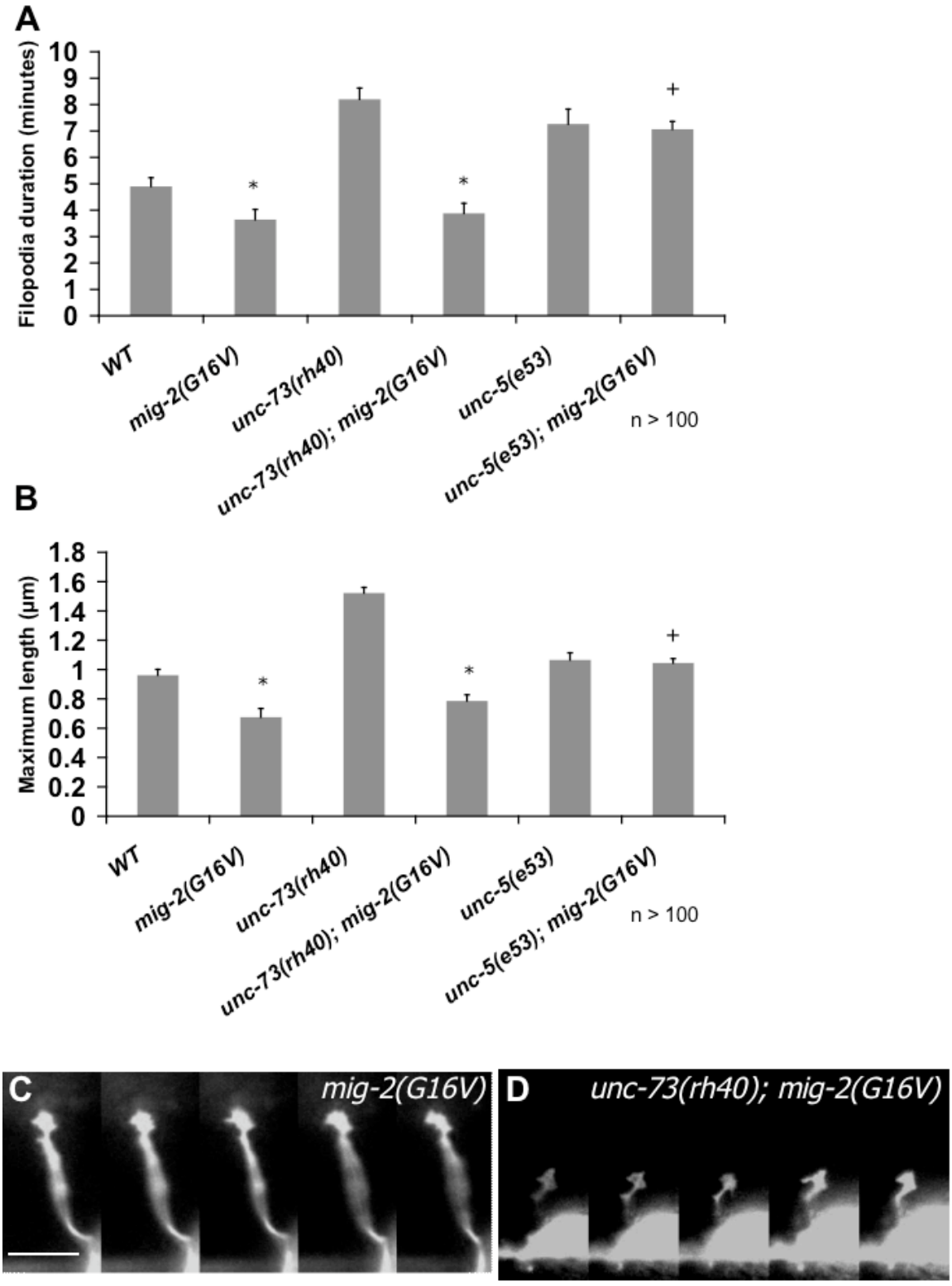
A
Filopodia duration (minutes)
0
1
2
3
4
5
6
7
8
9
10
*
*
+
WT
mig-2(G16V)
unc-73(rh40)
unc-73(rh40); mig-2(G16V)
unc-5(e53)
unc-5(e53); mig-2(G16V)
n > 100
B
Maximum length (µm)
0
0.2
0.4
0.6
0.8
1
1.2
1.4
1.6
1.8
*
*
+
WT
mig-2(G16V)
unc-73(rh40)
unc-73(rh40); mig-2(G16V)
unc-5(e53)
unc-5(e53); mig-2(G16V)
n > 100
C
mig-2(G16V)
D
unc-73(rh40); mig-2(G16V)

Figure 4.3 Expressing constitutively active MIG-2 in VD growth cones causes a reduction in extent of filopodia protrusion, and rescues filopodia dynamic defects observed in *mig-2(mu28); ced-10(n1993+)* and *unc-73(rh40)* mutants. Quantification of filopodia dynamics in VD growth cones. (A) Duration of filopodia (in minutes); and (B) Maximum length of filopodia (in μm). (C-D) Timelapse series of live growth cones, taken at 2 minutes per frame. (C) *mig-2*(G16V) growth cones; and (D) *unc-73(rh40); mig-2(G16V)* growth cones. Error bars represent standard error of the mean; asterisk denotes significant difference between wild-type and the mutant ($p < 0.01$), + denotes significant difference between *mig-2(G16V)* and double-mutant ($p < 0.01$); $n \geq 100$; scale bar represents 5 μm.

Figure 4.4

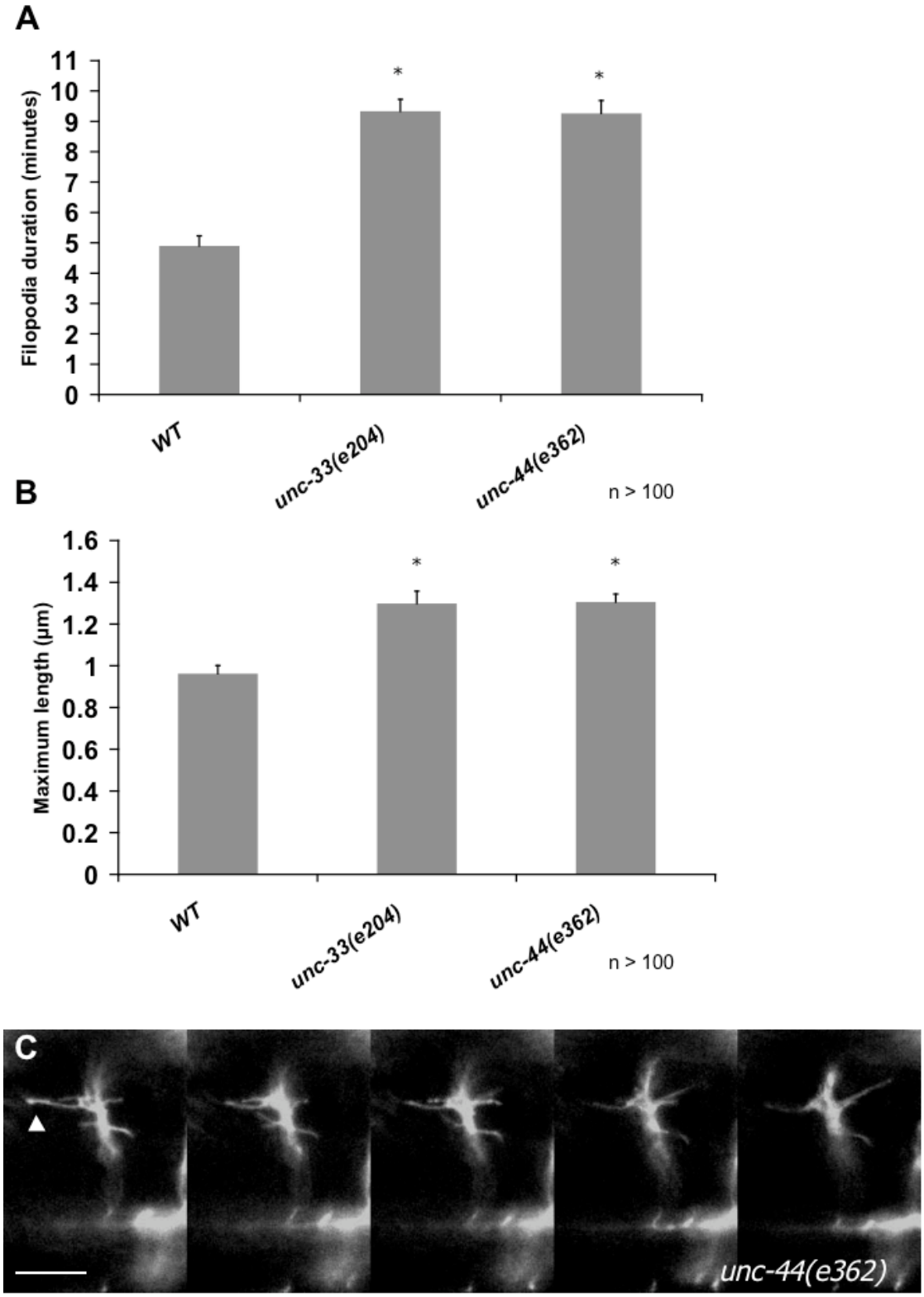
A
Filopodia duration (minutes)
11
10
9
8
7
6
5
4
3
2
1
0
*
*
WT
unc-33(e204)
unc-44(e362)
n > 100
B
Maximum length (µm)
1.6
1.4
1.2
1
0.8
0.6
0.4
0.2
0
*
*
WT
unc-33(e204)
unc-44(e362)
n > 100
C
unc-44(e362)

Figure 4.4 Mutations in *unc-33* or *unc-44* cause growth cone defects similar to those seen in *mig-2(mu28); ced-10(n1993M+)* and *unc-73(rh40).*

Quantification of filopodia dynamics in VD growth cones. (A) Duration of filopodia (in minutes); and (B) maximum length of filopodia (in μm). (C) Timelapse series of live *unc-44(e362)* growth cones, taken at 2 minutes per frame. Error bars represent standard error of the mean; asterisk denotes significant difference between wild-type and the mutant ($p < 0.01$); $n \geq 100$; scale bar represents 5 μm. Arrowhead shows excessively long, stable filopodium

Figure 4.5

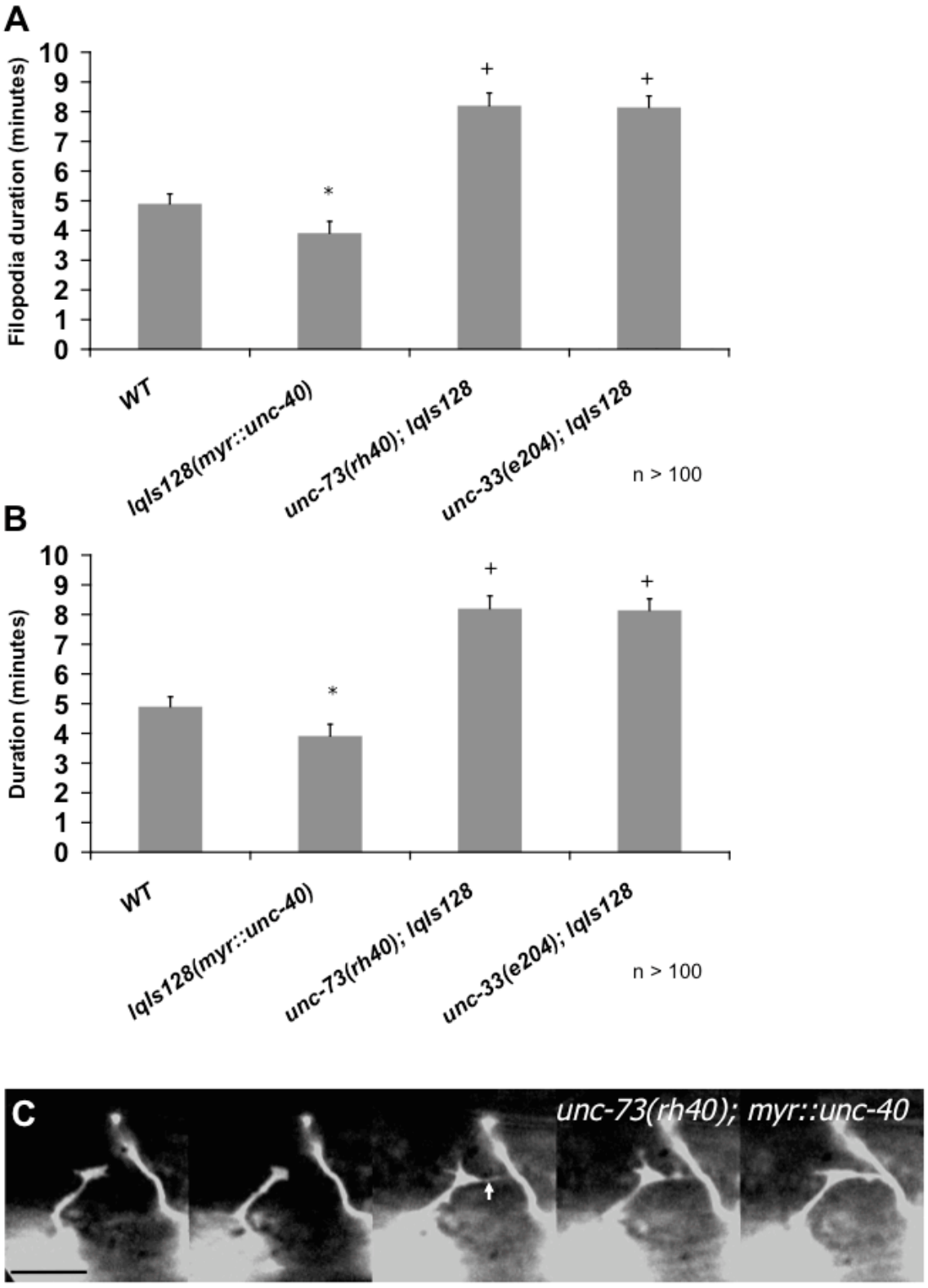
A
Filopodia duration (minutes)
0
1
2
3
4
5
6
7
8
9
10
*
+
+
WT
lqIs128(myr::unc-40)
unc-73(rh40); lqIs128
unc-33(e204); lqIs128
n > 100
B
Duration (minutes)
0
1
2
3
4
5
6
7
8
9
10
*
+
+
WT
lqIs128(myr::unc-40)
unc-73(rh40); lqIs128
unc-33(e204); lqIs128
n > 100
C
unc-73(rh40); myr::unc-40

Figure 4.5 Mutations in *unc-73, unc-33* and *unc-44* rescue the under-protrusive phenotype observed in *myr::unc-40* VD neurons. Quantification of filopodia dynamics in VD growth cones. (A) Duration of filopodia (in minutes); and (B) maximum length of filopodia (in μm). (C) Timelapse series of live *unc-73(rh40); myr::unc-40* growth cones, taken at 2 minutes per frame Error bars represent standard error of the mean; asterisk denotes significant difference between wild-type and the mutant ($p < 0.01$), + denotes significant difference between *myr::unc-40* and the double-mutant ($p < 0.01$); $n \geq 100$; scale bar represents 5 μm. Arrowhead shows unusually long, stable filopodium.

Chapter V

Discussion

The state of the axon pathfinding field is such that the vast majority of experiments are performed either on developed nervous systems at an endpoint-stage analysis, or on growth cones of dissociated neurons growing in vitro. The limitation of the former method is that conclusions about the developmental process are necessarily derived inferentially based on the endpoint phenotype. While such studies are highly useful and have advanced the field enormously, they lack the ability to give specific details about the cellular and molecular mechanisms controlling axon pathfinding during development. The latter method does provide such detail, but its main limitation is that the experiments are performed in artificial, *in vitro* conditions that are significantly different than the environment that a growth encounters *in vivo* in an organism. Thus, while *in vitro* growth cone studies are able to give a wealth of detailed information about the cellular and molecular aspects of axon pathfinding from a developmental standpoint, there is still the possibility that these mechanisms will be significantly different in growth cones challenged with the much more complex task of navigating an organism's extracellular milieu.

We set out to bridge the gap between these two experimental strategies by observing the cellular and molecular dynamics of live growth cones *in vivo* during the developmental process. We used *C. elegans* because of its invariant nervous system cell lineage and, most importantly, the fact that it is transparent and thus allows fluorescent tagging and imaging of neurons in intact, live organisms. A handful of neurons in *C. elegans* develop post-embryonically, and

are thus amenable to imaging in anesthetized worms. We utilized these neurons to learn about the normal development of the growth cone and used genetics to determine the morphological effects of axon pathfinding genes on the developing growth cone.

To date we have found over a dozen axon-pathfinding genes important for growth cone morphology and dynamics, as well as a few genes that do not appear to affect the morphology of the growth cone, through a candidate gene approach. The emerging theme of these studies is that changes in growth cone morphology, dynamics and polarity directly affect axon pathfinding. In Chapter II we proposed a link between proper filopodia formation and proper axon pathfinding. In Chapter III we showed that an attractive cue is correlated with stimulation of protrusion and a repulsive cue is correlated with inhibition of protrusion; we also showed that controlling the polarity of protrusion is linked with proper axon guidance. Finally, in Chapter IV we showed that failure to limit the extent of filopodia protrusion leads to the formation of ectopic axon branches in the adult. In sum, we are beginning to link morphological data about the growth cone to the final axon-pathfinding outcome, thus bridging the gap between in vitro growth cone studies and in vivo endpoint analysis studies.

These chapters detailed three major ways in which growth cone morphology and dynamics were linked with axon pathfinding outcomes. The first interesting link between growth cone dynamics and axon pathfinding was that mutations in genes that cause defects in filopodia formation also cause defects in axon pathfinding, especially in axons that tend to wander aberrantly from their

correct path. We speculate that this is due to the growth cone having a reduced sensitivity to the extracellular environment as a direct consequence of having reduced filopodia numbers.

The second link between the growth cone and axon pathfinding was that the Netrin signaling pathway affected both polarity and extent of growth cone protrusion, and that both extent and polarity of protrusion were involved in proper axon pathfinding. It is easy to imagine how loss of growth cone polarity could lead to axon pathfinding defects- the growth cone loses its ability to orient itself, and thus guide itself, in the proper direction. At the same time, the extent of protrusion of the growth cone must be controlled such that the proper balance is struck between growth cone protrusion toward a positive guidance cue and repulsion away from a guidance cue.

The final link that we have uncovered is between excessively long filopodia and ectopic axon branching. We show that in mutants that exhibit unusually long growth cone filopodia, they also exhibit ectopic axon branches in adults. We suggest, based on our results, that in fact the ectopic axon branches seen in these mutants are a direct consequence of excessively long filopodia that have failed to properly retract, but rather they continue to grow until they eventually consolidate and become mature axon branches. In each of these cases we have observed known axon pathfinding phenotypes and known or hypothesized growth cone phenotypes and shown how the two are related to each other, thus helping to bridge the gap between the understanding of the growth cone and how it affects the endpoint axon pathfinding phenotype.

The genes that we have studied are for the most part well-characterized axon pathfinding genes, but in each case little was known about how these genes were involved in the developing growth cone *in vivo*. We have thus elucidated the important growth-cone shaping roles of many important genes, such as Netrin and its receptors UNC-40/DCC and UNC-5, the Rac GTPases and their activating GEF UNC-73/Trio, and cytoskeletal regulators such as the Arp2/3 complex, UNC-44/Ankyrin and UNC-34/Enabled. We have shown that each of these important axon guidance molecules has a role to play in the dynamics and morphology of the developing growth cone *in vivo.*

There is still much work to be done. We have thus far only scratched the surface in terms of the number of genes required for axon pathfinding; it is likely that many new phenotypes will be uncovered as more and more genes are tested. We also would like to know more about the genetic pathways involved in many of these phenotypes. We have two powerful upstream phenotypes- the stimulation of protrusion with loss of the unc-5 guidance receptor, and the inhibition of protrusion with the myristoylation of the cytoplasmic domain of the unc-40 guidance receptor. These phenotypes have already born fruit in epistasis analysis (see Chapter IV) and have the potential to continue to do so in further studies of downstream signaling and effector genes.

Finally, there is still more work to be done to determine the causality between morphological characteristics of the growth cone and final endpoint status of the nervous system. This will require improved methods of growth cone imaging followed by subsequent rescue of the worm and re-imaging of the same

axon in the adult stage. While this has to some extent been accomplished, there are still some technical difficulties to overcome before this can become a standard procedure.

References

Adler, C. E., Fetter, R. D., and Bargmann, C. I. (2006), 'UNC-6/Netrin induces neuronal asymmetry and defines the site of axon formation', *Nat Neurosci,* 9 (4), 511-8.

Applewhite, D. A., et al. (2007), 'Ena/VASP proteins have an anti-capping independent function in filopodia formation', *Mol Biol Cell,* 18 (7), 2579-91.

Barzik, M., et al. (2005), 'Ena/VASP proteins enhance actin polymerization in the presence of barbed end capping proteins', *J Biol Chem,* 280 (31), 28653-62.

Bateman, J., Shu, H., and Van Vactor, D. (2000), 'The guanine nucleotide exchange factor trio mediates axonal development in the Drosophila embryo', *Neuron,* 26 (1), 93-106.

Bear, J. E. and Gertler, F. B. (2009), 'Ena/VASP: towards resolving a pointed controversy at the barbed end', *J Cell Sci,* 122 (Pt 12), 1947-53.

Beltzner, C. C. and Pollard, T. D. (2007), 'Pathway of actin filament branch formation by Arp2/3 complex', *J Biol Chem*.

Blangy, A., et al. (2000), 'TrioGEF1 controls Rac- and Cdc42-dependent cell structures through the direct activation of rhoG', *J Cell Sci,* 113 (Pt 4), 729-39.

Borisy, G. G. and Svitkina, T. M. (2000), 'Actin machinery: pushing the envelope', *Curr Opin Cell Biol,* 12 (1), 104-12.

Brenner, S. (1974), 'The genetics of *Caenorhabditis elegans*', *Genetics,* 77 (1), 71-94.

Chan, S. S., et al. (1996), 'UNC-40, a C. elegans homolog of DCC (Deleted in Colorectal Cancer), is required in motile cells responding to UNC-6 netrin cues', *Cell,* 87 (2), 187-95.

Chang, C., et al. (2006), 'MIG-10/lamellipodin and AGE-1/PI3K promote axon guidance and outgrowth in response to slit and netrin', *Curr Biol,* 16 (9), 854-62.

Colavita, A. and Culotti, J. G. (1998), 'Suppressors of ectopic UNC-5 growth cone steering identify eight genes involved in axon guidance in Caenorhabditis elegans', *Dev Biol,* 194 (1), 72-85.

Collet, J., et al. (1998), 'Analysis of osm-6, a gene that affects sensory cilium structure and sensory neuron function in Caenorhabditis elegans', *Genetics,* 148 (1), 187-200.

Davenport, R. W., et al. (1993), 'A sensory role for neuronal growth cone filopodia', *Nature,* 361 (6414), 721-4.

de Curtis, I. (2008), 'Functions of Rac GTPases during neuronal development', *Developmental neuroscience,* 30 (1-3), 47-58.

Dent, E. W., Tang, F., and Kalil, K. (2003), 'Axon guidance by growth cones and branches: common cytoskeletal and signaling mechanisms', *Neuroscientist,* 9 (5), 343-53.

Dent, E. W., et al. (2007), 'Filopodia are required for cortical neurite initiation', *Nat Cell Biol,* 9 (12), 1347-59.

Desai, C., et al. (1988), 'A genetic pathway for the development of the Caenorhabditis elegans HSN motor neurons', *Nature,* 336 (6200), 638-46.

Drees, F. and Gertler, F. B. (2008), 'Ena/VASP: proteins at the tip of the nervous system', *Curr Opin Neurobiol,* 18 (1), 53-9.

Duerr, J. S., et al. (1999), 'The cat-1 gene of Caenorhabditis elegans encodes a vesicular monoamine transporter required for specific monoamine-dependent behaviors', *J Neurosci,* 19 (1), 72-84.

Eden, S., et al. (2002), 'Mechanism of regulation of WAVE1-induced actin nucleation by Rac1 and Nck', *Nature,* 418 (6899), 790-3.

Engle, E. C. (2010), 'Human genetic disorders of axon guidance', *Cold Spring Harbor perspectives in biology,* 2 (3), a001784.

Friederich, E., et al. (1992), 'An actin-binding site containing a conserved motif of charged amino acid residues is essential for the morphogenic effect of villin', *Cell,* 70 (1), 81-92.

Fukata, Y., et al. (2002), 'CRMP-2 binds to tubulin heterodimers to promote microtubule assembly', *Nature cell biology,* 4 (8), 583-91.

Gallo, G. and Letourneau, P. C. (2004), 'Regulation of growth cone actin filaments by guidance cues', *J Neurobiol,* 58 (1), 92-102.

Garcia, M. C., et al. (2007), 'Role of Drosophila gene dunc-115 in nervous system', *Invert Neurosci,* 7 (2), 119-28.

Gatlin, J. C., et al. (2006), 'Myristoylated, alanine-rich C-kinase substrate phosphorylation regulates growth cone adhesion and pathfinding', *Mol Biol Cell,* 17 (12), 5115-30.

Gitai, Z., et al. (2003), 'The netrin receptor UNC-40/DCC stimulates axon attraction and outgrowth through enabled and, in parallel, Rac and UNC-115/AbLIM', *Neuron,* 37 (1), 53-65.

Gobel, V., et al. (2004), 'Lumen morphogenesis in C. elegans requires the membrane-cytoskeleton linker erm-1', *Dev Cell,* 6 (6), 865-73.

Goldberg, D. J. and Burmeister, D. W. (1986), 'Stages in axon formation: observations of growth of Aplysia axons in culture using video-enhanced contrast-differential interference contrast microscopy', *J Cell Biol,* 103 (5), 1921-31.

Hall, A. (2005), 'Rho GTPases and the control of cell behaviour', *Biochemical Society transactions,* 33 (Pt 5), 891-5.

Hall, A. and Nobes, C. D. (2000), 'Rho GTPases: molecular switches that control the organization and dynamics of the actin cytoskeleton', *Philosophical transactions of the Royal Society of London. Series B, Biological sciences,* 355 (1399), 965-70.

Hall, A. and Lalli, G. (2010), 'Rho and Ras GTPases in axon growth, guidance, and branching', *Cold Spring Harbor perspectives in biology,* 2 (2), a001818.

Hedgecock, E. M., Culotti, J. G., and Hall, D. H. (1990), 'The *unc-5, unc-6,* and *unc-40* genes guide circumferential migrations of pioneer axons and mesodermal cells on the epidermis in *C. elegans.*', *Neuron,* 4 (1), 61-85.

Hedgecock, E. M., et al. (1987), 'Genetics of cell and axon migrations in Caenorhabditis elegans', *Development,* 100 (3), 365-82.

Hong, K., et al. (1999), 'A ligand-gated association between cytoplasmic domains of UNC5 and DCC family receptors converts netrin-induced growth cone attraction to repulsion', *Cell,* 97 (7), 927-41.

Hopitzan, A. A., Baines, A. J., and Kordeli, E. (2006), 'Molecular evolution of ankyrin: gain of function in vertebrates by acquisition of an obscurin/titin-binding-related domain', *Molecular biology and evolution,* 23 (1), 46-55.

Innocenti, M., et al. (2004), 'Abi1 is essential for the formation and activation of a WAVE2 signalling complex', *Nat Cell Biol,* 6 (4), 319-27.

Ishii, N., et al. (1992), 'UNC-6, a laminin-related protein, guides cell and pioneer axon migrations in C. elegans', *Neuron,* 9 (5), 873-81.

Jin, Y., et al. (1999), 'The Caenorhabditis elegans gene unc-25 encodes glutamic acid decarboxylase and is required for synaptic transmission but not synaptic development', *J Neurosci,* 19 (2), 539-48.

Kim, A. S., et al. (2000), 'Autoinhibition and activation mechanisms of the Wiskott-Aldrich syndrome protein', *Nature,* 404 (6774), 151-8.

Kishore, R. S. and Sundaram, M. V. (2002), 'ced-10 Rac and mig-2 function redundantly and act with unc-73 trio to control the orientation of vulval cell divisions and migrations in Caenorhabditis elegans', *Dev Biol,* 241 (2), 339-48.

Knobel, K. M., Jorgensen, E. M., and Bastiani, M. J. (1999), 'Growth cones stall and collapse during axon outgrowth in Caenorhabditis elegans', *Development,* 126 (20), 4489-98.

Korobova, F. and Svitkina, T. (2008), 'Arp2/3 complex is important for filopodia formation, growth cone motility, and neuritogenesis in neuronal cells', *Mol Biol Cell,* 19 (4), 1561-74.

Kwiatkowski, A. V., et al. (2007), 'Ena/VASP Is Required for neuritogenesis in the developing cortex', *Neuron,* 56 (3), 441-55.

Lebrand, C., et al. (2004), 'Critical role of Ena/VASP proteins for filopodia formation in neurons and in function downstream of netrin-1', *Neuron,* 42 (1), 37-49.

Leonardo, E.D., Hinck, L., Masu, M., Keino-Masu, K., Ackerman, S.L., Tessier-Lavigne, M. (1997), 'Vertebrate homologs of C. elegans UNC-5 are candidate netrin receptors', *Nature,* 386 (6627), 833-38.

Letourneau, PC (1996), 'The cytoskeleton in growth cone motility and axon pathfinding', *Perspect Dev Neurobiol,* 4 (2-3), 111-23.

Leung-Hagesteijn, C., Spence, A.M., Stern, B.D., Zhou, Y., Su, M.-W., Hedgecock, E.M., Culotti, J.G. (1992), 'UNC-5, a transmembrane protein with immunoglobulin and thrombospondin type I domains, guides cell and pioneer axon migrations', *Cell,* 71, 289-99.

Li, W., Herman, R.K., Shaw, J.E. (1992), 'Analysis of the *Caenorhabditis elegans* Axonal Guidance and Outgrowth Gene *unc-33*', *Genetics,* 132, 675-89.

Lim, Y. S. and Wadsworth, W. G. (2002), 'Identification of domains of netrin UNC-6 that mediate attractive and repulsive guidance and responses from cells and growth cones', *The Journal of neuroscience : the official journal of the Society for Neuroscience,* 22 (16), 7080-7.

Lundquist, E. A. (2006), 'Small GTPases', *WormBook*, 1-18.

Lundquist, E. A., et al. (1998), 'UNC-115, a conserved protein with predicted LIM and actin-binding domains, mediates axon guidance in C. elegans', *Neuron,* 21 (2), 385-92.

Lundquist, E. A., et al. (2001), 'Three C. elegans Rac proteins and several alternative Rac regulators control axon guidance, cell migration and apoptotic cell phagocytosis', *Development,* 128 (22), 4475-88.

MacNeil, L. T., et al. (2009), 'UNC-129 regulates the balance between UNC-40 dependent and independent UNC-5 signaling pathways', *Nat Neurosci,* 12 (2), 150-5.

Mello, C. and Fire, A. (1995), 'DNA transformation', *Methods Cell Biol,* 48, 451-82.

Ming, G. L., et al. (1997), 'cAMP-dependent growth cone guidance by netrin-1', *Neuron,* 19 (6), 1225-35.

Montell, D. J. (1999), 'The genetics of cell migration in Drosophila melanogaster and Caenorhabditis elegans development', *Development,* 126 (14), 3035-46.

Moore, S. W., Tessier-Lavigne, M., and Kennedy, T. E. (2007), 'Netrins and their receptors', *Adv Exp Med Biol,* 621, 17-31.

Mortimer, D., et al. (2008), 'Growth cone chemotaxis', *Trends Neurosci*.

Norris, A. D., Dyer, J. O., and Lundquist, E. A. (2009), 'The Arp2/3 complex, UNC-115/abLIM, and UNC-34/Enabled regulate axon guidance and

growth cone filopodia formation in Caenorhabditis elegans', *Neural Dev,* 4, 38.

Otsuka, A. J., et al. (2002), 'Novel UNC-44 AO13 ankyrin is required for axonal guidance in C. elegans, contains six highly repetitive STEP blocks separated by seven potential transmembrane domains, and is localized to neuronal processes and the periphery of neural cell bodies', *Journal of neurobiology,* 50 (4), 333-49.

Otsuka, A.J., Franco, R., Yang, B., Shim, K.-H., Tang, L.Z., Zhang, Y.Y., Boontrakulpoontawee, P., Jeyaprakash, A., Hedgecock, E., and Wheaton, V.I. (1995), 'An Ankyrin-Related Gene (*unc-44)* Is Necessary for Proper Axonal Guidance in *Caenorhabditis elegans*', *J. Cell Biol.,* 129, 1081-92.

Pak, C. W., Flynn, K. C., and Bamburg, J. R. (2008), 'Actin-binding proteins take the reins in growth cones', *Nat Rev Neurosci,* 9 (2), 136-47.

Pan, Y., et al. 'Abnormal expression of netrin-G2 in temporal lobe epilepsy neurons in humans and a rat model', *Exp Neurol,* 224 (2), 340-6.

Pinyol, R., et al. (2007), 'Regulation of N-WASP and the Arp2/3 complex by Abp1 controls neuronal morphology', *PLoS ONE,* 2 (5), e400.

Quinn, C. C. and Wadsworth, W. G. (2008), 'Axon guidance: asymmetric signaling orients polarized outgrowth', *Trends Cell Biol,* 18 (12), 597-603.

Reddien, P. W. and Horvitz, H. R. (2000), 'CED-2/CrkII and CED-10/Rac control phagocytosis and cell migration in Caenorhabditis elegans', *Nat Cell Biol,* 2 (3), 131-6.

Sawa, M., et al. (2003), 'Essential role of the C. elegans Arp2/3 complex in cell migration during ventral enclosure', *J Cell Sci,* 116 (Pt 8), 1505-18.

Shakir, M. A., Gill, J. S., and Lundquist, E. A. (2006), 'Interactions of UNC-34 Enabled with Rac GTPases and the NIK kinase MIG-15 in Caenorhabditis elegans axon pathfinding and neuronal migration', *Genetics,* 172 (2), 893-913.

Shakir, M. A., et al. (2008), 'The Arp2/3 activators WAVE and WASP have distinct genetic interactions with Rac GTPases in C. elegans axon guidance', *Genetics,* 179 (August), 1-15.

Shekarabi, M. and Kennedy, T. E. (2002), 'The netrin-1 receptor DCC promotes filopodia formation and cell spreading by activating Cdc42 and Rac1', *Mol Cell Neurosci,* 19 (1), 1-17.

Shekarabi, M., et al. (2005), 'Deleted in colorectal cancer binding netrin-1 mediates cell substrate adhesion and recruits Cdc42, Rac1, Pak1, and N-WASP into an intracellular signaling complex that promotes growth cone expansion', *J Neurosci,* 25 (12), 3132-41.

Shen, K. and Bargmann, C. I. (2003), 'The immunoglobulin superfamily protein SYG-1 determines the location of specific synapses in C. elegans', *Cell,* 112 (5), 619-30.

Steven, R., et al. (1998), 'UNC-73 activates the Rac GTPase and is required for cell and growth cone migrations in C. elegans', *Cell,* 92, 785-95.

Strasser, G. A., et al. (2004), 'Arp2/3 is a negative regulator of growth cone translocation', *Neuron,* 43 (1), 81-94.

Struckhoff, E. C. and Lundquist, E. A. (2003), 'The actin-binding protein UNC-115 is an effector of Rac signaling during axon pathfinding in C. elegans', *Development,* 130 (4), 693-704.

Sulston, J. E. and Horvitz, H. R. (1977), 'Post-embryonic cell lineages of the nematode, Caenorhabditis elegans', *Dev Biol,* 56 (1), 110-56.

Svitkina, T. M. and Borisy, G. G. (1999), 'Arp2/3 complex and actin depolymerizing factor/cofilin in dendritic organization and treadmilling of actin filament array in lamellipodia', *J Cell Biol,* 145 (5), 1009-26.

Tessier-Lavigne, M. and Goodman, C. S. (1996), 'The molecular biology of axon guidance', *Science,* 274 (5290), 1123-33.

Tsuboi, D., et al. (2005), 'Regulatory machinery of UNC-33 Ce-CRMP localization in neurites during neuronal development in Caenorhabditis elegans', *Journal of neurochemistry,* 95 (6), 1629-41.

Van Furden, D., et al. (2004), 'The C. elegans ezrin-radixin-moesin protein ERM-1 is necessary for apical junction remodelling and tubulogenesis in the intestine', *Dev Biol,* 272 (1), 262-76.

Weinkove, D., et al. (2008), 'Overexpression of PPK-1, the Caenorhabditis elegans Type I PIP kinase, inhibits growth cone collapse in the developing nervous system and causes axonal degeneration in adults', *Dev Biol,* 313 (1), 384-97.

White, J. G., et al. (1986), 'The structure of the nervous system of the nematode *Caenorhabditis elegans*', *Philos. Trans. R. Soc. Lond.,* 314, 1-340.

Withee, J., et al. (2004), 'Caenorhabditis elegans WASP and Ena/VASP Proteins Play Compensatory Roles in Morphogenesis and Neuronal Cell Migration', *Genetics,* 167 (3), 1165-76.

Xu, Z., Li, H., and Wadsworth, W. G. (2009), 'The roles of multiple UNC-40 (DCC) receptor-mediated signals in determining neuronal asymmetry induced by the UNC-6 (netrin) ligand', *Genetics,* 183 (3), 941-9.

Yang, Y. and Lundquist, E. A. (2005), 'The actin-binding protein UNC-115/abLIM controls formation of lamellipodia and filopodia and neuronal morphogenesis in Caenorhabditis elegans', *Mol Cell Biol,* 25 (12), 5158-70.

Yu, S., et al. (1997), 'Guanylyl cyclase expression in specific sensory neurons: a new family of chemosensory receptors', *Proc Natl Acad Sci U S A,* 94 (7), 3384-7.

Zallen, J. A., Kirch, S. A., and Bargmann, C. I. (1999), 'Genes required for axon pathfinding and extension in the C. elegans nerve ring', *Development,* 126 (16), 3679-92.

Zallen, J. A., et al. (2002), 'SCAR is a primary regulator of Arp2/3-dependent morphological events in Drosophila', *J Cell Biol,* 156 (4), 689-701.

Zhou, F. Q. and Cohan, C. S. (2004), 'How actin filaments and microtubules steer growth cones to their targets', *J Neurobiol,* 58 (1), 84-91.

Zipkin, I. D., Kindt, R. M., and Kenyon, C. J. (1997), 'Role of a new Rho family member in cell migration and axon guidance in C. elegans', *Cell,* 90 (5), 883-94.